Progress in Oceanography 202 (2022) 102760

Contents lists available at ScienceDirect

Progress in Oceanography

journal homepage: www.elsevier.com/locate/pocean

Ocean shelf exchange, NW European shelf seas: Measurements, estimates and comparisons

John Huthnance [a,*], Jo Hopkins [a], Bee Berx [b], Andy Dale [c], Jason Holt [a], Philip Hosegood [d], Mark Inall [c], Sam Jones [c], Benjamin R. Loveday [e,1], Peter I. Miller [e], Jeff Polton [a], Marie Porter [c], Carl Spingys [f,2]

[a] UK National Oceanography Centre, 6 Brownlow Street, Liverpool L3 5DA, UK
[b] Marine Scotland Science, 375 Victoria Rd, Aberdeen AB11 9DB, Scotland, UK
[c] Scottish Association for Marine Science, Oban, Argyll PA37 1QA, Scotland, UK
[d] School of Biological and Marine Sciences, University of Plymouth, Reynolds, Drake Circus, Plymouth PL4 8AA, UK
[e] Plymouth Marine Laboratory, Prospect Place, Plymouth PL1 3DH, UK
[f] Department of Earth, Ocean and Ecological Sciences, University of Liverpool, 4 Brownlow Street, Liverpool L69 3GP, UK

ARTICLE INFO

Keywords:
Exchange
Shelf edge
Ekman transports
Slope current
Tidal currents
Internal tides
NW Europe
Celtic Sea
Malin-Hebrides shelf
West Shetland shelf

ABSTRACT

Transports across the continental shelf edge enhance shelf-sea production, remove atmospheric carbon and imply an active boundary to ocean circulation. We estimate relatively large overall transport across three contrasted sectors of north-west European shelf edge: the Celtic Sea south-west of Britain, the Malin-Hebrides shelf west of Scotland, the West Shetland shelf north of Scotland. The estimates derive from measurements in the project FASTNEt (Fluxes across sloping topography of the North East Atlantic): drifters, moored current meters, effective "diffusivity" from drifter dispersion and salinity surveys, other estimates of velocity variance contributing to exchange. Process contributions include transport by along-slope flow, internal waves and their Stokes drift, tidal pumping, eddies, Ekman transports in the wind-driven surface layer and bottom boundary layer.

Overall exchange across the shelf edge is estimated as several m^2s^{-1}: if extrapolated globally even 1 m^2s^{-1} is large compared with oceanic transports and potentially important to shelf-sea and adjacent oceanic budgets. In our context, most exchange is in tides, and other motion with periods ~ one day or less, and so effective only for water properties that evolve on such short time-scales. Nevertheless, cross-slope fluxes, and exchange by low-frequency motion (periods > two days), are large by global standards and also very variable. Deployment-mean fluxes nearest the shelf break were in the range 0.3–4 m^2s^{-1}; mean exchanges from low-frequency motion were 0.8–3 m^2s^{-1}. Deeper longer-term moorings and drifters crossing 500 m depth gave much larger fluxes and exchanges up to 20 m^2s^{-1}. These transports' significance depends on distinctive properties of the water, or its contents, and on internal shelf-sea circulation affecting further transport. For the NW European shelf, transports across the shelf edge enable its disproportionately strong CO_2 "pump".

The complex context, and small scales of numerous processes enabling cross-slope transports, imply a need for models. Measurements remain limited in extent and duration, but widely varied contexts, particular conditions, events, processes and behaviours are now available to support model validation, especially around the north-west European continental shelf edge. Variability still renders observations insufficient for stable estimates of transports and exchanges, especially if partitioned by sector and season; indeed, there may be significant inter-annual differences. Validated fine-resolution models give the best prospect of spatial and temporal coverage and of estimating present-day and potential future shelf-sea sensitivities to the adjacent ocean.

* Corresponding author.
E-mail addresses: jmh@noc.ac.uk (J. Huthnance), j.hopkins@noc.ac.uk (J. Hopkins), b.berx@marlab.ac.uk (B. Berx), Andrew.Dale@sams.ac.uk (A. Dale), jholt@noc.ac.uk (J. Holt), phil.hosegood@plymouth.ac.uk (P. Hosegood), mark.inall@sams.ac.uk (M. Inall), sam.jones@sams.ac.uk (S. Jones), ben.loveday@innoflair.com (B.R. Loveday), pim@pml.ac.uk (P.I. Miller), jelt@noc.ac.uk (J. Polton), Marie.Porter@sams.ac.uk (M. Porter), c.p.spingys@soton.ac.uk (C. Spingys).
[1] Now at Innoflair UG, Richard-Wagner-Weg 35, 64287 Darmstadt, Germany.
[2] Now at Ocean and Earth Science, University of Southampton, Waterfront Campus, National Oceanography Centre, European Way, Southampton SO14 3ZH, UK.

https://doi.org/10.1016/j.pocean.2022.102760
Received 23 April 2021; Received in revised form 24 December 2021; Accepted 8 February 2022
Available online 11 February 2022

1. Introduction

1.1. Global perspective of shelf seas

Society has a strong dependence on coastal and shelf-sea resources. Ocean margins are estimated to be responsible for more than one-fifth of the global marine primary production (Gröger et al. 2013) and for sequestering 40% of the global annual export of particulate organic carbon (e.g. Muller-Karger, 2005), much by lower-layer transport from shelf sea to deep ocean. For example, north-west (NW) European continental shelf modelling shows off-shelf transport removal of 40% or more of the carbon sequestered by one growing season before the next (Holt et al. 2009, Wakelin et al. 2012, Legge et al. 2020). Shelf and coastal waters include 90% of the world's commercial fish catch (Pauly et al. 2002). However, modelling suggests a substantial fraction of NW European continental shelf water originates from the open ocean to the south (Holt et al. 2012). Globally, transport from the open ocean across the shelf edge is estimated to bring most of the nitrogen and half of the phosphate used in shelf-sea export production (Liu et al., 2010) and supports the productive higher trophic levels there. However, model climate projections suggest that warming of the sea surface by about 2.0 K, and consequent change of stratification along the continental shelf break, would reduce the nutrient supply to the NW European shelf from the deep Atlantic by between 17% (Holt et al. 2012) and 50% (Gröger et al. 2013). Seasonal lack of oxygen tends to occur in wide-shelf sectors distant from "ventilation" from the ocean (other factors being equal; Monteiro et al. 2011). North Sea oxygen deficiency may expand and intensify in future climate scenarios (Wakelin et al. 2020).

From the reverse viewpoint, continental shelves are active ocean boundaries. Typical exchanges O(1 m^2s^{-1}) across a boundary length O (5×10^5 km) (Robinson et al. 2005; estimated on a scale 50–70 km) amount to O(500 Sverdrups (Sv); 1 Sv $\equiv 10^6$ m^3s^{-1}). From this perspective, the continental shelf break is far from being the closed ocean boundary sometimes assumed. For example, water leaving the Barents Sea constitutes 50–80% of the volume of Arctic Intermediate Water (Schauer et al. 1997). Cold, dense water masses generated over Antarctic continental shelves make a major contribution to the global thermohaline circulation. Transport and properties of these waters are constrained by cross-slope exchange and mixing of shelf and offshore water masses along the Antarctic shelf break (Gordon et al. 2009a). In summary, shelf-edge control of water, nutrient and carbon exchange between ocean and shelf-sea strongly influences both global climate and regional resources.

1.2. Constraints on exchange

Large-scale, slowly-varying flows are strongly constrained by geostrophy to follow f/h contours (where f is the Coriolis parameter and variations of water depth h dominate shelf-edge contours of f/h). As a result, cross-shelf gradients are usually greater than along-shelf gradients, but estimating cross-shelf flows is complicated by the general prevalence of along-shelf flow. Moreover, emphasis is thereby placed on the smaller time- and space-scale processes that enable cross-shelf flow but are harder to discern (e.g. Huthnance 1995; Brink 2016). For example, variability at small spatial and temporal scales modulates the contribution of Antarctic shelf seas to deep ocean circulation (Gordon et al. 2009a). Bottom Ekman layer transport below contour-following flows can be an effective means of ocean-shelf exchange (e.g. Shapiro and Hill 1997; Holt et al. 2009) and is directly related to along-slope forcing (Huthnance et al. 2020). Generally, interaction of ocean flow with the continental shelf edge is a difficult 4-D problem for measurements to resolve (Brink, 2016).

1.3. Previous studies of ocean shelf exchange

Various contrasting locations have been studied. Around European margins, down-slope particle fluxes were emphasised in the north-west Mediterranean (Guarracino et al. 2006; ECOMARGE – Monaco et al. 1990) and in the Bay of Biscay (e.g. ECOMARGE – Heussner et al. 1999). MORENA (off Portugal) emphasised mainly summer upwelling (enhanced off capes), along slope flow (more prominent in winter) and hydrography (Fiuza et al. 1998; Stevens et al. 2000). ARCANE, SEFOS and INTERAFOS measured general and mesoscale Lagrangian circulations over the Bay of Biscay abyssal plain and slopes (Serpette et al. 2006). OMEX studied physics and biogeochemical fluxes over Goban Spur (south-west of Britain) and off north-west Spain (Pingree et al. 1999; Huthnance et al. 2001, 2002; van Aken et al. 2005; Wollast and Chou 2001). The UK Shelf Edge Study (SES) and later winter cruises did likewise west of Scotland (e.g. Souza et al. 2001; Proctor et al. 2003; Hydes et al. 2004; Simpson and McCandliss 2013). ENAM emphasised Quaternary sediment processes in the Atlantic margin from Portugal to Norway (Meinert et al. 1998). Exchange across the NW European margin was reviewed by Huthnance et al. (2009). [More results from NW European margin studies are given in section 2.1.]

Off eastern North America, an early study was at the Scotian shelf edge (Smith 1978). "Shelf Edge Exchange Processes" (SEEP-I and –II) studied the Middle Atlantic Bight (Walsh et al. 1988; Biscaye et al. 1994). Other specific studies concern along-shelf convergence to infer off-shelf export near Cape Hatteras (Savidge and Bane, 2001) and Gulf Stream meanders interacting with Georges Bank (Lee and Brink, 2010). Physical transport and biogeochemical transformation processes affecting fluxes into, and out of, continental shelf systems, and their role in the global cycling of nitrogen (N) and carbon (C), were reviewed by Fennel (2010) who also modelled N and C budgets for the north-western North Atlantic continental shelf. Siedlecki et al. (2011) modelled the north-east USA shelf-break front, its response to winds (with modulation by summer stratification) and consequences for nutrient distributions. Off northern California, the response to wind forcing in CODE 1 and 2 (Beardsley and Lentz, 1987) included upwelling and filaments which were the focus of the Coastal Transition Zone program (Brink and Cowles, 1991). There are many studies of eastern boundary upwelling (see e.g. Barber, 2001).

Published estimates of transports in many locations are reviewed in section 5.6 for comparison with values in this study. Many concern specific processes expected to be effective in causing cross-slope flow: adjacent eddies, convergent along-shelf flows, Ekman transports from along-shelf winds and below along-slope currents, dense water flowing down-slope (often strongly guided by topography). An overview of many other studies is given in Johnson and Chapman (2011).

1.4. Physics governing exchange

Processes important to exchange may include tides (e.g. Huthnance et al. 1995), internal tides (e.g. Davies and Xing, 2005), internal waves (discussed by McPhee-Shaw 2006, Hopkins et al. 2012) and solitons (e.g. Huthnance 1995; Inall et al. 2000; Inall et al. 2001); along-shelf flow (e.g. Pingree et al. 1999) *via* associated secondary flows (e.g. Durrieu de Madron et al. 1999), frictional boundary layers (Houghton 1995) and an "Ekman Drain" (Simpson and McCandliss 2013); shelf edge meanders (e.g. Durrieu de Madron et al. 1999) and eddies (Pingree 1979); wind-driven transport (e.g. Huthnance et al. 2009; Ruiz-Castillo et al., 2022); wind-waves and swell (e.g. Huthnance 1995); upwelling, fronts and filaments (Barber 2001); fronts with eddies between shelf and slope waters (Houghton et al. 1988); downwelling (e.g. Huthnance et al. 2009), cascading (Shapiro and Hill 1997; Luneva et al. 2020) and the effects of entrainment and small-scale topography or canyons thereon; mixing and subsequent (geostrophic) adjustment or gravitational collapse with associated near-inertial motion (van Aken et al. 2005). Capes, spurs and canyons can be important in guiding the flow (e.g. Aagaard and Roach 1990; Moseidjord et al. 1999; Dinniman et al. 2011; Porter et al. 2016b) or facilitating cross-slope flow if depth contours bend sharply (e.g. Jordi et al. 2005, 2006; Skliris et al. 2002; Porter et al.

2018). Canyons in particular may reduce the local length scale of the flow, increasing the local Rossby number, so relaxing the geostrophic constraint (also moderated by strong stratification) and facilitating cross-isobath flow. Canyons cut across any along-slope tidal flow component, often generating baroclinic tides and internal waves; they can also focus internal waves. Allen et al. (2009) give a review of canyon effects.

1.5. Motivation for this study

Despite the previous studies reviewed above, we still lack knowledge of seasonal and inter-annual variability in behaviours of different exchange mechanisms. Measurements have been especially difficult in winter (when wind-forced mechanisms may be at their strongest). Yet seasonality in physical exchange is vital to meaningful estimates of biogeochemical fluxes. There also remains a challenge to integrate individual processes for regional-scale estimates of transports across the shelf edge as: (a) individual process contributions based on measurements may not be simply additive; (b) the small-scale physical processes enabling transport across steep slopes may not be resolved or parameterised in regional numerical models. Improved understanding of exchange requires numerical modelling to provide evidence with a density and coverage beyond the scope of observations alone. However, we need measurement data of sufficient variety to test such models' representation of numerous known significantly-contributing processes (as listed above). "Variety" implies different seasons and contrasting shelf-edge sectors. Accordingly, project FASTNEt (Fluxes across sloping topography of the North East Atlantic) around the NW European shelf edge included aims:

(i) To determine through measurements the *seasonality* of physical gradients and exchange across the shelf edge;
(ii) To quantify key exchange mechanisms and obtain new data to test and improve fine-resolution models of the shelf edge, by carrying out process studies in *contrasting* shelf-edge sectors.

The second aim entails fine spatial resolution of transports, at scales comparable to or less than model resolution, to understand the very local scale (10′s km or less) variability in exchange, in varied shelf-edge sectors having different combinations of exchange processes.

Here we attempt to synthesise estimates of transports and contributions thereto, on the basis of the varied measurements and some model simulations, both from FASTNEt and from other studies, including the Hebrides Shelf Edge Study in 1995–1996 and the Shelf Sea Biogeochemistry (SSB) programme in the Celtic Sea in 2014–2015. We describe the NW European shelf-edge context (section 2.1), an outline of FASTNEt observations (2.2), definition of fluxes (net transports) and exchanges (2.3) and an outline of the utilised fine-resolution model

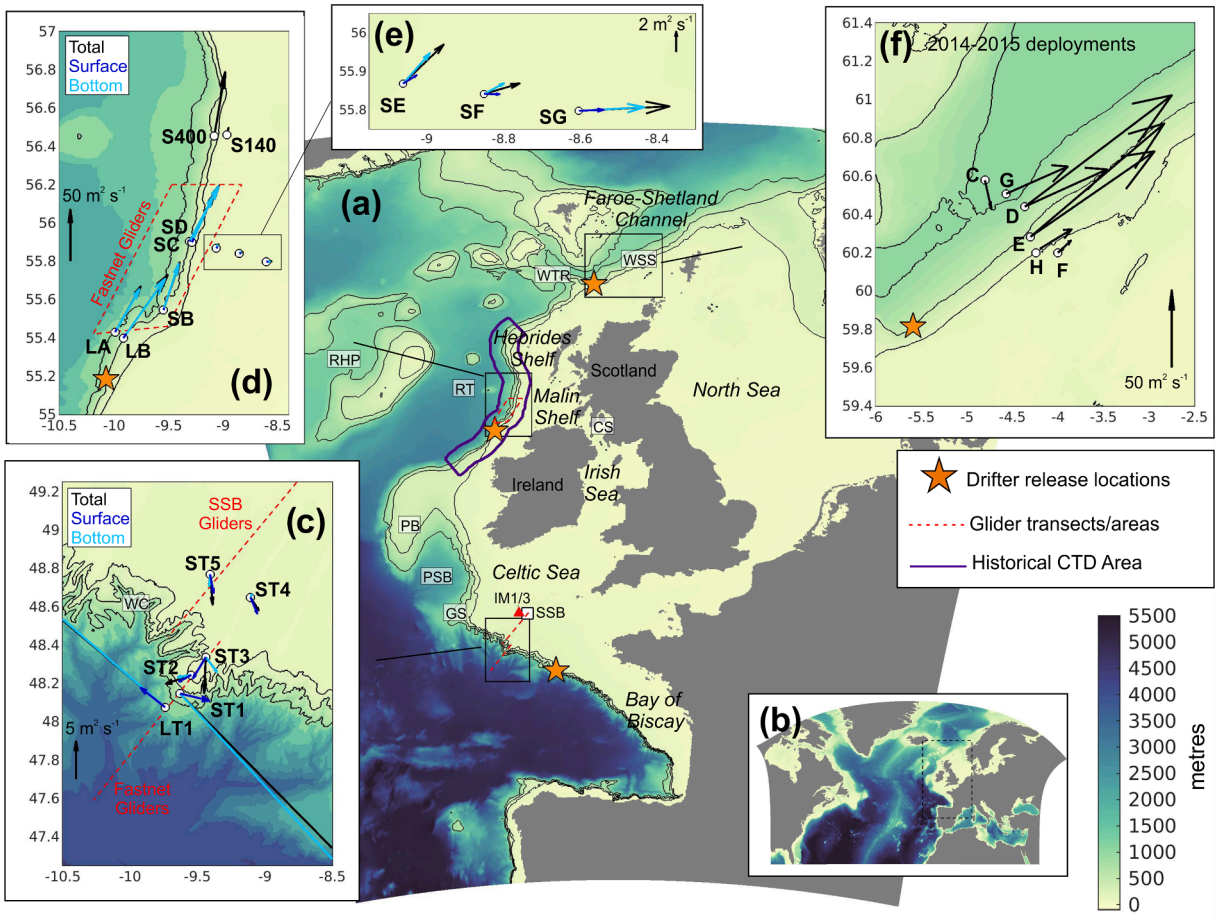

Fig. 1. North West European shelf modelling and observations. (a) AMM60 model domain and bathymetry. (b) Northern North Atlantic (NNA) model domain and bathymetry. (c) Celtic Sea mooring locations and deployment mean fluxes; full water column (black), surface (dark blue), bottom (light blue). FASTNEt and Shelf Sea Biogeochemistry (SSB) glider tracks: dashed red lines. (d) Malin and Hebrides shelf mooring locations and deployment mean fluxes. Red dashed box: area of FASTNEt glider operations in 2013. Orange star is the 2013 drifter release location. (e) Shallow water Malin shelf moorings and deployment mean fluxes. (f) Locations and deployment mean fluxes for the Faroe-Shetland channel NWS-moorings in 2014–2015. Orange star is the 2014 drifter release location. Location codes (south to north): WC = Whittard Canyon (in c); GS = Goban Spur; PSB = Porcupine Sea Bight; PB = Porcupine Bank; CS = Clyde Sea; RT = Rockall Trough; RHP = Rockall-Hatton Plateau; WTR = Wyville Thomson Ridge; WSS = West Shetland Slope.

(2.4). Methodology and results for estimation of fluxes and exchange are described for each type of observation in turn in section 3. Estimates of some process contributions thereto are presented in section 4. A discussion section (5) includes some global comparisons and significance for shelf-sea budgets and cycling. Conclusions (section 6) include Table 15 summarising distinctive characteristics of North-west European shelf-edge sectors studied here.

2. Context, fluxes and exchanges, fine-resolution model

2.1. North-west European shelf edge; dynamical background

The shelf seas bordering the NE Atlantic are broad and irregular, from ~50 km wide around Ireland to as much as 400 km in the Celtic Sea (Fig. 1). Depths are typically between 100 and 150 m. The shelf slope is steep (super-critical to internal tides) in the south, becoming less steep (sub-critical) north-west of Scotland. The Celtic Sea margin is irregular. The definition of "along-slope" varies locally owing to the many canyons which may focus internal waves instigating sediment movement and creating bedforms (Lo Iacono et al. 2020). The Porcupine Seabight is a 2000 m deep indentation into the shelf at ~50°N. North of this, the Malin and Hebrides shelf edge and slope are much smoother, except that there is a distinct shallow canyon and "rough" upper-slope topography near 55.5°N. The west Shetland slope of the Faroe-Shetland Channel is broader (less steep) than the Celtic and Malin-Hebrides slopes.

Adjacent ocean stratification in southern sectors relates to Eastern North Atlantic Water (ENAW) overlying Mediterranean Outflow Water (MOW), below which ENAW mixes with Labrador Sea Water (LSW). In the Faroe-Shetland Channel, extensions of the poleward warm North Atlantic Current overlie cold overflow water, flowing in the opposite sense from the Nordic Seas as discussed in Chafik et al. (2020). Freshwater inputs to these shelf seas are moderate; salinity is typically within 1 or 2 psu of oceanic values except in the Scottish Coastal Current inshore of the shelf break west of Scotland (e.g. Hill et al. 1997; Inall et al. 2009) resulting from reduced-salinity outflows from the Irish and Clyde Seas. There is also a clockwise-flowing Irish Coastal Current. The dominant variability in buoyancy is seasonal, e.g. across the Celtic Sea (Ruiz-Castillo et al. 2019): a shallow thermocline (~50 m) develops in spring and is eroded each autumn and winter, deepening below the shelf break (to as much as 800 m in the Rockall Trough). These contrasting contexts suggest varied exchange processes.

Prevailing south-westerly winds vary seasonally in strength and drive downwelling on average. At the Celtic Sea margin, except on the shelf, currents resulting from these winds (and eddies) are typically O (0.1 m s^{-1}) or less and decrease with depth (Huthnance et al. 2001). Over the Hebrides slope west of Scotland, Painter et al. (2016) estimated shoreward wind-driven surface Ekman transports of 1.9–2.2 m^2s^{-1} in October-November 2014 (slightly exceeding other literature estimates). These transports are very variable; the proportions of Atlantic-origin to coastal-source water on the Hebrides shelf around 57°N 7°W vary from more than 62%:38% to less than 6%:94% as winds vary from strong westerly to strong easterly for sustained periods (Jones et al. 2018). Salinity here and on the Malin shelf is strongly affected by these ratios of Atlantic- and coastal-source waters (and hence by wind stress and direction; Jones et al. 2018); there is no particular periodicity but salinity variability is greater in winter. Prevailing winds are often strong, generating large waves, turbulence and consequent mixing, to which strong tidal currents also contribute (see below).

This is an eastern ocean boundary; there is no strong (wind-driven) western boundary current, nor large associated eddies. However, along the upper continental slope there is a current, which is usually poleward. The North Atlantic Current meets the continental slope off the Celtic Sea and in Rockall Trough; 1 – 2 Sv of its transport is converted to barotropic transport over the slope. The slope current transport increases significantly from Rockall Trough to the Faroe-Shetland Channel (Zhou and Nost 2013). This slope current is believed to be the result of increasing poleward density at the sloping ocean margin (Huthnance 1986); Stashchuk et al. (2017) show an additional tidal residual contribution over the upper Malin slope. The slope current is warm and saline, nearly-barotropic (Souza et al. 2001), in near-geostrophic balance and typically centred over the 500 m isobath (Pingree and LeCann 1989; Huthnance et al. 2001) albeit variable seasonally (Pingree and LeCann 1990; Souza et al. 2001), interannually and spatially (Xu et al. 2015). The flow along the Celtic Sea slope, O(0.05 m s^{-1}), may decrease and even tend to equatorward flow in spring (March-April or later), a seasonal September/October – March/April variation (Pingree et al. 1999). The slope current here is perhaps weaker than further north owing to non-meridional alignment and indentations in the Celtic Sea slope; around Goban Spur it may sometimes overshoot off-shelf rather than follow the depth contours (Pingree et al. 1999).

Slope current transport is determined by a balance between the meridional oceanic density gradient, wind stress and bottom friction over the slope (Huthnance et al. 2020). Where the slope current is poleward, the bottom frictional boundary layer is expected to give off-shelf Ekman transport. Measurements over the Hebrides slope west of Scotland showed slope-current speeds of order 0.2–0.3 m s^{-1} and upper-bound estimates 0.7–2.7 m^2s^{-1} for down-slope bottom Ekman transports in October-November 2014 (Painter et al. 2016); Simpson and McCandliss (2013) estimated 1.6 m^2s^{-1} in August 1995 to January 1996. The west Shetland slope current being just as strong, comparable down-slope Ekman transport is expected on the upper slope. However, an opposing Faroe Shetland Channel jet against the lower slope (Chafik et al. 2020) reverses this expected Ekman transport. There is evidence in literature of meanders and eddies, larger here than west of Scotland and with preferred locations (Sherwin et al. 2006).

Rockall Trough has mesoscale activity (Sherwin et al. 2015; Smilenova et al. 2020), with a majority of cyclonic eddies south of Rockall–Hatton Plateau and anticyclonic eddies along the path of the slope current (possibly from instabilities thereon where and when the slope current is strong enough; Ullgren and White 2012). Such eddies are typically small-scale compared with western boundary current eddies; stratification is weak and Coriolis frequency is high, so the Rossby radius is small relative to sub-tropical values. Nevertheless, on occasion eddies may combine to divert slope current water from the Hebrides slope across Rockall Trough; 5 Sv transport during December 2009 to February 2010 is estimated in Sherwin et al. (2015).

Evidence of cascading has been found at the Celtic Sea and Malin shelf edge (Cooper and Vaux 1949; Hill et al. 1998) but is not considered to contribute significant volume to cross slope exchange on the NW European shelf.

Tidal currents are mainly semi-diurnal (super-inertial) and strong in this region. Barotropic tidal currents O(0.2 m s^{-1}) are typical on the shelf, reach 0.5 m s^{-1} in the southern Celtic Sea but are O(0.1 m s^{-1}) or less over most of Goban Spur. They drive internal tides all along the shelf break, particularly bordering the Celtic Sea and over the Wyville-Thomson Ridge. Solitary wave amplitudes over the Celtic Sea shelf edge have exceeded 100 m (Vlasenko et al. 2014) and internal tides have shown coherence over more than 170 km or about five wavelengths onto the Celtic Sea shelf (Pingree and New, 1995; Inall et al. 2011). Internal tides and waves are susceptible to stratification and hence to mixing. Wind-, tide- and wave-forced currents may be the most consistent agents of cross-slope exchange O(1 m^2 s^{-1}). Topographic effects are important locally (canyons, spurs). For example, Whittard Canyon in the Celtic Sea continental slope was studied in April 2011, 2012 and June 2013 (Wilson et al. 2015) and reviewed in Amaro et al. (2016). By focusing and wave reflections, canyon topography may intensify currents, especially in upper reaches near the bottom (>0.4 m s^{-1} in Whittard Canyon; Amaro et al. 2016).

Oceanic, slope and shelf waters are less distinct at the Celtic Sea shelf edge than at the Malin shelf edge, suggesting more cross-slope exchange at the former (based on temperature, salinity and nutrient concentrations). On the central Malin Shelf (8°W) a water age of 400 days, relative

to ocean water crossing the shelf break, is suggested on the basis of nitrate:phosphate ratios (Hydes et al. 2004); 400 days is probably an upper limit owing to an assumption that nitrate depletion is solely due to denitrification. A six-year transit time for water from the Atlantic Ocean to cross the Celtic Sea to the central Irish Sea (Hydes et al. 2004, on the same basis as for the Malin shelf) reflects slow mean transport and the great breadth of the Celtic Sea rather than the rate of cross-slope exchange. Celtic shelf-edge transports O(1 m^2s^{-1}) were diagnosed by Ruiz-Castillo et al. (2019): off-shelf in winter and onto-shelf in summer (of nitrate-rich bottom water). These values correspond to Celtic Sea volume in O(1 year) but the summer-winter reversal implies much longer transit time. On Porcupine Bank a dense dome of cold, relatively less-saline water forms in winter, with more nutrients than in water at the same depth on either side. In 1995 the dome persisted until at least July and retained relatively high nutrient values, suggesting restricted shelf–ocean exchange here (White et al. 1998).

2.2. FASTNEt observations

In outline, FASTNEt carried out an observational campaign in each of three contrasted shelf/slope sectors (Fig. 1).

- 2012 in the Celtic Sea / Bay of Biscay (very broad shelf, steep slope heavily indented with canyons) focusing on internal tides: their generation, lenses (as previously observed; Hopkins et al. 2012), contributions to transport and mixing; deployments included moorings, drifters, gliders, turbulence profilers and an undulator (Scanfish – this also in 2008; Inall et al. 2011);
- 2013 on the Malin shelf north of Ireland focusing on the density-driven slope current, its meanders (onto the shelf), associated secondary circulation and Ekman Drain, canyon influence and wind forcing; moorings, drifters, gliders and turbulence profilers were deployed along with dye tracing;
- 2014 on the West Shetland slope (Faroe-Shetland Channel) with moorings and drifters.

Remote sensing was also used for surface temperature, thermal fronts and chlorophyll distributions, and long-term altimetry to estimate surface currents. We also draw upon 1-year mooring timeseries collected during the UK Shelf Edge Study (SES) on the Hebrides upper slope and on glider transects collected during the Shelf Sea Biogeochemistry Programme (SSB) in the Celtic Sea. Details are given where pertinent in sections 3 and 4.

2.3. Definitions: Fluxes (net transports), exchanges

At any one location we define *flux F* as the net transport through depth $(-H < z < 0)$ in a layer:

$$flux\ F = \int \overline{\boldsymbol{u}} dz \tag{1}$$

where $\overline{\boldsymbol{u}}$ is the profile of current $\boldsymbol{u}$ averaged over time T. Moreover

$$exchange\ E = 1/2 \int \left|\boldsymbol{u}'\right| dz \tag{2}$$

where $\boldsymbol{u}' = \boldsymbol{u} - \overline{\boldsymbol{u}}$ is the local instantaneous departure from the time-mean flow and $|..|$ denotes *magnitude* (also averaged over time T; magnitude avoids cancellation of flows reversing in time or space that comprise exchange and, being linear unlike standard deviation, avoids giving extra "weight" to large values).

For a layer above or below a moving interface at $z = -h(t)$, flux in the layer is taken as

$$flux\ F = T^{-1} \int_0^T \int \boldsymbol{u}\, dz\, dt \tag{3}$$

where the z-integration is over the ranges $(-h, 0)$ and $(-H, -h)$ respectively for the layers. This is relevant for (e.g.) biogeochemical interests which may want transport estimates in a 2-layer framework, e.g. to account for nutrient imports supporting production along with carbon export in a bottom layer. The sum of upper-layer flux F_U and lower-layer flux F_L should equal the full-depth integral, $F = F_U + F_L$.

2.4. Fine-resolution model

To support FASTNEt, an Atlantic margin model "AMM60" was developed with resolution 1 nautical mile = 1/60° (~1.8 km) and 51 hybrid s-sigma terrain-following layers (Guihou et al. 2018). It is based on version 3.6 of the NEMO ocean model (Madec et al. 2016). AMM60 spans from Spain to Norway, including all this sector of the Atlantic margin and the North Sea (Fig. 1). Lateral viscosity is 50 m^2s^{-1}, lateral diffusion is Smagorinsky (1963) with factor $k_H = 0.7$, vertical mixing is GLS Canuto A (k-ε) formulation with background viscosity 10^{-7} m^2s^{-1}.

Surface forcing is by the ERA-interim atmospheric reanalysis (Dee et al. 2011). Lateral oceanic forcing for AMM60 is from a NEMO-based Northern North Atlantic model "NNA" using the same atmospheric and tidal forcing (Holt et al. 2014). Freshwater input from rivers is also included from a synthesized dataset (see Guihou et al. 2018). Initial conditions (temperature, salinity, sea surface height), derived from 5-day-mean NNA output, are consistent with the oceanic forcing.

AMM60 model validation in respect of tidal elevations and currents, surface temperature and thermocline depth (varying with internal waves) is described in Guihou et al. (2018). The model is able to represent the complexity of Celtic Sea internal tides (wavelength about 30 km corresponding to internal Rossby radius ~ 4 km), fronts and some small-scale processes unresolved by basin-scale and coarser-resolution shelf models. The finer resolution improved on the 7 km resolution (UK) Met Office operational forecast model of that time (O'Dea et al. (2012) and has led to a 1.5 km resolution successor (Graham et al. 2018a; Tonani et al. 2019).

AMM60 was run from 5th January 2010 to December 2013. 5-day-mean 3D fields of temperature, salinity and currents were produced, along with daily surface values and 1D hourly values at Celtic Sea and Malin shelf mooring locations.

3. Estimates of fluxes, exchange and effective diffusivity

In this section each observational method is considered in turn. Precise methodology for the data-type is given, which then allows flux, exchange and effective diffusivity to be evaluated. Directly following each precise methodology, results are presented and discussed without reference to other results. Later, in Section 3.6 and the discussion of Sections 4 and 5, the variously derived estimates of fluxes, exchange and effective diffusivity are synthesised.

3.1. Fluxes and exchange from moorings

Fluxes and exchanges were calculated from moorings deployed in the Celtic Sea, on the Malin and Hebrides shelves and on the West Shetland slope (the eastern side of the Faroe-Shetland Channel) (Fig. 1). Mooring terminology, duration, location, depth range sampled and sampling interval are given in Table S1.

At each location, the across-slope component of flow, u, was defined based on the orientation of the local bathymetric slope and the observed deployment-mean current direction at mid-depths over the slope (presumed best-geostrophically-constrained along the slope; details are provided in the respective sections below, Appendix B and Table S3). The barotropic tidal component (u_{bt}) of each current time series was calculated from a harmonic fit of six tidal constituents (M_2, S_2, N_2, O_1, K_1, M_4) to the depth-mean current (u_{dmc}). A tidal residual (u_{res}) containing the baroclinic tide and the non-tidal components of the flow was

then defined: $u_{res} = u - u_{bt}$. [However, for exchanges E calculated from these components, $E_{res} \neq E - E_{bt}$.] The baroclinic component of flow, $u_{bc} = u - u_{dmc}$, was also calculated. [u_{bc} omits all barotropic flow remaining in u_{res}.] By definition, the full-depth integrals of the baroclinic fluxes are zero; however, fluxes in the surface and bottom layers may indicate the direction of seasonally important transports driven by the baroclinic current field in each layer. Lastly, filtered time series of the across-slope component of flow, u_{filt}, were generated, retaining only frequencies less than 1/48 cycles h^{-1}, thus removing all high frequency and directly tidal oscillations, useful when considering process attribution. Transports computed using the residual currents are typically larger than those computed from the low pass filtered currents; more of the tide and other motion with frequencies greater than 1/48 cycles h^{-1} are removed by the filter. Equivalent notation applies to the along-shelf component v and vector velocity $\boldsymbol{u}$. For the Hebrides and West Shetland data with multiple deployments at (nominally) the same site, the procedures used to determine u_{bt}, u_{res}, u_{bc} and u_{filt} were applied to each deployment's data independently. (Time-mean) flux calculations omitted an integer number of M_2 tidal periods spanning gaps between deployments.

At all moorings, the barotropic tidal and tidal residual exchanges are each less than the exchange by the total current. However, according to whether tidal currents are dominant or not, usually either the tidal or the tidal residual exchange is close to the total; their sum is always greater than the total, i.e. contributions to exchange are not simply additive.

We report standard deviations (±in respective tables) for each of the deployment mean total across-shelf flux and exchange calculations and also 95% confidence intervals (meaning 2½% to 97½%; in parentheses in respective tables) based on Student's t-distribution. The numbers of degrees of freedom (df) were calculated as

$$df = \frac{N\Delta t}{\int |acf|} \tag{4}$$

where acf is the autocorrelation of the depth integrated flux/exchange (x) calculated using u_{res} (tidal signal removed), Δt is the sampling interval and N the total number of data points.

3.1.1. Celtic Sea

Flux and exchange were calculated for five sites (ST1-ST5 within 30 km of the shelf break; Table S1, Fig. 1c) over an 11-day period in June 2012 (21 M_2 tidal periods) when all the moorings were in the water simultaneously. Along- and across-slope direction was determined from the long-term mooring LT1 on the slope (Table S1, Fig. 1c), see Appendix B and Table S3. The definition of surface and bottom layers is detailed in Appendix A and Table S2. [At the short-term moorings modal analysis was used to identify the isotherms most representative of the mode-1 zero crossing point and used to define time-varying surface and bottom layer depths. At ST3, where a temperature chain was not deployed along-side the ADCP and therefore time-varying isotherm depths could not be identified, a fixed depth of 75 m was chosen based on analysis of CTD casts at this site; see Table S1 for full details.] Tables 1, 2 and S4 show across-slope fluxes, cross-slope exchanges and along-slope fluxes respectively for all these moorings, including LT1. On the shelf (ST2-ST5) the baroclinic currents at each site were dominated by a mode-1 semi-diurnal internal tidal wave structure, with opposing surface and bottom layer current directions (Figure S1). Maximum baroclinic current velocities reached 0.2–0.4 m s^{-1}, much exceeding Malin shelf (2013) values of order 0.1 m s^{-1} (section 3.1.2).

On the shelf (ST2-ST5), deployment-mean flux directions (Fig. 1c) and off-shelf components were very varied (Table 1), 1–4 m^2s^{-1} in the space of 30–40 km. Full-depth fluxes calculated from the filtered (u_{filt}) current time-series closely match the total; low-frequency (<1/48 cycles h^{-1}) processes were responsible for most of this transport. ST4 alone had an on-shelf flux, in the bottom layer.

Mooring ST1 on the slope was dominated by a 0.1 m s^{-1} equatorward slope current for an along-slope flux of 57 m^2s^{-1} (Fig. 1c and Table S4). Across-shelf flux (Table 1) was attributable to low-frequency processes, as for the on-shelf sites but much larger.

Across-shelf transports varied substantially within the 11 days common deployment at all sites ST1-ST5 (Figure S1). Bottom-layer transports (shown only for ST5) changed at ST3 and ST5 from on– to off-shelf on day 169, and at ST4 from off- to on-shelf on day 172.

The 297 days at mooring LT1 (Table S1, Fig. 1c) in 1503 m depth show seasonal variability in cross-shelf fluxes. Time-series of flux and exchange averaged over four semi-diurnal periods are shown in Fig. 2; monthly across- and along-slope fluxes are shown in Fig. 3. Monthly across-slope fluxes (Fig. 3a, c) were largest in March and April 2013 and weakest in September to December 2012 but consistently off-shelf in November 2012 to January 2013. On seasonal timescales the fluxes were dominated by low-frequency dynamics. Along-slope transport, poleward

Table 1
Deployment mean and standard deviation (±) of across-shelf fluxes at the Celtic Sea mooring sites.

Mooring	Depth	Fluxes	based on					$\int \lvert acf \rvert$	df
		m^2s^{-1}	$\boldsymbol{u}$	$\boldsymbol{u_{bt}}$	$\boldsymbol{u_{res}}$ ± std (95% CI)	$\boldsymbol{u_{bc}}$	$\boldsymbol{u_{filt}}$	hours	
ST1	688	**Total**	**−13.8**	**0.15**	**−13.9** ± 12.7 (−18, −10)	**0**	**−13.9**	**5.4**	**48**
		surface	1.2	−0.10	1.2 ± 4.1 (−0.6, 3.1)	2.1	1.6	12.6	21
		bottom	−15.0	0.2	−15.2 ± 12.1 (−19, −11)	−2.1	−15.5	7.0	37
ST2	184	**Total**	**−2.7**	**0.01**	**−2.7** ± 4.3 (−4.8, −0.6)	**0.03**	**−2.7**	**14.3**	**18**
		surface	−1.5	0.13	−1.7 ± 4.5 (−5.0, 1.7)	0.15	−1.4	27.9	9
		bottom	−1.1	−0.12	−1.0 ± 2.8 (−3.1, 1.1)	−0.13	−1.3	29.1	9
ST3	144	**Total**	**−4.1**	**−0.02**	**−4.1** ± 4.4 (−6.6, −1.6)	**0**	**−4.1**	**18.4**	**14**
		surface	−3.2	−0.01	−3.2 ± 5.3 (−8.5, 2.1)	−1.1	−3.2	43.2	6
		bottom	−0.92	−0.01	−0.91 ± 4.6 (−4.7, 2.8)	1.1	−0.93	32.1	8
ST4	156	**Total**	**−0.90**	**−0.11**	**−0.79** ± 3.7 (−1.9, 0.3)	**0**	**−0.99**	**5.7**	**46**
		surface	−1.4	−1.5	0.18 ± 2.6 (−1.0, 1.3)	0.40	0.14	12.1	22
		bottom	0.46	1.4	−0.97 ± 4.0 (−2.6, 0.6)	−0.40	−1.1	10.2	26
ST5	169	**Total**	**−3.2**	**−0.14**	**−3.1** ± 3.0 (−4.8, −1.4)	**0**	**−3.1**	**18.4**	**14**
		surface	−1.8	−0.96	−0.88 ± 2.3 (−2.4, 0.6)	0.03	−0.99	22.7	11
		bottom	−1.4	0.82	−2.2 ± 3.9 (−4.8, 0.4)	−0.03	−2.1	24.2	11
LT1[a]	1503	**Total**	**9.9**	**0**	**9.9** ± 38 (−14, 34)	**0**	**9.9**	**587**	**12**
		surface	0.56	0	0.56 ± 22.4 (−15, 16)	−1.9	0.51	717	10
		bottom	9.4	0	9.4 ± 31 (−9, 28)	1.9	9.4	542	13

95% confidence intervals (CI) calculated using $\boldsymbol{u_{res}}$ and Student's t-distribution (see section 3.1). Negative flux is off-shelf. Calculated from $\boldsymbol{u}$: total current; $\boldsymbol{u_{bt}}$: barotropic tidal current; $\boldsymbol{u_{res}}$: tidal residual current; $\boldsymbol{u_{bc}}$: baroclinic current; $\boldsymbol{u_{filt}}$: low-pass filtered current (see section 3.1). [a]At LT1 the base of the surface layer was defined as 500 m, the maximum depth of winter mixing based on analysis of the World Ocean Atlas Climatology.

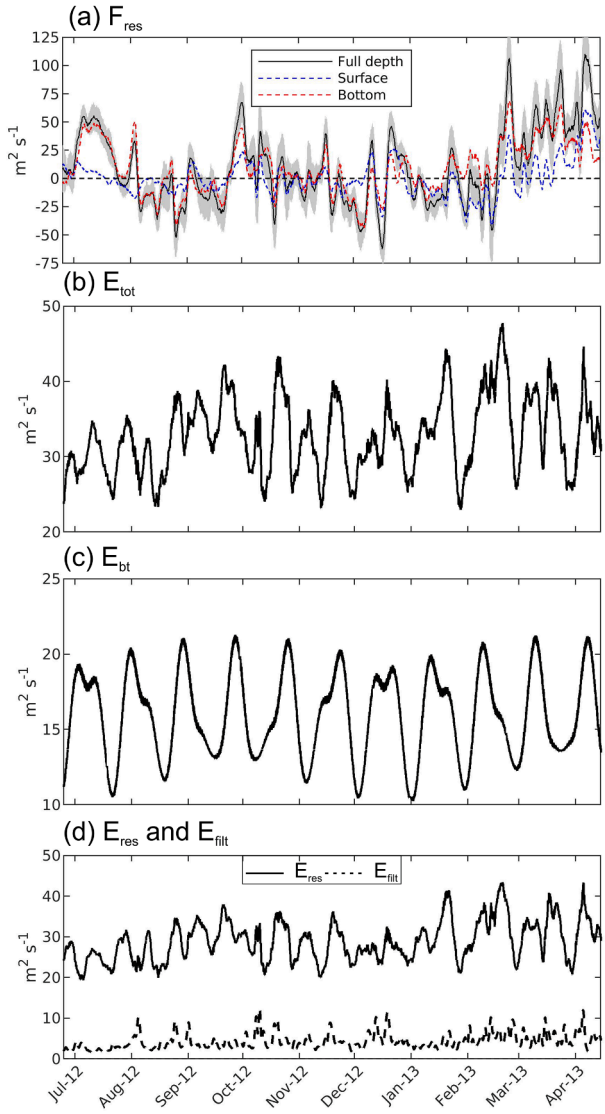

Fig. 2. (a, b) **Across-shelf flux (F) and (c-e) exchange (E) at LT1 in the Celtic Sea.** Calculated within 4 × M_2 period windows. Gray shading in (a) is for the 95% confidence interval around the full depth fluxes. Subscripts tot, bt, res and filt refer to fluxes and exchanges calculated for the total, barotropic, residual and filtered across-shelf currents.

on average, also varied substantially. There was equatorward monthly-averaged transport in June-July 2012 and April 2013 (Fig. 3b) as well as in three shorter intervals during winter 2012–2013 (Porter et al. 2016b). The four-year AMM60 model run suggests that this observed variability in along-slope flux results from changes in slope-current strength (rather than changes in its path causing variability in fixed-point observations).

In many months, the sign of the across-shelf flux was the same in the surface (top 500 m) and bottom layers (Fig. 3c). Exceptions were September 2012, December 2012 and especially February 2013.

Most exchange on the shelf at ST3 to ST5, and at ST1 on the slope, was driven by the barotropic tide (Table 2). Close to the shelf break, at ST2 and ST3, total across-shelf exchange was smaller although exchange associated with residual currents (u_{res}) was comparable with ST4 and ST5. Within the internal tide generation zone (ST1 and ST2) the exchange had a large tidal residual component comprising baroclinic and non-tidal currents (Table 2). ST1 on the slope had a ~ 100 m thick bottom boundary layer where maximum across-shelf exchange took place (Figure S1; discussed in section 5.3). Spring-tide exchanges on the shelf (ST3 to ST5) exceeded those at neaps, but were smaller than at neaps on the upper slope (ST1 and ST2).

Exchange (total and all contributions except barotropic tidal) was much greater at the deepest mooring LT1 than at the others (Table 2). However, that attributed to the tidal residual u_{res} retains a tidal contribution (Fig. 2d).

3.1.2. *Malin and Hebrides shelf*

Flux and exchange were calculated for eight sites (LA, LB, SB-SG on the upper slope and across the Malin shelf to about 40 km from the shelf break; Table S1, Fig. 1d,e) over an 11-day period in July 2013. The separation of surface and bottom layers and definition of along- and across-slope directions are detailed in Appendices A, B and Tables S2, S3. LA and LB were south of SB that was in a canyon at 55½°N; SD was further north with SC to SG aligned across the shelf. Flux and exchange were also calculated for S140 and S400 deployed for longer periods on the Hebrides shelf and slope in the UK Shelf Edge Study, 1995–1996 (Table S1, Fig. 1d). Tables 3, 4 and S5 show across-shelf fluxes, across-slope exchanges and along-slope fluxes respectively.

Poleward along-slope flux was dominant at the slope moorings LA, LB, SB-SD and S400 (Table S5); across-shelf flow was always < 0.05 m s^{-1}. North of the Malin canyon, along-slope flow at SC, SD was almost barotropic and poleward throughout the deployment. In the canyon (SB) there was a 2-day reversal in the top 100–200 m. Further south (LB), the strongest flow was in the bottom 200 m. In deeper water (LA), the along-shelf currents were weaker (<0.1 m s^{-1}) and there were three occasions of reversal (−0.1 m s^{-1}) between 600 and 800 m and the bottom. At the longer-term Hebrides sites S140 and S400, along-slope flow and transport were stronger during autumn–winter (Fig. 4; Souza et al. 2001). S140 displayed sporadic flow reversals lasting a few days. Correlation between S140 and S400 filtered depth-mean velocities was weak; R^2 (variance "explained") was 0.18, mainly attributable to large "events" common to both locations. S140 was more subject to weather over the shallower shelf.

Across-shelf flow at LA and LB had reversals associated with fluctuations in the along-shelf current. Near-bed transports up-slope at LA and down-slope at LB (Figures S2c, S2b respectively) implied convergence. In the canyon (SB) there was persistent downslope flow extending from the bottom up to typically 100 m below the surface (Figure S2b) resulting in a large off-shelf transport (Table 3; downslope "Ekman drainage" is estimated in section 4.3), especially at times of strong along-shelf current. Periods of on-shelf flow were confined to the top 200 m. Thus LB, SB and SD were all in similar water depths but their across-shelf fluxes were quite different (Table 3). On the shelf (SE to SG) across-shelf transport increased with distance from the shelf-edge as the direction of total transport veered (Table 3, Fig. 1e). At all of SB to SG, across-shelf fluxes were almost entirely attributable to low-frequency processes (periods > 48 h).

Down-slope pulses below 250 m at Hebrides site S400 resulted in net off-shelf (depth-integrated) flux (Figure S3), unlike the shelf site S140 having net on-shelf flux. Strongest S400 down-slope flow coincided with the strongest along-slope current as expected for a bottom Ekman layer. Filtered across-shelf flow (u_{filt}) at S140, typically O(±0.05 m s^{-1}), had a baroclinic element, particularly during summer and autumn (Figure S3) and overall on-shelf flow at mid-depth, off-shelf flow above and below. Time-mean across-shelf flux for the whole S140 time-series is similar to that for the 194 days common with S400 (Table 3). Cross-shelf flux estimates by month (Fig. 4) highlight net off-shelf flux at S400 in January 1996, apparently downslope flow associated with a strong slope current, and large bottom-layer contributions at S140 (Fig. 4c). The largest feature (on-shelf flux and exchange) in both mooring time series occurred around 13th February 1996 (Fig. 4), coinciding with southward along-shelf flow. At S400, such a reversal of the slope current appears to be unusual; it was associated with a negative sea-surface height anomaly on the shelf (and unremarkable weather), but cause and effect are not clear.

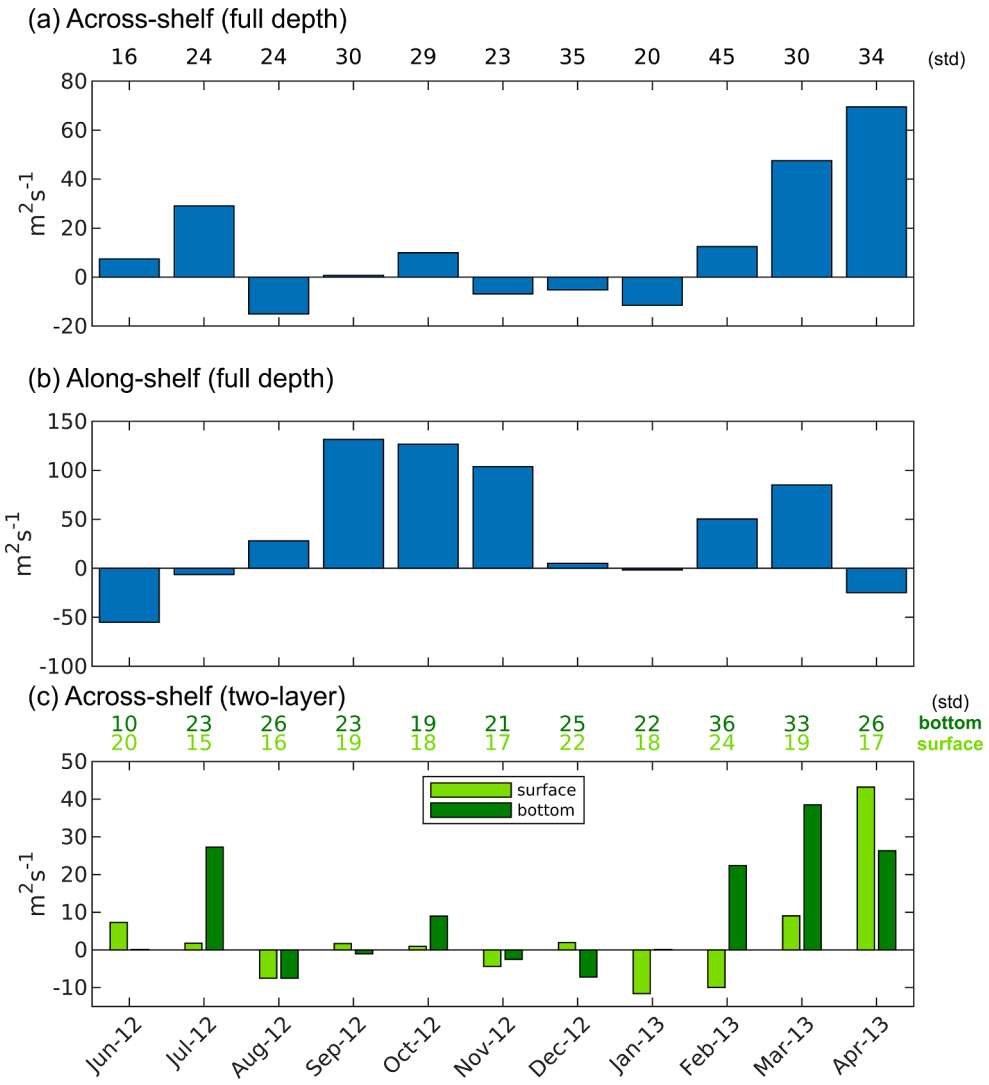

Fig. 3. Average monthly fluxes at mooring LT1 in the Celtic Sea. (a-b) Total across- and along-shelf fluxes. (c) Total across-shelf flux in the surface (500 m; light green) and bottom (dark green) layers. Monthly across-shelf standard deviations are provided along the top of the plots.

Table 2
Deployment mean and standard deviation (±) of **cross-shelf exchanges at Celtic Sea mooring sites**.

Mooring exchanges	Based on						
m^2s^{-1}	$\boldsymbol{u}$ ± std (95% CI)	u_{bt}	u_{res} ± std (95% CI)	u_{bc}	u_{filt}	$\int\|acf\|$**hours**	***df***
ST1	22.8 ± 6.7 (18.6, 27.1)	16.3	16.0 ± 6.0 (12.2, 19.7)	15.3	2.8	22.5	12
ST2	4.6 ± 2.1 (3.4, 5.8)	1.2	4.6 ± 2.1 (3.3, 5.8)	4.2	1.3	20.2	13
ST3	9.4 ± 3.7 (7.2, 11.5)	8.1	5.3 ± 2.0 (4.2, 6.4)	5.0	1.2	18.2	14
ST4	16.6 ± 7.9 (14.4, 18.8)	16.4	4.3 ± 1.3 (3.9, 4.6)	4.0	0.65	5.1	52
ST5	15.8 ± 7.5 (12.6, 19.0)	15.6	3.4 ± 1.5 (2.7, 4.0)	3.0	0.85	10.8	24
LT1	37.7 ± 12.5 (32.0, 43.3)	16.0	34.4 ± 11.6 (29.1, 39.6)	31.0	19.3	335	21

95% confidence intervals (CI) calculated using $\mathbf{u}_{res}$ and Student's t-distribution (see section 3.1). Calculated from $\mathbf{u}$: total current; $\mathbf{u}_{bt}$: barotropic tidal current; $\mathbf{u}_{res}$: tidal residual current; $\mathbf{u}_{bc}$: baroclinic current; $\mathbf{u}_{filt}$: low-pass filtered current (see section 3.1)

Most exchange on the Malin and Hebrides shelves at SE to SG, S140, and at SB in the canyon, was driven by the barotropic tide (Table 4) as was a majority at S400 (Fig. 5c, d). The long series show a tidal spring-neap cycle (~29½ days for two unequal cycles). At the other slope locations, the largest contributions were from tidal residual or baroclinic currents (u_{res}, u_{bc}; these have much in common, section 3.1). In contrast

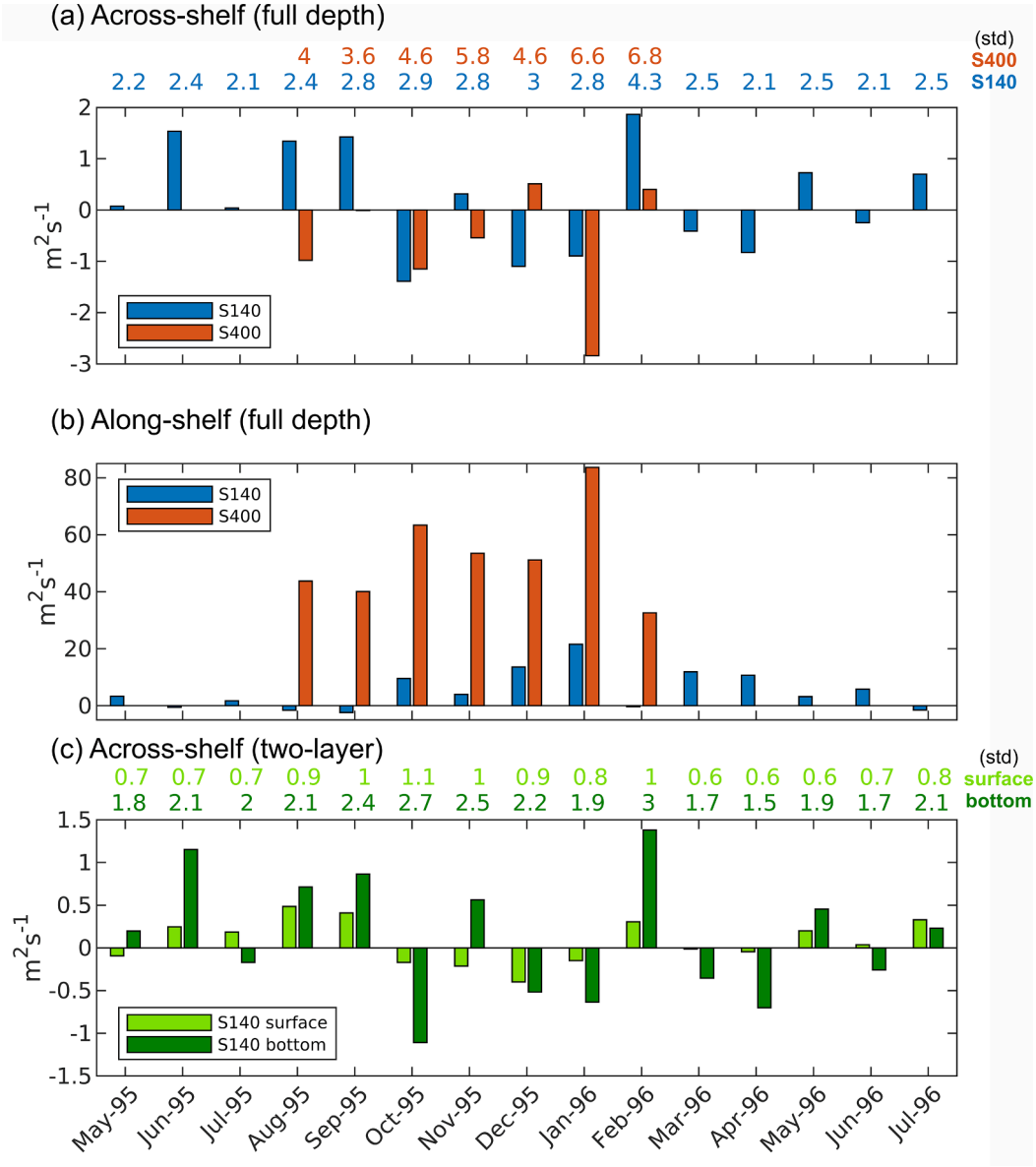

Fig. 4. Monthly average fluxes at S140 and S400. (a-b) Total across- and along-shelf fluxes at S140 (blue) and S400 (red), Hebrides shelf and slope. (c) Total across-shelf flux in the surface (light green) and bottom (dark green) layers at S140. Monthly standard deviations (std) are provided along the top of the plots.

with the Celtic Sea, total exchange decreased from the slope across the shelf (SD to SG; Table 4). The long-term moorings show no clear seasonal cycle (Fig. 5c-e), although the largest values based on filtered currents occurred during the autumn and winter.

3.1.3. *West Shetland slope*

Flux and exchange were calculated for six long-term Marine Scotland Science mooring locations across the Faroe-Shetland Channel (Table S1, Fig. 1f). Values in Tables 5 and 7 are for the FASTNEt period with all six moorings, April-September 2014 and October 2014-April 2015.

At all mooring locations except NWS-C, long-term mean fluxes were primarily along the channel to the north-east (Fig. 1f). At NWS-C near the north-western side of the Channel, long-term mean flux was southward. Thus cross-shelf mean fluxes (Table 5) were much smaller than respective mean along-slope fluxes $\geq$ 4.6 (NWS-F), 24.8 (NWS-E,H), 43.2 m^2s^{-1} (NWS-D,G; Table S7). Differences between mean fluxes based on total and filtered currents are insignificant (Table 5 shows only the former). Fluxes were strongest on mid-slope, decreasing to the shelf edge (Fig. 1f). Cross-shelf flux was generally onto the shelf, although some sustained off-shelf fluxes occurred in winter 2014/15 (Fig. 6a, c).

Much variability on time-scales of two days or more is indicated by the standard deviations in Table 5. [The confidence intervals are narrowed by the many degrees of freedom in 6–12 month records]. Monthly-mean fluxes retain a substantial fraction of this variability (e.g. at NWS-E; Fig. 6a, c). Multi-year deployments showed larger mean fluxes along the slope in winter than in summer (Table 6), in accord with the seasonal cycle of slope current transport in the Faroe-Shetland Channel in Berx et al. (2013). The mainly-winter deployments suggested (with exceptions) less across-slope flux and more cross-slope exchange than mainly-summer deployments (Table 6).

Total cross-slope exchange (u; Table 7) decreased from deepest Channel up the slope to NWS-F. The barotropic tidal contribution u_{bt} was similar at all moorings, whereas the contributions calculated from u_{res}, u_{bc} and especially lower frequencies (u_{filt}) decreased markedly over the upper slope.

Table 3
Deployment mean and standard deviation (±) of **across-shelf fluxes at Malin and Hebrides shelf mooring sites**.

Mooring	Depth	Flux	based on					$\int \lvert acf \rvert$	*df*
		m^2s^{-1}	u	u_{bt}	u_{res} ± std (95% CI)	u_{bc}	u_{filt}	hours	
Malin									
LA	964	**Total**	**0.88**	**−0.05**	**0.93 ± 16 (−10, 12)**	**0**	**0.97**	**28.1**	**10**
		surface	−0.17	0.00	−0.17 ± 2.0 (−2.0, 1.7)	−0.21	−0.15	38.2	7
		bottom	1.1	−0.05	1.1 ± 15 (−9.8, 12)	0.21	1.1	27.6	10
LB	499	**Total**	**−0.33**	**−0.14**	**−0.20 ± 8.1 (−4.2, 3.8)**	**0**	**−0.10**	**15.1**	**18**
		surface	−0.12	−0.01	−0.11 ± 2.4 (−1.9, 1.7)	−0.10	−0.09	31.4	9
		bottom	−0.21	−0.13	−0.08 ± 7.9 (−3.9, 3.7)	0.10	−0.01	14.3	19
SB	504	**Total**	**−5.5**	**0.11**	**−5.6 ± 9.0 (−10.6, −0.6)**	**0**	**−5.7**	**18.2**	**15**
		surface	0.18	0.01	0.18 ± 1.3 (−0.4, 0.7)	0.43	0.17	11.3	24
		bottom	−5.7	0.11	−5.8 ± 8.8 (−10.6, −1.0)	−0.43	−5.9	17.8	15
SD	544	**Total**	**1.4**	**−0.30**	**1.7 ± 8.8 (−1.8, 5.2)**	**0**	**1.5**	**10.5**	**26**
		surface	0.04	−0.01	0.05 ± 0.73 (−0.6, 0.6)	0.02	0.05	32.6	8
		bottom	1.4	−0.29	1.6 ± 8.7 (−1.8, 5.2)	−0.02	1.5	10.3	27
SC	400	**Total**	**−1.7**	**−0.27**	**−1.4 ± 6.8 (−5.2, 2.4)**	**0**	**−1.6**	**17.9**	**15**
		surface	0.01	−0.03	0.04 ± 3.5 (−3.4, 3.5)	0.21	0.07	46.2	6
		bottom	−1.7	−0.24	−1.4 ± 7.5 (−5.6, 2.7)	−0.21	−1.6	18.0	15
SE	149	**Total**	**0.32**	**−0.08**	**0.40 ± 3.0 (−1.4, 2.3)**	**0**	**0.38**	**23.1**	**12**
		surface	0.31	0.00	0.30 ± 3.0 (−1.5, 2.1)	0.18	0.26	21.8	13
		bottom	0.02	−0.08	0.10 ± 3.3 (−2.1, 2.3)	−0.18	0.13	24.6	11
SF	129	**Total**	**1.3**	**0.03**	**1.3 ± 3.3 (−0.3, 2.8)**	**0**	**1.3**	**13.8**	**20**
		surface	0.77	0.01	0.76 ± 2.6 (−0.6, 2.2)	0.33	0.79	17.4	16
		bottom	0.52	0.02	0.51 ± 3.2 (−1.2, 2.2)	−0.33	0.48	16.1	17
SG	117	**Total**	**4.2**	**0.04**	**4.2 ± 3.5 (1.4, 7.0)**	**0**	**4.2**	**33.2**	**8**
		surface	1.2	−0.10	1.3 ± 2.2 (0.1, 2.5)	−0.06	1.3	17.1	16
		bottom	3.1	0.14	2.9 ± 3.1 (1.2, 4.7)	0.06	2.9	19.6	14
Hebrides									
S140 (194 d)	148	Total	0.24	−0.01	0.25 ± 3.6 (−8.7, 9.2)		0.27	344	12
S140 (447 d)	148	Total	0.22	0.01	0.23 ± 4.0 (−5.3, 5.7)		0.22	346	30
S400 (194 d)	396	Total	−0.76	−0.02	−0.74 ± 6.2 (−11.2, 9.7)		−0.78	304	14

95% confidence intervals (CI) calculated using u_{res} and Student's t-distribution (see section 3.1). Negative flux is off-shelf. Surface fluxes at LA and SD should be treated with extra caution since only 2 m of this layer were sampled. Calculated from u: total current; u_{bt}: barotropic tidal current; u_{res}: tidal residual current; u_{bc}: baroclinic current; u_{filt}: low-pass filtered current (see section 3.1).

3.2. Fluxes and exchanges from drifters crossing depth contours

In areas of complex topography, it can be difficult to define "along-slope" or "cross-slope" direction, yet transport estimates from mooring data are sensitive to these definitions, especially for the Malin shelf. With our interest in cross-slope flow, we wish to avoid identifying "along-slope" with current direction. Even with defined directions at a mooring, flow may not maintain the same angle relative to depth contours downstream. Tracked drifters may avoid these difficulties. Clusters of drifters were deployed in 2012 at the Celtic Sea shelf edge (Porter et al. 2016a), in 2013 at the Malin shelf edge (Porter et al. 2018; Jones et al. 2020) and in 2014 in the Faroe-Shetland Channel (Fig. 7a; deployment locations, numbers and drogue depths are given in Table S8). Subsequent drifter positions and hence corresponding water depths were recorded every three hours. Thus we know which depth contours were crossed by the drifters and hence by the water, assuming that the drifters followed the water. [While the drifters remained drogued, their tracks were taken as largely representative of upper water column movements (Porter et al. 2016a)].

For each of the 500 m, 200 m and 150 m depth contours, all drifter crossings (to shallower or deeper water, and regarded as independent) in time intervals $\Delta T = 3$ or 24 h were identified in approximate months. For each contour and "month", the water-depth changes Δh in time ΔT pertaining to the crossings were analysed for a mean $\overline{\Delta h}$ and a mean absolute deviation $\overline{|\Delta h - \overline{\Delta h}|}$. Dividing by ("slope" × ΔT) gave estimates of cross-slope flux $\overline{u}$ and exchange $|u^{'}|$ (velocities; Tables S9-S11).

An obvious estimate of "slope" would be via direct multiple regression of Δh on Δx and Δy (east and north displacements respectively). However, for complex topography (notably the Biscay slope) this averages out irregular steep slopes to a much smaller mean. A somewhat modified multiple regression was therefore used based on a model

$$|slope\ \ along\ \ direction\ \ \Theta| = |s\ \cos(\Theta - \Theta_0)\,| \quad \text{or} \quad |\Delta h|/l = s|\Delta x\ \ cos\Theta_0 + \Delta y\ \ sin\Theta_0|/l \tag{5}$$

where $|..|$ denotes absolute value, s is the maximal slope (along $\Theta = \Theta_0$), $l^2 = (\Delta x)^2 + (\Delta y)^2$. By squaring both sides

$$|\Delta h/l|^2 = a + b\left[(\Delta x)^2 - (\Delta y)^2\right]\Big/l^2 + c\Delta x\Delta y\Big/l^2$$

$$\text{or}\ \ |\Delta h/l| = \left\{a + b\left[(\Delta x)^2 - (\Delta y)^2\right]/l^2 + c\Delta x\Delta y/l^2\right\}/|\Delta h/l| \tag{6}$$

to avoid over-weighting crossings with steep slopes. In either case $|\Delta h/l|$ and the displacements on the right-hand side are known; multiple regression determines a, b, c and hence s. In this formulation, topographic complexity weakens the dependence on direction Θ but the typical slope steepness is retained through the constant term a.

Flux and exchange estimates, from drifter crossings of depth contours, are shown in Table 8 for the Celtic, Malin and West-Shetland deployments. The estimates are based on daily 24-hour-average positions (derived from 3-hourly recorded positions) so as to remove most of the tidal displacements. We do not expect bias from the choice of depth contours; some depth contour is crossed in any interval ΔT; the chosen contours are of interest (as "conventional" depth choices) but should be representative. However, the fact of analysing only occasions of contour crossing may introduce bias (contours are probably more likely to be crossed when flow is faster). Such bias can be estimated by comparing mean distance travelled on contour-crossing occasions with the overall mean distance travelled in (three or) 24 h. This was carried out for the daily positions and the "bias" (factor) for the contour-crossing occasions is shown at the foot of the respective tables. The bias factor is between 0.96 and 1.46 in all cases (i.e. not large; a value 1 means no bias) and typically less at 500 m than at 200 m or 150 m.

Table 4
Deployment mean and standard deviation (±) of **cross-shelf exchanges at Malin and Hebrides shelf mooring sites.**

Mooring exchanges m^2s^{-1}	based on					$\int \|acf\|$	*df*
	u ± std (95% CI)	u_{bt}	u_{res} ± std (95% CI)	u_{bc}	u_{filt}	hours	
Malin							
LA	15.5 ± 4.3 (12.7, 18.4)	2.2	15.4 ± 4.3 (12.6, 18.3)	13.9	5.8	24.5	11
LB	8.1 ± 2.5 (6.8, 9.3)	2.6	7.7 ± 2.4 (6.5, 8.9)	7.0	1.7	15.8	17
SB	15.2 ± 7.4 (12.2, 18.3)	13.1	7.6 ± 2.1 (6.8, 8.5)	6.8	2.3	10.9	25
SD	15.6 ± 3.5 13.7, 17.4)	8.0	13.5 ± 2.2 (12.3, 14.7)	13.0	1.7	17.0	16
SC	12.1 ± 4.5 (10.1, 14.0)	8.8	8.2 ± 2.5 (7.1, 9.2)	7.6	2.6	12.1	23
SE	8.1 ± 4.2 (6.4, 9.8)	7.6	3.1 ± 1.4 (2.6, 3.7)	2.9	0.89	10.8	25
SF	7.0 ± 3.0 (6.3, 7.6)	6.0	3.6 ± 1.0 (3.4, 3.9)	3.4	0.84	3.7	73
SG	5.4 ± 2.3 (4.8, 6.0)	4.6	3.1 ± 0.9 (2.9, 3.4)	2.8	1.1	4.4	63
Hebrides							
S140	7.2 ± 4.5 (3.8, 10.6)	6.0	3.5 ± 1.2 (2.7, 4.4)	2.6	1.5	524	8
S400	9.8 ± 5.2 (6.4, 13.1)	7.2	6.8 ± 1.9 (5.7, 7.8)	7.4	1.7	351	12

95% confidence intervals (CI) calculated using u_{res} and Student's t-distribution (as section 3.1). Calculated from u: total current; u_{bt}: barotropic tidal current; u_{res}: tidal residual current; u_{bc}: baroclinic current; u_{filt}: low-pass filtered current (see section 3.1)

In most cases here, exchange velocities $|u'|$ exceeded the magnitude of the mean $\overline{u}$ but (inherent in their calculation) are less variable within months; errors in exchange estimates are proportionately less. Transport estimates $\overline{hu}$ and $\frac{1}{2}h|u'|$ are comparable in more cases. [The values of $\frac{1}{2}h|u'|$ are increased by tidal excursions if 3-hourly positions are used.] N.B. u, $|u'|$ derive from the drifters drogued at depths 15 to 70 m and may represent the upper water column rather than the whole.

The bias of 500 m crossings to shallower water (positive $\overline{u}$) is influenced by drifters' initial deployment locations and trajectories. In stark contrast is the consistent crossing to depth > 500 m soon after the June 2012 Celtic Sea deployments, showing the effect of a storm at the time. This indicates strong dependence of the upper 50 m flow on the particular wind forcing. Subsequently most drifters moved south-eastwards. Their displacement to deep Biscay waters led to encounters with open-ocean eddies; some drifters over the slope were apparently caught in short-lived eddies that often exist over the Biscay slope (in association with the irregular topography) and appear to favour ocean-shelf exchange there (Porter et al. 2016a). The strongest drifter-derived cross-contour currents ($\overline{u}$ and $|u'|$) from the three FASTNEt areas (Tables S9-11) were from the Celtic Sea deployment, supporting the suggestion that the irregular Biscay topography favours ocean-shelf exchange.

For the *Malin* deployment, an integrated on-shelf transport of 0.2 Sv was estimated from near-eastward drifter velocities multiplied by a corresponding area of high salinities in a near-meridional glider transect on the shelf (Porter et al. 2018; Jones et al. 2020). This estimate is a small fraction O(10%) of the typical along-slope transport O(2 Sv) in the poleward slope current (Souza et al. 2001). However, it represents a substantial diversion onto the shelf in a sector of only O(80–100 km) along the slope, especially for waters above ~150 m depth. Two of the drifters crossing onto the shelf in December 2013 reached speeds up to

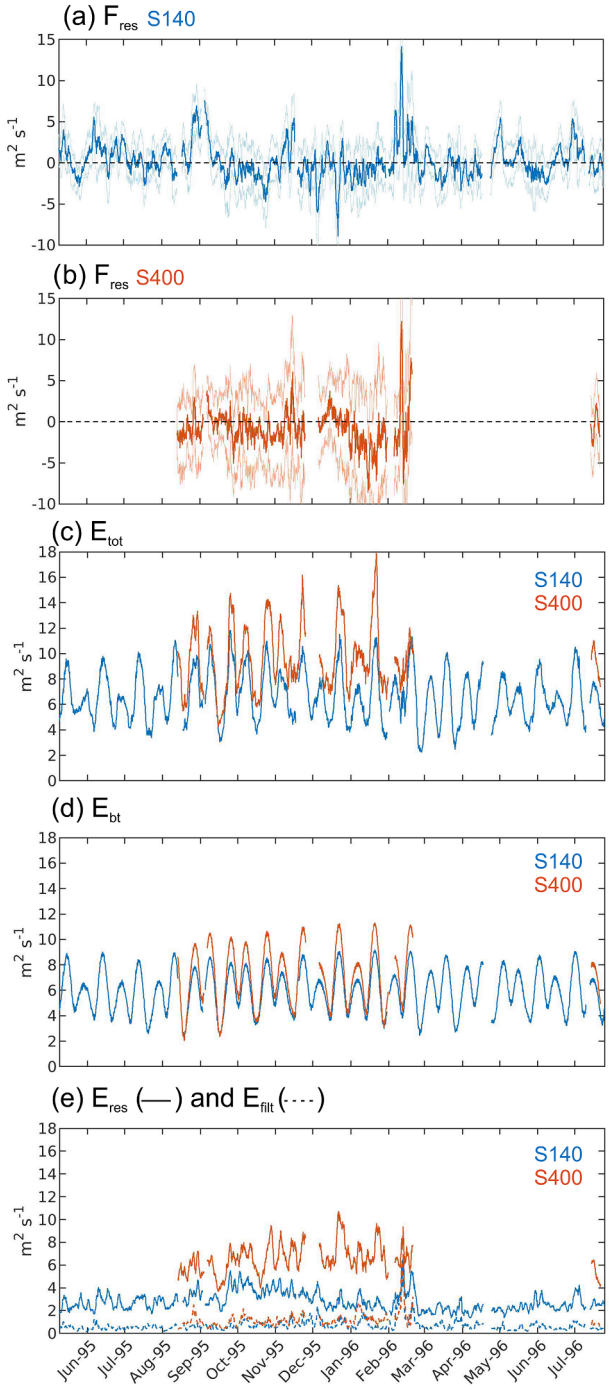

Fig. 5. (a-b) **Across-shelf flux** (F) **and** (c-e) **exchange** (E) at moorings S140 (blue) and S400 (red), Hebrides shelf and slope. Calculated within 4 × M_2 period windows. Light blue and red lines in (a, b) show the standard deviation of the contributing full depth flux values within the windows. Subscripts tot, bt, res and filt refer to fluxes and exchanges calculated for total, barotropic, residual and filtered across-shelf currents (see section 3.1).

0.6 m s^{-1} in a storm, suggesting an onto-shelf transport up to 0.48 Sv if the flow's cross section was as in the previous summer (Jones et al. 2020).

Typically, Celtic Sea exchange flows $|u'|$ > Malin flows > Faroe-Shetland Channel flows (Tables S9-S11). Exceptions were large Faroe-Shetland exchange flows across the 200 m and especially 500 m contours. Exchange flows $|u'|$ across the 500 m and 200 m contours were typically comparable and less than $|u'|$ across the 150 m contour. Large

Table 5
Deployment mean and standard deviation (±) of total across-shelf fluxes at Faroe-Shetland Channel mooring sites, for deployments during 2014–2015.

Mooring	Deployment	Depth	Flux u_{res} ± std (95% CI), m^2s^{-1}	$\int \lvert acf \rvert$, hours	*df*
NWS-C	June 2014-May 2015	1070	17.5 ± 61 (-15, 50)	525	16
NWS-G	April 2014-April 2015	1090	11.2 ± 62 (-18, 40)	426	20
NWS-D	April 2014 -September 2014	690	14.4 ± 67 (-17, 46)	181	20
	October 2014-April 2015		1.9 ± 60 (-16, 20)	104	47
NWS-E	April 2014 -September 2014	490	−4.0 ± 22 (-18, 10)	295	12
	October 2014-April 2015		6.5 ± 28 (-1.9, 15)	109	45
NWS-H	June 2014-May 2015	200	3.2 ± 10 (1.1, 5.4)	101	82
NWS-F	April 2014 -September 2014	165	0.28 ± 4.7 (-1.2, 1.8)	92	39
	October 2014-April 2015		−0.67 ± 8.5 (-2.8, 1.5)	80	61

Negative flux is off-shelf. Values shown here are within 4% of values using u_{filt}. The barotropic tide contribution is O(0.01 m^2s^{-1}) or less. 95% confidence intervals (CI) calculated using u_{res} and Students t-distribution (see section 3.1).

Faroe-Shetland Channel exchange flows across the 500 m contour were again an exception. These comparisons seem to reflect slope steepness (less at 150 m depth allowing freer cross-contour flow), strong Celtic Sea tides over complex topography and meanders of the strong slope current in the Faroe-Shetland Channel (and beyond as drifters went further north and east).

The estimates are large. [3-hourly positions crossing 150 m depth give typically 0.5–7 m^2s^{-1} transport and 10 m^2s^{-1} exchange.] Estimates from daily positions (omitting most of the tidal contribution) and allowing for the "bias" are typically 2–4 m^2s^{-1} transport and 2–7 m^2s^{-1} exchange, significantly less but still large compared with exchange estimates from FASTNEt moorings' u_{filt} (sections 3.1, 3.6) and compared with exchange estimates elsewhere (sections 1.3, 5.6). These large estimates may be biased by drifter drogues at depths 15–70 m in the upper, typically faster-moving, part of the water column.

3.3. Exchanges from altimetry

Surface currents (for fluxes and variance in the FASTNEt region) have been estimated from altimetry for October 1992 – December 2012 (Xu et al. 2015). The variance suggests typical weekly velocity fluctuations O(1 mm s^{-1}) at 200 m for the Celtic Sea shelf edge and the Malin-Hebrides shelf edge in winter. There is more variance in summer off NW Ireland; Malin-Hebrides along-shelf variability is larger. Then exchange $\frac{1}{2}h|u'|$ (section 2.3) is estimated from these values as ~ 0.5 to 1 m^2s^{-1} (range given by standard error) or more in summer off NW Ireland. As the estimates are based on weekly maps of altimetry interpolated to a regular grid, they can fully represent only low-frequency, large-scale motion and are probably under-estimates (albeit aliasing may add a contribution from higher-frequency motion). Moreover, the ageostrophic component of variability is not considered, reinforcing the view that the altimetry variance represents a lower bound for the velocity variance.

3.4. Effective diffusivity from drifters

Relative dispersion of deployed drifter clusters (Table S8) enables calculations of effective diffusivity. Dispersion along co-ordinate x is defined as $D_x^2 = < (s_i - s_{i0})^2 >$ where $< .. >$ denotes an average over all drifter pairs (labelled i); s_i is the x-separation between two drifters with initial x-separation s_{i0}. Dispersion along co-ordinate y is defined similarly. The x-diffusivity K_x is estimated after Batchelor (1952) as $K_x = \frac{1}{2}\, d(D_x^2)/dt$ and y-diffusivity K_y similarly. 90% confidence intervals (5th and 95th percentiles) were defined as $K(1 \pm 1.65\,(2/N)^{1/2})$, where K is the (x- or y-) diffusivity and N is the number of drifters, as in e.g. LaCasce and Bower (2000). A synthesis of the results from the three FASTNEt

Table 6
Mean along-slope fluxes, across-slope fluxes and across-slope exchanges ± standard errors based on u_{filt} over all mooring deployments separated into those mainly in winter (November-March) and those mainly in summer, Faroe-Shetland Channel. Numbers of seasons in parentheses.

m^2s^{-1}	Along-slope flux		Across-slope flux		Across-slope exchange	
Site	winter	summer	winter	summer	winter	summer
D	56.4 ± 10.8 (15)	35.0 ± 12.3 (17)	12.1 ± 3.5 (15)	26.1 ± 6.0 (17)	20.5 ± 1.1 (15)	21.0 ± 1.3 (17)
E	74.7 ± 6.9 (16)	65.6 ± 9.5 (13)	4.7 ± 1.1 (16)	3.9 ± 1.9 (13)	5.7 ± 0.4 (16)	3.2 ± 0.6 (13)
F	12.1 ± 0.3 (4)	7.0 ± 0.8 (2)	0.06 ± 0.6 (4)	0.9 ± 0.2 (2)	1.1 ± 0.1 (4)	0.8 ± 0.1 (2)

Table 7
Deployment mean and standard deviation (±) of cross-shelf exchanges at Faroe-Shetland Channel mooring sites.

Mooring exchanges m^2s^{-1}	based on u ± std (95% CI)	u_{bt}	u_{res} ± std (95% CI)	u_{bc}	u_{filt}	$\int \lvert acf \rvert$ hours	*df*
NWS-C	30.1 ± 16.8 (22.7, 37.5)	4.5	30.1 ± 16.4 (22.8, 37.4)	19.2	23.7	377	22
NWS-G	28.2 ± 18.4 (19.8, 36.5)	5.3	27.7 ± 18.0 (19.5, 35.8)	14.9	20.5	410	21
NWS-D	33.6 ± 19.7 (26.6, 40.6)	6.8	31.9 ± 17.9 (25.6, 38.3)	18.5	17.3	113	33
	28.4 ± 16.7 (23.4, 33.4)	4.3	28.1 ± 16.5 (23.2, 33.0)	15.3	14.1	105	46
NWS-E	12.9 ± 6.7 (10.8, 15.0)	5.7	11.7 ± 5.7 (9.9, 13.5)	8.0	6.6	83	43
	15.8 ± 9.0 (13.0, 18.5)	7.7	13.8 ± 7.8 (11.4, 16.2)	8.0	6.4	114	43
NWS-H	8.4 ± 4.5 (6.7, 10.1)	6.5	5.4 ± 2.8 (4.4, 6.4)	4.0	1.5	276	30
NWS-F	6.7 ± 3.4 (5.4, 8.0)	5.8	3.5 ± 1.5 (2.9, 4.0)	2.9	0.82	128	28
	6.5 ± 3.9 (5.7, 7.3)	5.2	4.1 ± 2.4 (3.6, 4.6)	2.4	1.2	55	89

NWS-H and NWS-C are mean exchanges between June 2014 and May 2015. NWS-G is the deployment mean between April 2014 and April 2015. Deployment mean exchanges for NWS-F, NWS-E and NWS-D are for April-September 2014 (upper row) and October 2014 – April 2015 (lower row). Calculated from u: total current; u_{bt}: barotropic tidal current; u_{res}: tidal residual current; u_{bc}: baroclinic current; u_{filt}: low-pass filtered current (see section 3.1). 95% confidence intervals (CI) calculated using u_{res} and Students t-distribution (see section 3.1).

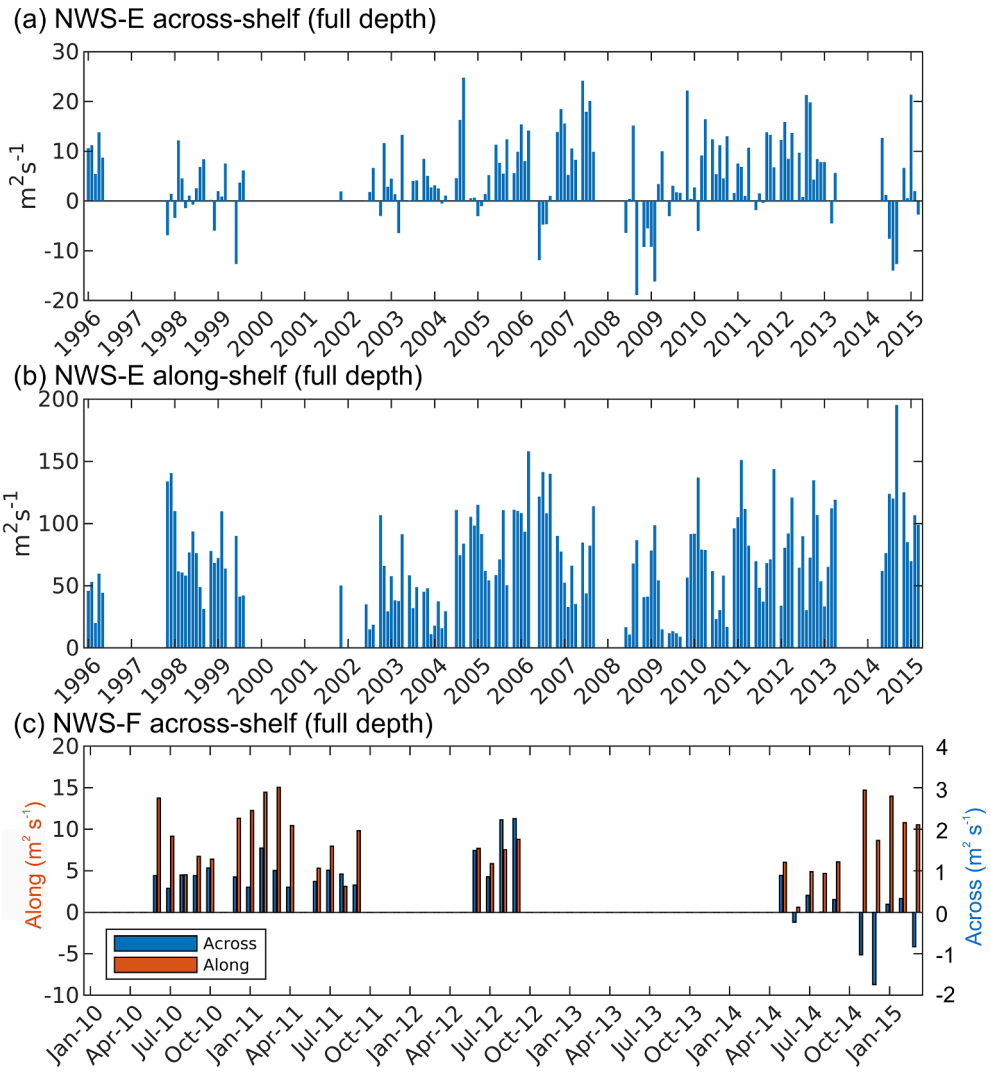

Fig. 6. Average monthly fluxes at NWS-E and NWS-F, Faroe-Shetland Channel. (a-b) Respective across- and along shelf fluxes at NWS-E. (c) Across- (blue) and along-shelf (red) fluxes at NWS-F. Note the different scales on the left (along) and right (across) y-axes.

drifter releases is shown in Fig. 7.

The 2012 *Celtic Sea* drifters (Fig. 7a) moved south-south-west to deeper water for about a week, then equatorwards in the along-slope direction influenced by an absolute dynamic topography "high" (Porter et al. 2016a). Six drifters returned to the slope and subsequently moved onto the shelf; too few for diffusivity estimates there. The remainder continued to the south-east. Their relative dispersion in along- and cross-slope directions is shown in Fig. 5 of Porter et al. (2016a) and corresponding diffusivities in Fig. 7b here. During days ~ 30–50, along-slope dispersion was close to t^3 suggesting fully turbulent flow dominated by shear and turbulent eddies (Porter et al. 2016a). Across-slope dispersion roughly followed a t^2 curve for the first 10 days. Once away from the slope, the across-slope dispersion was roughly linear in t (as Fickian diffusion). For the first 60 days overall (13 drifters, mostly over the abyssal plain), drifters' relative dispersion indicated effective diffusivity of about 700 m^2s^{-1} along and across the slope. Nevertheless, the dispersion character was anisotropic: along-slope dispersion was dominated by turbulence and shear; across-slope separation was driven mostly by diffusive-like processes (Porter et al. 2016a).

For the *Malin Shelf*, drifters in 2013 mostly moved northwards and then typically east-north-eastwards onto the shelf near 55.5°N (Fig. 7a), although some moved with a westward component over Rockall Trough. Movement on the shelf subsequently turned northwards again. Components were calculated along and across the general flow (as defined by the centre of "mass" of the drifters) onto and over the shelf (clockwise around Scotland; Porter et al. 2018). Effective along-flow diffusivity for the drifters drogued at 15 m was estimated as a few 100 m^2s^{-1} or less up to day 14, then rapidly rising to a maximum exceeding 6000 m^2s^{-1} around day 35 (Fig. 7c). Transverse diffusivity was much less, estimated on average as less than 100 m^2s^{-1} up to day 30 and peaking at 300–350 m^2s^{-1} around day 42 (Fig. 7c and Porter et al. 2018). Thus effective diffusivity was strongly anisotropic, far greater in the overall direction of movement, unlike the Celtic Sea.

The 2014 *Faroe-Shetland Channel* drifters initially moved north-eastwards (Fig. 7a). Two entered the North Sea between Orkney and Shetland, two moved to deeper water in the Faroe-Shetland Channel and the others dispersed across the slope in 0°-1°W. Meridional and zonal relative dispersion (squared separations) appear to evolve similarly but there is a clear magnitude difference between along- and across-slope components (Fig. 7d). Both show a near-exponential increase (e-folding time ~ 10 h) for the first three days, after which the relative growth rate slows (e-folding time increases). During days 8 to 30, both relative dispersion components increase approximately as t^2 (across-slope relative dispersion with more fractional fluctuation). Then along-slope effective diffusivity increases ~ linearly to O(3700 m^2s^{-1}); across-slope diffusivity fluctuates with a mean value ~ 140 m^2s^{-1} over days 8 to 30 but arguably a linear increase to O(280 m^2s^{-1}). This exponential

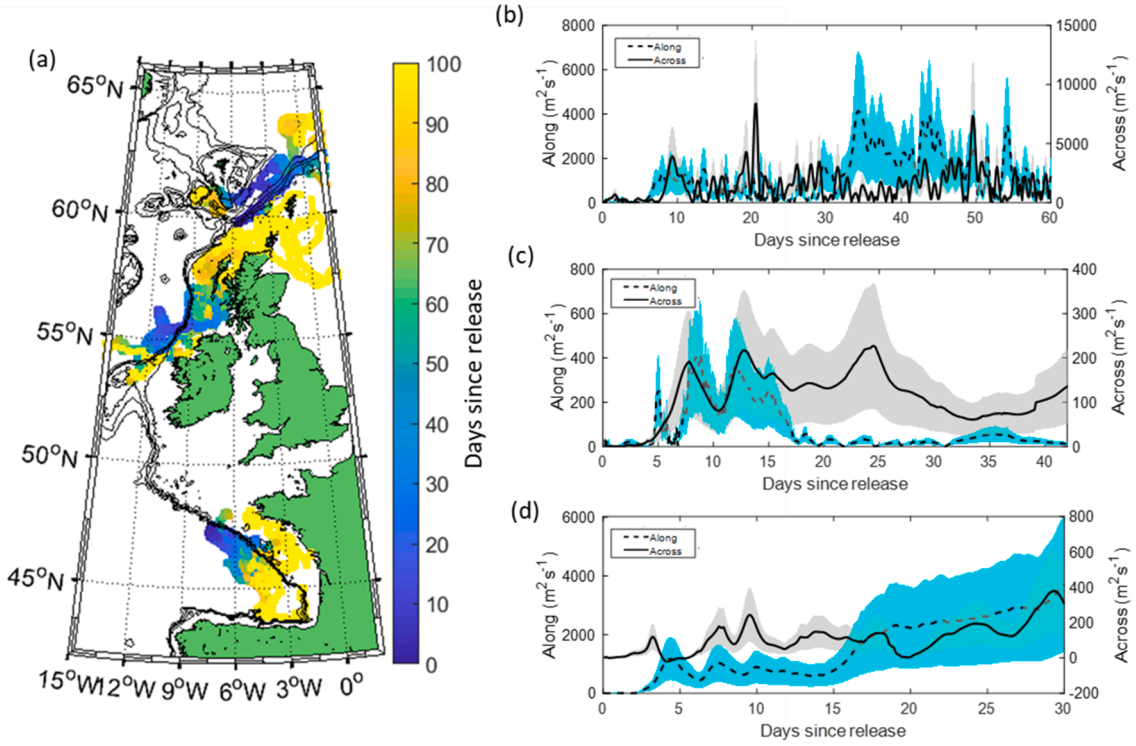

Fig. 7. Drifter trajectories and derived effective diffusivities. (a) Trajectories for the 2012, 2013 and 2014 FASTNEt releases shaded according to the number of days since release. (b) Along- and across slope diffusivity from the Celtic Sea (2012), as published in Porter et al. (2016), calculated as in section 3.4 from all (91) drifter pairs with initial separation distances ≤ 5 km. (c) Across- and along-flow diffusivity from the Malin Shelf (2013), as published in Porter et al. (2018) and calculated relative to the centre of mass of the drifters. (d) Across- and along-slope diffusivity from the Shetland-Channel (2014). (Statistics were calculated between drifter pairs. Shading indicates 90% confidence intervals as in section 3.4. Note the different scales for "Along" and "Across".)

Table 8
Contour-crossing components of flux and exchange from drifters' daily-average positions and depths, ± error estimate = (standard deviation for month)/(crossings in month)$^{1/2}$. In parentheses: (crossings over all months) for each depth. Blanks: ≤ two crossings in the month.

500 m (17)		200 m (28)		150 m (64)		Celtic, 2012
$h\bar{u}$	$\lvert\frac{1}{2}hu'\rvert$	$h\bar{u}$	$\lvert\frac{1}{2}hu'\rvert$	$h\bar{u}$	$\lvert\frac{1}{2}hu'\rvert$	m^2s^{-1}
−8.8 ± 0.3	0.18 ± 0.09					"June"
2.5 ± 8.6	5.7 ± 1.4			1.1 ± 6.2	5.7 ± 1.8	"July"
6.9 ± 16.2	9.8 ± 4.2	−1.1 ± 2.3	3.3 ± 0.4	−1.2 ± 1.9	3.5 ± 0.4	"August"
7.5 ± 12.9	8.5 ± 2.3	1.7 ± 2.3	3.4 ± 0.6	4.2 ± 2.5	3.5 ± 0.8	"September"
−9.4 ± 12.7	9.0 ± 3.7	6.7 ± 4.4	3.4 ± 1.4	0.09 ± 1.4	2.9 ± 0.4	"October"
0.96		1.20		1.26		Bias factor
500 m (29)		**200 m (34)**		**150 m (88)**		**Malin, 2013**
$h\bar{u}$	$\lvert\frac{1}{2}hu'\rvert$	$h\bar{u}$	$\lvert\frac{1}{2}hu'\rvert$	$h\bar{u}$	$\lvert\frac{1}{2}hu'\rvert$	m^2s^{-1}
0.50 ± 4.2	7.1 ± 0.4	3.3 ± 1.6	2.1 ± 0.5	2.8 ± 0.2	0.20 ± 0.04	"July"
14.3 ± 3.9	6.3 ± 1.2	13.3 ± 2.4	4.7 ± 0.6	3.6 ± 2.2	4.8 ± 0.7	"August"
				4.4 ± 4.4	8.8 ± 1.4	"September"
				1.9 ± 4.7	6.9 ± 1.7	"October"
				−8.5 ± 11.0	6.7 ± 2.7	"November"
1.26		1.46		1.33		Bias factor
500 m (38)		**200 m (27)**		**150 m (16)**		**Faroe-Shetland 2014**
$h\bar{u}$	$\lvert\frac{1}{2}hu'\rvert$	$h\bar{u}$	$\lvert\frac{1}{2}hu'\rvert$	$h\bar{u}$	$\lvert\frac{1}{2}hu'\rvert$	m^2s^{-1}
−8.0 ± 21.1	46.5 ± 3.7	20.1 ± 9.8	18.3 ± 2.6	3.9 ± 1.8	1.8 ± 0.6	June
11.2 ± 14.7	24.5 ± 3.3	−0.75 ± 2.7	2.3 ± 1.0	0.03 ± 1.9	2.0 ± 0.6	July
1.17		1.41		1.11		Bias factor

and then transition to t^2 increase, with increasing time and separation scales, appears to prevail in the North Atlantic (Corrado et al. 2017). It typically represents sub-mesoscale random separations and shear dispersion on scales O(100 km).

3.5. Effective diffusivity from glider, ARGO and historic salinity sections

To estimate diffusivity from salinity gradients, we consider a steady-state salinity (S) budget. In Appendix C for an along-shelf sector "box" of length L from "south" (subscript S) to "north" (subscript N), (C2) becomes

$$(S_S - S_N)(q_S + q_N)\Big/2 = \sum_{inflows} |q_i|(\widehat{S} - S_i) - \sum_i Lh_iK_i\partial S\Big/\partial n_i \quad (7)$$

where inflow q_S (salinity S_S) from the south leads to northern outflow q_N

(salinity S_N), $\widehat{S} \equiv (S_S + S_N)/2$ and h_i is the depth of side i. In along-slope flow (carrying greater-than-ambient salinity from south to north), let x label streamlines. Along the shore side (E), suppose total river inflow q_R with zero salinity, Δq_R of which flows out through the offshore side (W) while the remainder adds to northern outflow: $q_N = q_S + (1-\Delta)q_R$. Assuming that the along-slope fluxes greatly exceed along-slope (diffusive) exchanges, (7) becomes

$$[Kh\partial S/\partial x]_W^E = \widehat{S} q_R/L + \partial S/\partial y(q_S + (1-\Delta)q_R/2) \quad (8)$$

(8) formalises the approach to estimating exchange used by Hill and Mitchelson-Jacob (1993) for the Hebridean shelf and by Daniault et al. (1994) off Iberia. It shows that slope current salinity may decrease ($\partial S/\partial y < 0$) as its excess salinity diffuses shorewards ($\partial S/\partial x|^E < 0$) and freshwater arrives ($q_R > 0$). If the offshore side (W) is a maximum-salinity streamline at the centre of the along-slope flow; then $hK\partial S/\partial x|_W = 0$ so that LHS (8) becomes $Kh\partial S/\partial x|^E$ and (8) becomes explicit for K. We use (8) to estimate K, other terms being "known", i.e. estimated as follows.

$\partial S/\partial x$ was obtained from repeated FASTNEt 2012 *Celtic* glider sections orientated approximately along N 37° E (Fig. 1c); distance "x" along sections was projected along a line in this direction through 47.78°N, 10.4°W. Many sections show an off-shelf "W" salinity maximum where $\partial S/\partial x|_W$ is taken as zero. $\partial S/\partial x|^E$ (values in Table 9) was estimated by regression of salinity values against x between the salinity-maximum location and either the shelf end of the section or a salinity-minimum location if closer to the maximum. A similar approach was also applied to E-W glider transects in 2013 across the *Malin-Hebrides* shelf edge (Fig. 1d). An estimate 2 Sv for slope current transport is based on (rather varied) literature values, e.g. Pingree and LeCann (1989, 1990), Souza et al. (2001), Holliday et al. (2015), Painter et al. (2016), Marsh et al. (2017). [5-day means from the AMM60 model run for 2010–2013 give estimates in the ranges 1.1–1.6 Sv, 0.6–1.5 Sv, 0.9–2.0 Sv respectively for the Celtic Sea, Malin Shelf and Hebrides/SES sections. These may be underestimates owing to the offshore limits of the sections, especially the Malin Shelf section to 10°W]. Hence we take $q_S = 10^6$ m^{3}s^{-1} (inshore of the salinity maximum). $\partial S/\partial y$ is estimated as -10^{-4}/km from a Celtic-to-Malin salinity decrease ~ 0.27 (from the glider profiles in 2012 and 2013–2014 respectively); depth $h = 200$ m for the Malin shelf onshore. [For typical values $\widehat{S} = 35$ and run-off $q_R = 10^3$ m^{3}s^{-1} in $L = 10^3$ km, we have $q_R/2 \ll q_S$ and $\widehat{S} q_R/L$ is 35% of $q_S|\partial S/\partial y|$]. These contributions to estimate K have uncertainties: formal (standard) errors in $|\partial S/\partial x|$ (Table 9) are relatively small; the necessary use of "global" values on the right-hand side of (8) and possible non-coincidence of $\partial S/\partial x|^W = 0$ with the centre of slope-current transport suggest possible errors ± 50% in the Table 9 values for K.

Effective diffusivity K has equivalence with exchange. Constituent transport by unresolved small-scale processes is typically represented as $\overline{u'C'} = -K\partial C/\partial x$ (x-component; constituent concentration C). Here K representing the dispersive effect is related to fluid motion as follows (c. f. section 3.4 for drifter dispersion). Along co-ordinate x,

$$K = \tfrac{1}{2} \frac{d}{dt} < (s_i - s_{i0})^2 > \quad (9)$$

after Batchelor (1952), where $< .. >$ denotes an ensemble average; s_i is the i th pair's x-separation with initial x-separation s_{i0}. Hence

$$K = < u'^2 > T_d \quad \text{where} \quad T_d = \int R\, dt \quad (10)$$

$R(t)$ is the auto-correlation of the component of flow pertaining to K. Hereby effective exchange $|\dot{u}|$ is inferred as $(K/T_d)^{1/2}$, T_d being evaluated at shelf break moorings where the estimate of exchange *via* K is most relevant. In practice T_d (in Table 9) is taken as $\int |acf|$ where acf is the autocorrelation of the depth integrated low-pass filtered current, consistent with the section 3.1 equation (4) estimates of degrees of freedom in time series. Equivalent exchange values are then derived as $\tfrac{1}{2}h(K/T_d)^{1/2}$ and shown in Table 9. There is further uncertainty in that time-series of order one year have larger values T_d (in parentheses in Table 9) suggesting longer-term correlations that are not represented in the FASTNEt records of order two weeks. The larger values T_d in Table 9 reduce the Malin and Celtic exchange estimates by factors 0.38, 0.23 respectively.

In the *Shelf-Sea Biogeochemistry* project (SSB) in the *Celtic Sea*, glider transects were carried out in late 2014 to summer 2015 in ~110–200 m depth (~107–130 km extent), orientated approximately along N 33° E (Fig. 1a,c). Distance "x" along the SSB transects was their projection along a line through 49°N 9°W in the FASTNEt-defined on-shelf direction N 32° E (Table S3). SSB transects were entirely on the shelf side of (did not include) the salinity maximum or "core" of the along-slope flow; in (8) we took $\partial S/\partial x|^W = 0$ and $\partial S/\partial x|^E$ as estimated by a least-squares fit of a quadratic to $S(x)$ along the whole length of each transect. Depth h was taken as the greatest depth in the transect (variously 151 to 202 m); as previously, $q_S = 10^6$ m^{3}s^{-1} was taken as the along-slope transport. Celtic Sea values of $|\partial S/\partial x|^E$ found in SSB (2014–2015) are typically larger than in FASTNEt (2012) but partly offset by lesser water depth h;

Table 9
Effective diffusivity and derived exchange across the Malin and Celtic shelf edge from glider sections.

	On-shelf $\lvert\partial S/\partial x\rvert$, 10^{-3}/km, Depth range (m)				K, m^{2}s^{-1}	T_d, hours	Exchange, m^{2}s^{-1}
	0–50	50–100	100–150	Average	±50%		
Malin November 2013 – April 2014	0.64 ± 0.29	0.28 ± 0.20	0.90 ± 0.42	0.53 ± 0.15	610	51 (348)	4.3 (×0.38)
Celtic 2012:							
July	2.7 ± 0.32	1.4 ± 0.33	1.3 ± 0.10	1.6 ± 0.31	200	38 (712)	2.8
August	1.9 ± 0.11	1.7 ± 0.20	1.4 ± 0.15	1.7 ± 0.12	190		2.7
September	1.8 ± 0.2	2.9 ± 0.41	1.8 ± 0.31	2.1 ± 0.25	160		2.4
October	0.96 ± 0.14	3.4 ± 0.35	2.5 ± 0.72	1.8 ± 0.61	180		2.6
November	0.97 ± 0.25	0.81 ± 0.29	1.2 ± 0.16	1.0 ± 0.10	320		3.5
December	0.63 ± 0.09	0.79 ± 0.06	1.0 ± 0.13	0.79 ± 0.09	410		3.9 (×0.23)
SSB 2014–15:	0–30	middle	bottom 30				
December	1.46 ± 0.09	1.26 ± 0.05	1.01 ± 0.05	1.21 ± 0.11	280	38 (712)	3.3
February	2.47 ± 0.21	2.45 ± 0.20	2.43 ± 0.22	2.45 ± 0.13	180		2.6
April	2.56 ± 0.16	2.73 ± 0.10	2.85 ± 0.15	2.72 ± 0.11	160		2.4
May/June	4 transects over 25 days			2.20 ± 0.07	170		2.5
July/August	1.62 ± 0.19	2.49 ± 0.19	2.66 ± 0.29	2.20 ± 0.30	150		2.4

± values for $|\partial S/\partial x|$ are standard errors. Values of diffusivity K rounded to two significant figures. T_d values in parentheses come from long-term moorings; corresponding reduction factors for exchange estimates are in the right-hand column.

resulting estimates of K_S and exchange are broadly comparable.

July/August 2015 in particular illustrates limitations of this approach to estimating diffusivity and exchange primarily on the basis of salinity gradient. Fitted quadratics reversed from concave to convex between the upper and lower layers. Visually, salinity along the transect changed rather abruptly; gradient changes were at different locations along the section in the different layers. This suggests patches of water of differing salinity and influence of the heavily "corrugated" shelf edge and slope. Excepting July/August 2015, the separate SSB layer estimates are consistent.

Much Argo and CTD data for 1975–2015 between the *Hebrides* and Rockall, held by ICES, includes repeats of the Ellett line of CTD stations along ~ 57°N, for which mean summer and winter sections are shown in Figure S4. The data allow a similar analysis for the 1975–2013 period-average, albeit there are fewer data to estimate $\partial S/\partial y$ (Jones 2016). Estimates here are for six sectors between 54°N and 58½°N; each sector extends 40 km off-shelf and 35 km on-shelf from the 500 m depth contour (outlined "Historical CTD sections" in Fig. 1a); $\partial S/\partial x$ was estimated for each and an overall value for $\partial S/\partial y$ was estimated. Separate summer and winter calculations were made (Jones 2016). Effective diffusivities (Table 10) follow from (8) using assumed values of the slope-current transport which was supposed centred with a salinity maximum at 500 m depth. Equivalent exchange values were derived as for the Malin shelf using slope current transport q and T_d as shown in Table 10. Salinity gradients may be underestimated: they come from salinity values in many sections, tending to cause scatter in regression against cross-slope location. Hence K and derived exchange $½h(K/T_d)^{1/2}$ in turn may be over-estimated. Here $h = 500$ m has been used both onshelf and offshelf. At typical shelf-edge depths 150 m this results in an under-estimate of K by a factor 3.3 but an over-estimate of exchange by a factor 1.8. Again, the larger values T_d from long-term moorings reduce exchange estimates. The related uncertainty is discussed further in section 5.2.

Comparing summer and winter, Tables 9 and 10 suggest increased effective diffusivity in winter, when cross-slope salinity gradients were smaller (Table 9). For the Hebrides shelf (Table 10), cross-slope salinity gradients were similar despite a stronger winter slope current tending to intensify them.

3.6. Overall summary by region of total fluxes and cross-slope exchange

3.6.1. Celtic Sea

On the Celtic Sea shelf, fluxes estimated from moorings in June 2012 were largely off-shelf, but ST4 on the shelf had an on-shelf bottom-layer flux 0.46 m^2s^{-1} (discussed in section 4.1). On-shelf moorings showed exchange as great as 16 m^2s^{-1} if semidiurnal tides are included. Excluding coherent barotropic tides, exchanges were O(5 m^2s^{-1}) near the shelf break and areas of internal tide generation, O(3 to 4 m^2s^{-1}) further on-shelf; low-frequency exchanges (periods > 48 h) were O(1 m^2s^{-1}). Smaller cross-slope salinity gradients in winter (section 3.5) suggest a greater effective diffusivity K, by a factor of about two compared with other seasons.

In the deeper slope locations, upper-level fluxes varied at low frequencies, presumably driven by the wind. The deepest short-term mooring at 688 m depth showed the largest exchanges and especially large fluxes. Drifter dispersion (section 3.4) also suggests large exchanges in much deeper Biscay waters. Clearly different deeper-water dynamics do not apply to exchange across the shelf break.

Table 11
Summary of cross-slope exchanges from indicated moorings and drifter crossings, ± (standard) error estimates for these mean values derived from respective tables in sections 3.1, 3.2.

Cross-slope exchanges, m^2s^{-1}	Shelf break			Deep	
	Mooring Total	Mooring Low-pass	Drifters, 150 & 200 m	Mooring Low-pass	Drifters, 500 m
FSC 2014–15	F & H: 7.2 ± 0.4	1.2 ± 0.2	4.5 ± 0.8	G: 20 ± 1	30 ± 4
Hebrides 1995–96	S140: 7.2 ± 0.1	1.5 ± 0.1	n/a	S400: 1.7 ± 0.1	n/a
Malin 2013	SE: 8.0 ± 0.2	0.9 ± 0.1	3.6 ± 0.9	LA: 6.0 ± 0.7	5 ± 0.6
Celtic 2012	ST2&3: 7.0 ± 1.7	1.25 ± 0.1	3.0 ± 0.4	LT1: 19.3 ± 0.2	7 ± 2.1

3.6.2. Malin and Hebrides shelves

On the Malin shelf, July 2013 moorings showed persistent downslope transport in the canyon at 500 m depth: more than 5 m^2s^{-1} estimated in the bottom 300 m; stronger episodes correlated with stronger along-shelf flow. This canyon location recorded the largest flux (Table 3), off the shelf. In locations LA to the west-south-west and SD to the north, fluxes at depth tended to be on-shelf. Excepting the canyon and the shallowest location SG on the shelf, fluxes were O(1 m^2s^{-1}) associated with low-frequency variability (periods > 48 h), as for the Celtic Sea. Exchanges in 500 m and deeper were as large as 15 m^2s^{-1} if tides are included, but low-frequency exchanges (periods > 48 h) were O

Table 10
Effective diffusivity across Hebrides slope from long-term salinity sections.

Variable, units	Sector	$\lvert\partial S/\partial x\rvert$, 10^{-3}/km		$\partial S/\partial y$, 10^{-4}/km	q, 10^6 m^3s^{-1}	K, m^2s^{-1}		T_d, hours	Exchange, m^2s^{-1}	
		Offshelf	Onshelf			Offshelf	Onshelf		Offshelf	Onshelf
Summer	1	0.42	0.16	−0.454	1.5	160	430	51 (348)	7.4	12.1
	2	0.19	4.98			350	13		11.0	2.1
	3	0.46	1.05			150	65		7.1	4.7
	4	0.58	3.67			120	18		6.3	2.5
	5	0.48	2.37			140	28		7.0	3.1
	6	0.24	0.39			280	180		9.8	7.7
Summer mean ± standard error						200 ± 35	120 ± 63		8.1 ± 0.8	5.3 ± 1.6
Winter	1	0.28	1.29	−0.996	2	720	130	51 (348)	15.7	6.7
	2	0.55	4.24			360	47		11.1	4.0
	3	0.33	2.66			600	74		14.3	5.0
	4	0.46	3.85			430	51		12.1	4.2
	5	0.66	1.47			300	140		10.1	6.8
	6	0.33	1.17			600	170		14.3	7.6
Winter mean ± standard error						500 ± 63	100 ± 22		12.9 ± 0.9	5.7 ± 0.6

Based on Jones (2016), depth h = 500 m. Values of diffusivity K rounded to two significant figures. T_d values in parentheses are from long-term moorings; corresponding reduction factors for exchange estimates are 0.38. ± values for K and exchanges are standard errors and do not take account of different depths and uncertainties in $\partial S/\partial y$, q and T_d discussed in the text.

(5 m^2s^{-1}) or less (Table 4). On-shelf exchanges were O(7 m^2s^{-1}) including tides, O(1 m^2s^{-1}) due to low frequencies. Drifters' transverse "diffusivities" increased from less than 100 m^2s^{-1} to a maximum 300–350 m^2s^{-1}; they correspond to exchange estimates $½h(K/T_d)^{1/2}$ up to 3 m^2s^{-1} if depth $h = 140$ m, $T_d = 42$ h (Table 9). Effective diffusivities from cross-slope salinity gradients in winter glider sections average to a corresponding exchange 5.7 m^2s^{-1}.

On the Hebrides shelf in 1995–96, typical filtered cross-shelf fluxes were ± 3 m^2s^{-1} at both moorings (Table 3). In 140 m, there was a baroclinic element; on-shelf flow (0.025 to 0.075 m s^{-1}) formed in an intermediate layer at/just below the seasonal thermocline from early summer to the end of autumn. Off-shelf flow above 50 m and below 100 m was stronger during winter months. The overall depth integral was on to the shelf and small on long-term average (Table 3) By contrast, in 400 m, down-slope pulses below 250 m resulted in net off-shelf (depth-integrated) flux. Strongest down-slope flow there coincided with the strongest along-slope current as expected for a bottom Ekman layer, notably in January 1996. The largest feature in both mooring time series occurred over three tidal cycles around 13th February 1996. On-shelf flux briefly reached 14 m^2s^{-1} and exchange almost 7 m^2s^{-1}, coinciding with southward along-shelf flow and apparently associated with a pause in the (usually northward) slope current and corresponding local pressure gradient changes. Cross-slope salinity gradients (from 1975 to 2015) were very variable but similar on average between summer and winter despite a stronger winter slope current tending to intensify them. Correspondingly, inferred effective off-shelf diffusivity doubled from summer to winter. Derived exchange estimates $½h(K/T_d)^{1/2}$ are of order 8 (13) m^2s^{-1} in summer (winter) off-shelf, O(6 m^2s^{-1}) on-shelf if depth $h = 500$ m, $T_d = 51$ h (Table 10) but subject to possible reductions given uncertainty in these values.

3.6.3. Faroe-Shetland Channel/West Shetland shelf

From the Faroe-Shetland Channel/West Shetland shelf moorings, fluxes were primarily along the Channel, to the north-east except on the Faroes side, with a component onto the shelf in general, excepting some sustained off-shelf fluxes in winter 2014/15. Cross-slope exchange decreased markedly from the centre of the Channel to shallower slope waters, from O(20 m^2s^{-1}) to O(1 m^2s^{-1}) in the case of low-frequency contributions; the barotropic tidal contribution O(4 to 7 m^2s^{-1}) varied much less. Along-slope flux and cross-slope exchange tended to be stronger in October-April than May-September. Drifters' transverse "diffusivities" up to 280 m^2s^{-1} correspond to exchange estimates $½h(K/T_d)^{1/2}$ up to 1.9 m^2s^{-1} using $h = 200$ m and $T_d = 225$ h corresponding to FASTNEt moorings NWS-F, -H.

3.6.4. Summary of cross-slope flux and exchange estimates

Fluxes vary markedly in space on scales of 10–30 km, as shown by the contemporaneous (albeit short-duration) moorings, and in time on scales from days to seasons, as shown by the (albeit few) longer-duration moorings. Exchanges are more consistent; they have a large tidal contribution whilst longer-period contributions generally decrease from deeper water to the shelf break. Exchange estimates derived from Tables 2, 4, 7 (moorings) and Table 8 (drifters) are given in Table 11. In the three studies with drifters, shelf-break exchange estimates from daily drifter positions are 2.4 to four times those from low-frequency currents $\boldsymbol{u}_{filt}$ at comparable-depth moorings, but much less than the values from those moorings' total currents. For comparison, surface-current variance derived from altimetry (section 3.3) suggests exchange ~ 1 m^2s^{-1}; this is a lower bound as higher-frequency or smaller-scale motion breaking geostrophy may not be included. Estimates via effective diffusivity from salinity sections consistently exceed the estimates from moorings and drifters, possibly in part as a result of under-estimated "diffusive" timescale T_d as discussed further in section 5.2.

4. Process contributions to fluxes and exchange

In Section 3, fluxes, exchange and effective diffusivity were presented without regard to process attribution. Process mechanisms are considered in this Section, including: lenses and internal waves (4.1); Ekman transport from wind (4.2) and at the bottom (4.3); boundary/slope currents and associated diversions, meanders and eddies (4.4); tides (4.5).

4.1. Lenses and internal waves

Transport in a layer between two isopycnals, separation $h(t)$, was analysed by Spingys et al. (2020) as a combination of Eulerian transport $\boldsymbol{U}_E$ and Stokes' transport $\boldsymbol{U}_S$. The Eulerian transport is diagnosed as $\overline{\boldsymbol{u}_{\overline{h}}}\,\overline{h}$ which is equivalent to averaging the transport at a fixed depth. The Stokes' transport is diagnosed as $\overline{\boldsymbol{u}_{h'}}\,\overline{h} + \overline{\boldsymbol{u}'h'}$ combining a term driven by the interaction of isopycnal displacement and shear, and another driven by covariances in the layer thickness and velocity (McDougall and McIntosh 2001). Here $\overline{\boldsymbol{u}_{h'}}$, is the layer average velocity over the instantaneous layer extent and $\overline{\boldsymbol{u}_{\overline{h}}}$ is the average over the mean layer extent.

Tidal motion may provide multiple contributions to the Stokes' transport terms driven by baroclinic (internal) tides, barotropic tides and their interaction. For simple stratification and mode 1 vertical structure, the Stokes' transport tends to be in the direction of internal wave propagation in the upper and lower water column (through the bolus transport) and reversed at mid-depth (through the shear term $\overline{\boldsymbol{u}_{h'}}\,\overline{h}$). However, barotropic tides co-varying with baroclinic-tide-driven layer thickness can add another contribution to the bolus transport within layers. These covariances drive opposing transports in the upper and lower layers with strong spatial variability depending on the local phase relation between the baroclinic and barotropic tides (Spingys 2017). In some settings the Stokes' transport may be partially, or completely, compensated by the Eulerian transport; however, this does not appear to be the case at the shelf break (Spingys et al. 2020).

4.1.1. Celtic Sea

Cross-slope tidal flows and consequent internal tides are particularly strong at the Celtic Sea shelf edge. The internal wave field observed within 30 km of the Celtic Sea shelf-edge is complex owing to small-scale topography; internal tidal velocity profiles at ST2 and ST3 were almost mirror images of each other. These observations reflect the spiral type internal wave generation at the headland predicted by MITgcm modelling (Vlasenko et al., 2014). At ST4 the baroclinic bolus and shear components of Stokes' transport were consistent with theory, being respectively in the same (E-W) and opposite (W-E) direction as the internal tide propagation rather than directly on–off-shelf. Eulerian transport was eastward in the upper layer (offsetting the Stokes' transport) and westward in the lower layer (reinforcing the Stokes' transport). Eastward Stokes' transport prevailed in the middle layer. At both ST4 and ST5 the transport driven by the barotropic velocity ($\mathbf{u}_{bt}$ in Table 1) was directed on-shelf for the bottom layer, resulting from a thick bottom layer coinciding with on-shelf barotropic tidal currents, and directed off-shelf in the surface, with off-shelf barotropic tidal velocities coinciding with thick surface layers. Stokes transports are summarised here in Table 12; for a discussion of the associated error estimates see Spingys et al. (2020).

The seasonal variability of the Stokes transport in the surface, pycnocline and bottom layers was explored at a *Shelf-Sea Biogeochemistry* (SSB) mooring 100 km from the Celtic Sea shelf break (Fig. 1a) in 2014–2015 (Ruiz-Castillo et al., 2022; summarised in Table 12). Stokes transport was strongest during summer 2014. Within the pycnocline the Stokes' transport was off-shelf (0.21 m^2s^{-1}) in September and was offset by transport in the layers above and below. Stokes transport was weaker, 0.01–0.03 m^2s^{-1} throughout autumn and early winter 2014 and during

Table 12
Internal tide Stokes transport in the Celtic Sea and on the Malin Shelf.

Stokes transport, m^2s^{-1}	Bottom layer	Pycnocline layer	Surface layer
[a]Celtic Sea 2010 IM1 (+ve to SW)		0.07	
[a]Celtic Sea 2010 IM3 (+ve to SW)		0.09	
[b]Celtic Sea 2012 ST4 (+ve to W)	0.33 ± 0.01	−0.43 ± 0.01	0.15 ± 0.06
[c]Celtic Sea 2014–2015 CCS	0.01 to 0.09	0.01 to 0.21	0.01 to 0.12
[b]Malin Shelf 2013 SG (+ve to SE)	0.02 ± 0.012	−0.035 ± 0.011	0.025 ± 0.025

[a] magnitude of the Stokes transport reported
[b] magnitude of the Stokes transport in direction of baroclinic energy flux (from Spingys et al., 2020)
[c] magnitude of the Stokes transport in the across-shelf direction from Ruiz-Castillo et al. (2022).

the spring and summer months of 2015. Typically, its magnitude was consistent with the values reported for the IM1 and IM3 moorings (Table 12) but less than those in Spingys et al. (2020), perhaps due to the distance from the shelf-break source of internal tides.

Shorter period variability was observed in June 2012, when wind-driven vertical mixing through the upper 50 m permitted increased on-shelf transport of baroclinic semi-diurnal energy; 28–48 W m^{-1} over the 2-week deployment (Stephenson et al., 2015). A 25–43% increase in positive on-shelf energy flux resulted from nonlinear interaction between (i) the vertical shear of wind-generated near-inertial oscillations and (ii) the vertical velocity associated with the semidiurnal internal tide (Hopkins et al. 2014). The interaction introduced a 2-day counter-clockwise "beating" in the energy transport. Mass flux directions also changed around days 168–169, coincident with the wind-driven changes in stratification; notably the bottom layer flux at ST5 changed from on– to off-shelf (Figure S1a).

Saline lenses offer an alternative estimate of the transport onto the shelf using a salt flux calculation. In June 2010, saline lenses were observed within the pycnocline at the shelf-edge and up to 100 km on-shelf in the Celtic Sea. Hopkins et al (2012) estimated that these lenses propagated from the shelf edge (their formation site) at average speeds of 1–2 cm s^{-1}. Following Spingys et al. (2020) the baroclinic transport within the pycnocline and its Stokes components were calculated for two moorings, IM1 and IM3, located 7 km apart near 8.94°W, 49.4°N, in 137 m water depth and 100 km from the shelf break (Fig. 1a). They remained in the water for 12.5 days (24 integer M_2 wave periods) during which the deployment-mean baroclinic transport within the pycnocline was 0.07 m^2s^{-1} on-shelf at IM1 and 0.14 m^2s^{-1} off-shelf at IM3, a difference (within just 7 km) that highlights the complex nature of the Celtic Sea internal wave field across the entire inner shelf. At both locations however, the Stokes component of transport (0.07–0.09 m^2s^{-1}; Table 12) was directed off-shelf, consistent with on-shelf propagating internal waves.

Celtic Sea 2012 FASTNEt data and numerical models were used to investigate 3-D dynamics of baroclinic tides and consequent internal (solitary) waves over the shelf-slope (Vlasenko et al. 2014; Vlasenko and Stashchuk 2015). Internal solitary waves had maximum amplitudes up to 105 m. Short-scale internal waves were generated (i) over spurs; (ii) in an area with several canyons (4.1.3 below). Local intensification at ST1 (in 688 m) was explained in terms of a tidal beam formed over super-critical bottom topography. Internal solitary waves generated over the shelf break, and propagating seaward, disintegrated locally over the continental slope due to the steep sea floor, their energy going to higher baroclinic modes. Transports were not estimated but the largest soliton's size (Vlasenko et al. 2014, Fig. 5), and a typical speed 0.5 m s^{-1}, suggest a transport of order 10^5 m^2 per semi-diurnal tide. More typically 3 to 4 solitons of amplitude ~ 30 m (e.g. Vlasenko et al. 2014, Fig. 4) suggest a transport at ST1 of order 1 m^2s^{-1} (~ 4.5×10^4 m^2 per semi-diurnal tide).

4.1.2. Malin shelf

On the Malin shelf, FASTNEt 2013 moorings showed the internal tide consistently propagating onto the shelf. Stokes' transports at mooring SG, about 30 km onto the shelf, were much smaller than at Celtic mooring ST4 deployed at a comparable distance from the shelf edge (Table 12 based on Spingys et al. (2020)). Indeed, the resulting depth-integrated transport is statistically indistinguishable from zero. The Eulerian transport was larger than, but nearly perpendicular to, the Stokes' transport in each layer, but its depth-integral is likewise statistically indistinguishable from zero.

[Eddy transports $\overline{u'h'}$ by internal waves at mooring SE near the shelf break were comparable with 2012 Celtic Sea values in the bottom layer, somewhat less in the upper layer (Spingys, 2017). Eddy transports were smaller at SG. Thus Malin eddy transports were smaller than Celtic Sea eddy transports at comparable distances onto the shelf.]

4.1.3. Topographic effects

3-D focusing of internal tidal energy in Petite Sole Canyon (Celtic Sea) was analysed by Vlasenko et al. (2016) from FASTNEt observations and by numerical modelling. Deep (500–800 m) in the canyon, shear variance was intensified by an order of magnitude, as multiple internal tidal beams generated at the shelf break propagated downwards and were focused. A near-circular canyon head, and bottom slope steeper than the tidal beam, create favourable conditions for the focusing. Resultant greatly intensified local diapycnal mixing led to local formation in the model of a baroclinic eddy, the reality of which was supported by LADCP measurements (Vlasenko et al. 2016). Modelled circulation was of order 10^4 m^3s^{-1} in each of two superposed layers over O(10 km) extent, i.e. an exchange of order 2 m^2s^{-1} locally. However, most of this did not cross depth contours.

Malin shelf observations (2013) around a shallow canyon near 55.5°N show much more tidal energy in the canyon and downstream (i.e. at SC) than upstream. SC showed enhanced energy through the internal wave band. Modelling showed (i) energy focusing in the canyon, as a tidal beam generated at the shelf break radiated energy downwards, and (ii) a bottom-trapped internal wave propagating northwards along the slope after generation by tidal flow over a local prominence (Stashchuk and Vlasenko, 2017).

A (rare) downslope-moving front of cold water over near-bottom warm water was seen north of the Malin slope canyon, at SD, in July 2013 (van Haren and Hosegood 2017). This front occurred between fronts propagating upslope with tidal periodicity; it resembled a gravity current and had strong convective turbulence coming from the interior. The downslope transport was of order 50 m (depth) × 0.1 m s^{-1} (downslope velocity component), i.e. 5 m^2s^{-1}, a large value, but one 2-hour occurrence in 15 days of record implies a small transport overall. The authors suggest that the front was generated by oblique propagation of internal (tidal) waves and flow over a nearby upstream promontory.

4.2. Ekman transport from wind

Daily values of (along-shelf windstress)/(ρf), i.e. the onto-shelf (downwelling) component of Ekman transport, are shown in Fig. 8 for the three FASTNEt deployment periods and during SES. Much day-to-day variability implies that mean values hardly represent the range as listed in Table 13. Mean values are naturally biased towards extremes. However, median values (in Table 13) are relatively close to the means; extremes O(5 m^2s^{-1}) of downwelling transports on the Scottish shelves did not have a large effect on estimates of typical or mean values. Scottish median and mean values ranged from 0.04 to 0.71 m^2s^{-1} for the periods shown; the positive values show onto-shelf transport. Median and mean Celtic Sea transports, however, were in an upwelling sense under prevailing south-westerly to westerly winds (owing to the orientation of the shelf-edge: 302°). They perhaps show a trend from upwelling in summer to downwelling in autumn. In SSB 2014–15, Ekman

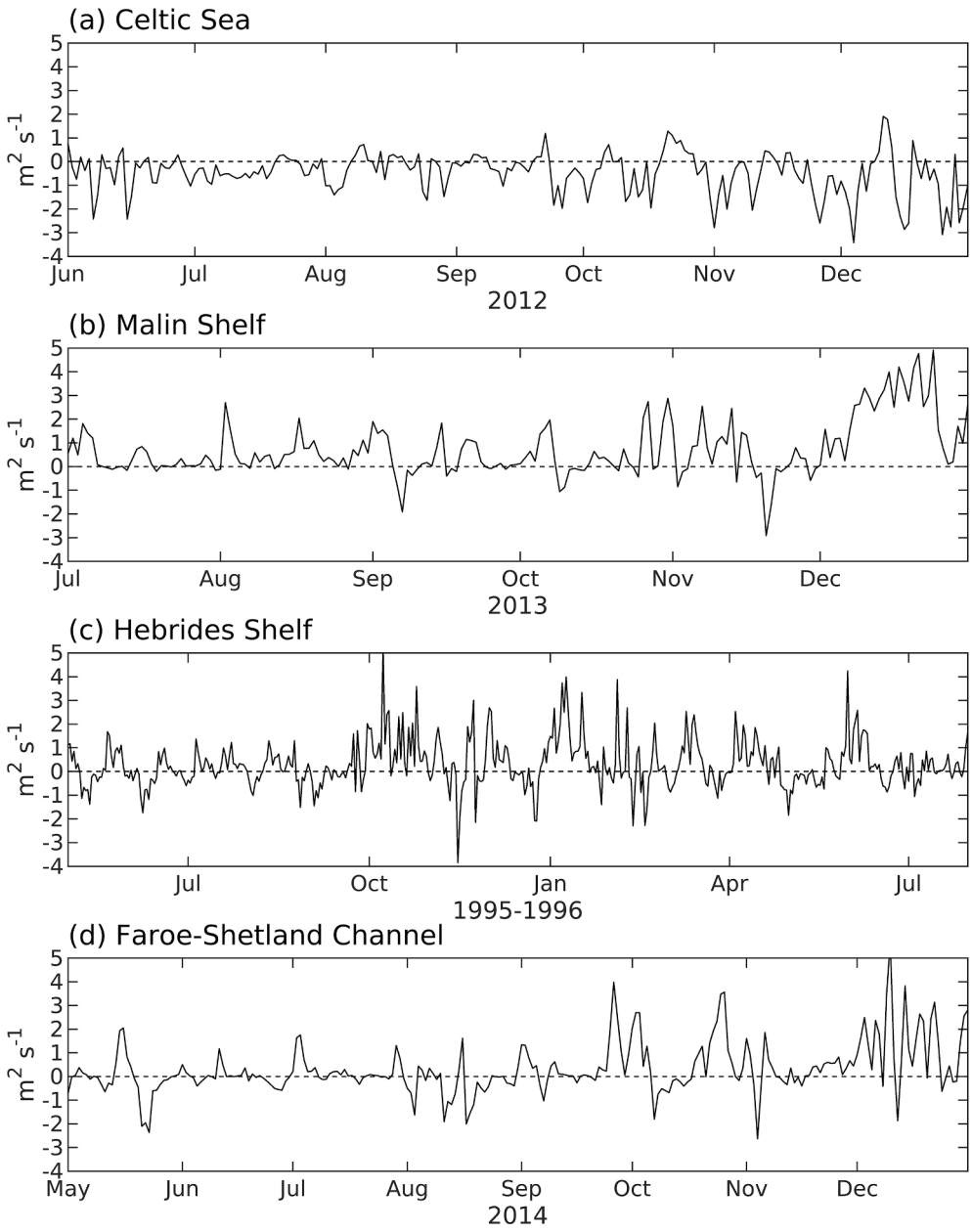

Fig. 8. Wind driven across-shelf Ekman transport. (a) Celtic Sea 2012, (b) Malin Shelf 2013, (c) Hebrides Shelf 1995–1996 and (d) Faroe-Shetland Channel 2014. Positive values are on-shelf transport (downwelling).

transports at CCS, 100 km in from the Celtic Sea shelf break, are shown in Table 13. Values are moderate throughout compared with the Scottish extremes.

4.3. Bottom Ekman transport ("Ekman Drain")

Estimates of bottom Ekman transport *EK* were made for *Malin Shelf* moorings LB, SB and SD/SC, respectively "upstream", "canyon" and "downstream" for their 2-week deployments during 2013.

$EK = \tau_b/(\rho_0 f) = (k_b/f)(U^2 + V^2)$ where τ_b is the bottom drag, f is the Coriolis parameter, $k_b = 2.5 \times 10^{-3}$ is a drag coefficient chosen for consistency with Souza et al. (2001). U and V (across- and along-slope velocities, squared first and then filtered to calculate *EK*) were obtained at each mooring from a downward-looking 300 kHz RDI ADCP, 100 m above the bed sampling in 2 m vertical bins to within 10 m above the bed, and an upward-looking RDI 75 kHz ADCP above, sampling in 8 m bins. 4th order low-pass elliptic filtering had a cut-off period of 71 h; subsampling to hourly intervals allowed comparison with Simpson & McCandliss (2013). "Along" and "across" the slope were defined based on the flow direction within the geostrophic interior, as in section 3.1.2. Excepting the initial four days of mooring deployments, during which wind speeds exceeded 15 m s^{-1} and caused a reversal in the along-slope current, the low pass filtered current direction at 350 m depth matched that of the depth contours in accord with Taylor-Proudman theory.

The resulting downslope transport was integrated within the bottom Ekman layer, defined (in the absence of turbulence measurements) as the layer adjacent to the seabed within which the (filtered) current rotated anticlockwise towards the bed in a manner consistent with Ekman dynamics. [This definition is consistent with that used by Simpson & McCandliss (2013) to enable comparison with their earlier nearby mooring.] Typical bottom boundary layer thickness exceeded 100 m and, whilst larger during periods of stronger flow, differed little in a time-mean sense between moorings. A well-defined veering layer within the mean current was deflected up to 20° at all locations other

Table 13
Minimum, mean, maximum and standard deviations of **cross-slope wind-driven Ekman transport** (from daily values, in sense of upwelling). [a]from Ruiz-Castillo et al. (2022).

Cross-slope wind-driven Ekman transport, m^2s^{-1}						
Location	Dates	Min	Median	Mean	Max	StD
Celtic	2012, June 1 to December 31	−3.43	−0.29	−0.47	1.91	0.87
Malin	2013, July 1 to December 31	−2.91	0.35	0.71	4.91	1.18
Hebrides SES	1995, May 1 to 1996, July 31	−3.85	0.13	0.30	5.24	1.00
Faroe-Shetland Channel	2014, May 1 to December 31	−2.63	0.04	0.32	5.68	1.09
[a]Celtic Sea SSB; mean (peak) values and mean direction	2014, June 22 to August 18	0.34 (1.5) to SW (off-shelf)				
	2014, August 23 to November 17	0.40 (1.5) to SE (slightly on-shelf)				
	2014, November 22 to December 26	0.67 (2.5) to SW (off-shelf)				
	2015, April 25 to July 23	0.36 (1.2) to SSE (slightly off-shelf)				

than SD which is not included in this analysis because of the strong influence of downslope propagating bores (van Haren & Hosegood, 2017, and section 4.1). The downstream location (SC) is notable due to the pronounced intensification in poleward along-slope flow, commencing on day 192 and accompanied by a distinct on-shore flow that persisted for 2 days.

Instantaneous integrated Ekman transports throughout the mooring deployment are largely directed downslope (negative values in Fig. 9a) and fluctuate in magnitude: 0 to 10 $m^2\ s^{-1}$. Largest values were at the canyon head (SB, 7.8 $m^2\ s^{-1}$) and at the shallower downstream mooring (SC, 8.0 $m^2\ s^{-1}$). The downstream impact of the canyon on slope current stability, and consequently the Ekman drain, is apparent as the anomalously large upslope transport (max. = 22.86 $m^2\ s^{-1}$) on days 192–193.

Time-mean Ekman (downslope) transport, calculated over the period of each mooring deployment, is given in Table 14. [Beyond the scope of this study is an evaluation of the correct slope heading within the canyon, which due to the curvature of the canyon makes such a determination challenging. Future work could investigate the impact of curvature in the flow induced by the underlying bathymetry and how this impacts on estimates of cross-slope transport as the flow may not follow isobaths as closely as along straight slopes.] Bottom Ekman transport was largest within the canyon (SB) where a persistent anti-clockwise veering in current direction was observed (Fig. 9b). Although these records are shorter than was hoped for (the long term moorings were lost to trawling), they are long enough to provide a clear comparison of Ekman transport at sub-inertial timescales from the three locations located upstream, downstream and within the canyon. They show the influence of the canyon (rather than dynamical influence of longer timescale processes) where the largest time-mean value occurred. The largest bottom Ekman layer transport at a given moment, however, occurred downstream of the canyon at SC on day 192 due to an instability in the along-slope current (Fig. 9); this enhanced transport up the slope. Despite the strong up-slope transport on days 192–193, the mean at SC was weakly downslope.

Table 14
Bottom time-mean **Ekman transports at Malin slope moorings.**

Malin bottom Ekman transports	Upstream (LB)	Canyon (SB)	Downstream (SC2)
Depth (m)	499	504	396
Time mean integrated EK (m^2s^{-1})	−0.90 ± 1.32	−3.12 ± 2.38	−0.31 ± 9.69
	(-2.4, 0.6)	(-3.8, −2.4)	(-5.3, 4.7)

Negative is down-slope. Values ± standard deviations with 95% confidence intervals in parentheses (see section 3.1).

Estimates of down-slope bottom Ekman transport a little further north off the Hebrides shelf were 1.6 m^2s^{-1} in SES (over 167 days in 1995–6 with veering ~ 10-20° in a bottom boundary layer; Simpson and McCandliss, 2013) and 0.7–2.7 m^2s^{-1} (upper-bounds) in October-November 2014 (Painter et al. 2016).

4.3.1. *Dye experiment*

Two dye experiments were carried out at the Malin-Hebrides shelf edge west of Scotland in July 2013 (Dale et al. in preparation; the second is described in section 4.4). In the first, seeking the source of water in the Ekman Drain, 50 kg of density-adjusted fluorescein dye was injected at depth 112 m (i.e. above the bottom Ekman layer) in 201 m water depth (i.e. over the shelf break) at 55.19°N on 7th July (Fig. 10 "Dye1"). The dye patch was repeatedly surveyed using an MSS turbulence profiler as it was tracked northwards along the shelf break (near 200 m water depth). The surveying gave excellent resolution including microstructure but poor coverage of the patch meant difficulty budgeting the dye.

The dye showed weak tendencies to cool (~ 0.015 °C day^{-1}), increase density (~ 0.002 kg m^{-3} day^{-1}) and move down in the water column by 10 ± 4.7 m day^{-1} (95% confidence limits). These tendencies

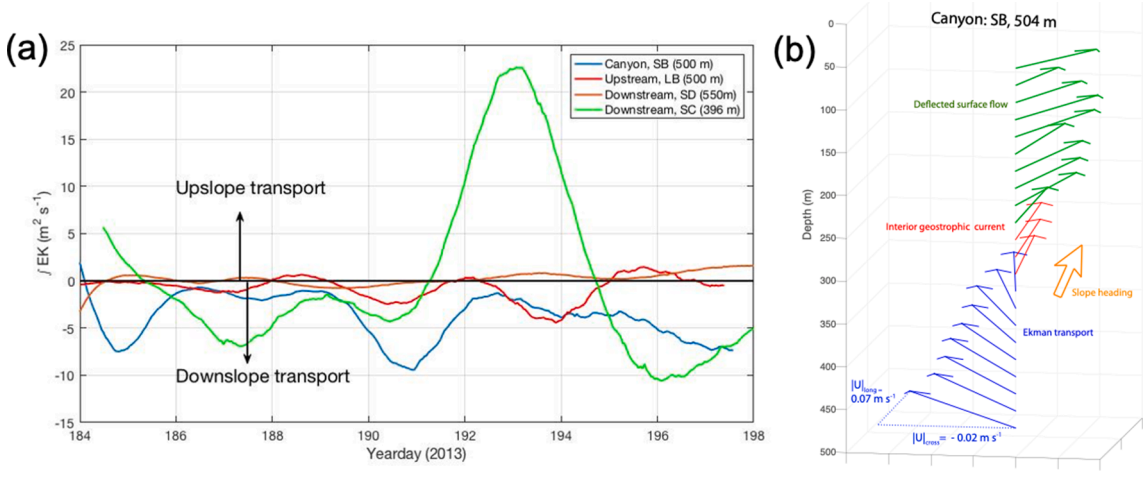

Fig. 9. (a) **Integrated Ekman transports within the veering layer above the seabed** at moorings SB, LB, SD and SC on the Malin shelf. (b) **Deployment-mean velocity vectors** at mooring SB.

Table 15
Distinctive characteristics of FASTNEt areas.

	Celtic	Malin-Hebrides	Faroe-Shetland
Topography (2.1)	Broad shelf, steep slope, many canyons	Fairly regular slope with shallow double canyon	Sub-critical nearly straight slope
Water masses (2.1)		Scottish Coastal Current; wind affects ratio with Atlantic Water hence salinity on shelf	North Atlantic Current over cold Overflow Water
Poleward Slope current	Seasonal weakening or reversal (2.1), especially June-July 2012 (3.1, 3.2), Goban Spur overshoots (2.1)	Autumn-winter maximum, small eddies (2.1); reversal "event" 13 February 1996 with sea-surface height anomaly and flux onto shelf	Stronger, reverse flow on lower slope, large meanders (2.1); drifters' evidence (3.2)
Ekman "drain"		(2.1) Spatially variable (3.1.2, 4.3), clearest relation to slope current at S400 (3.1.2)	(2.1)
Cascading	(2.1)	(2.1)	
	Seasonal thermocline (2.1)		
	Strong wind, wave and tidal mixing (2.1)		
Up-/Down-welling winds	varied, more upwelling than downwelling, especially summer (4.2)	Downwelling, occasionally very strong (to 4 $m^2 s^{-1}$; 2.1, 4.2)	
Wind "event"	June 2012 storm (3.2) with off-shelf flow		
Tidal currents	Strong (up to 0.5 m s^{-1}; 2.1, 3.1). Dominate HF exchange (3.1)	O(0.2 m s^{-1}; 2.1, 3.1). Rectified on upper slope (2.1). Dominate HF exchange (3.1)	O(0.2 m s^{-1}; 2.1, 3.1). Minority of exchange (3.1)
Baroclinic tide	(2.1); mode 1 dominates shelf baroclinic currents (3.1.1), much local variability, [P]canyons intensify (4.1)	(2.1); [P]Focusing in canyon, generation and northward propagation (4.1.3); [P]associated fronts (4.1.3)	(2.1)
Bottom boundary layer flow	Thick downslope at ST1 (3.1.1)	Thick downslope in canyon (4.4)	
Cross-slope fluxes	Most from LF motion; largely offshelf, spatially and temporally variable; not clearly seasonal (3.1.1)	Most from LF motion; spatially variable (3.1.2), [P]strongly on-shelf near 55.5°N (topographic guidance? 3.2)	Most from LF motion; variable month-to-month; winter < summer (3.1.3)
Cross-slope exchange	Drifters suggest irregular topography increases exchange (3.2)		winter exchange > summer (3.1.3)
	Cross-slope exchange (especially from LF motion) is generally minimised near the shelf break		
Drifter dispersion	Along- and cross-slope effective diffusivities had similar value but different character [P](3.4)	Transverse ≪ along-flow [P](3.4)	Across-slope ≪ along-slope (3.4)

Reference to section 2: published elsewhere. Reference to sections 3 to 5: reported here. [P]FASTNEt but also published elsewhere.
HF = high frequency, LF = low frequency,

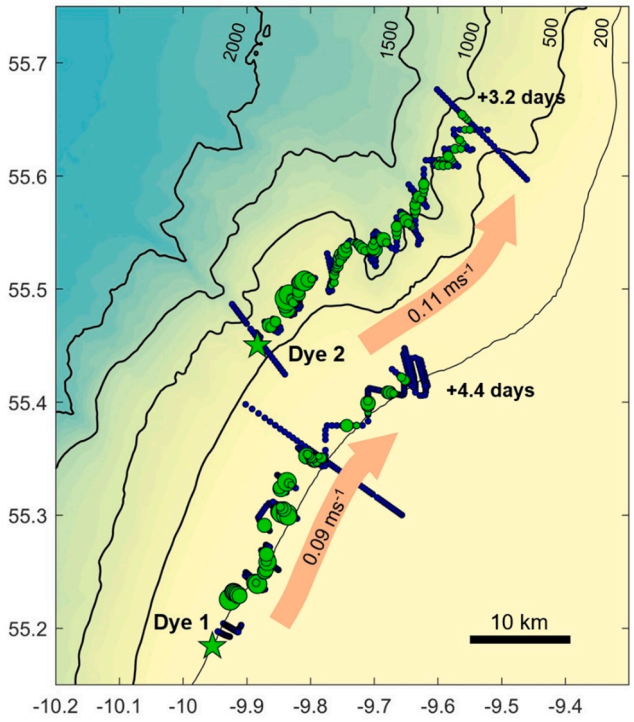

Fig. 10. Tracks of two dye releases at the Malin-Hebrides shelf edge in July 2013. Dye-containing profiles are shown as green discs, the size of which represents the dye load of the water column. Dye-free profiles are shown blue. The indicated speeds reflect net displacement from the release to the last detection.

appear to be broadly consistent with diapycnal flow needed to supply the divergent bottom Ekman layer from above; down-slope Ekman transport is expected to increase beyond the shelf break towards the maximum in the poleward slope current at O(500 m or greater) water depth. However, the ultimate source of the water supplying this Ekman "drain" remains unclear; a convergence of cross-shelf transport is probable but whether *via* onshore transport from the ocean or offshore transport from nearer-shore is not yet determined and, in a local study such as this, the role of along-slope convergence cannot be dismissed.

This section 4.3 clearly shows down-slope flow near the bottom, albeit of unresolved origin. Along-slope flow that is weaker on the shelf than over the slope implies divergence of the bottom Ekman layer. This could be supplied by local along-slope convergence, but a more extensive, regional down-slope flow must be supplied principally from cross-slope convergence and downwelling of overlying water (e.g. as shelfward flow, balancing along-slope density and pressure gradients, encounters the slope). The relative contributions of oceanic and shelf water are not known.

4.4. Boundary/slope currents and associated features

Currents along the continental slope do not directly give cross-slope transport or exchange. However, associated features may do so. (i) Bottom Ekman transport is associated with along-slope flow as discussed in section 4.3. (ii) Any misalignment of a slope current O(2 Sv) can cause relatively large cross-slope transport, as exemplified by the estimated transport 0.2 Sv or more onto the Malin shelf (section 3.2). (iii) Slope current meanders and eddies are prominent in Biscay (affecting the FASTNEt 2012 Celtic Sea drifters) and in the Faroe-Shetland Channel.

Regarding slope current alignment and meanders (ii and iii), alignment of flow at individual moorings is problematic (Appendix B): the along-slope component tends to be relatively strong, so that any misalignment has a large effect on cross-slope estimates; moreover, effective direction of meandering depth contours is ill-defined. Hence drifters

may give better estimates of effective cross-slope transport and exchange resulting from slope-current meanders (section 3.2 and Table 8). The results from daily-average positions and depths are most relevant because they omit most of the high-frequency contributions (c.f. section 5.3). The monthly transports represented by $\overline{\boldsymbol{u}}$ are fairly consistently onto the Malin and West Shetland shelves (as well as poleward) but are variable at the Celtic Sea shelf edge; values (multiplying by 150 m depth) are typically 3 m^2s^{-1}. Exchanges $\frac{1}{2}h|u'|$ are 2 to 4 m^2s^{-1}.

Capes and canyons can divert and strain the slope current. An example of diversion at Goban Spur (Celtic Sea west of the FASTNEt sites) is shown in Pingree et al. (1999). May 1991 infrared remote-sensed images show cool water there separating from the upper slope (~1 km water depth), to WNW and to SSW (i.e. the off-slope "overshoot" directions for poleward and equatorward flows). We cannot quantify the associated transports from these images of the surface. Any such transports at the FASTNEt sites are included in the overall estimates of sections 3.1 to 3.3 but are not separable from other contributions thereto. Upwelling across the Celtic Sea shelf-break, in two small sub-canyons of width O(½ internal Rossby radius) near Whittard Canyon, was shown by gliders in July-August 2012 (Porter et al. 2016b). Upwelled features were identified as sub-pycnocline saline water on the shelf, upwelled from 300 m depth. During equatorward flow, unbalanced pressure gradient (ageostrophy) can lead to upwelling along canyon axes. The slope current subsequently reverted to poleward flow, the upwelling stopped and upwelled remnants were mixed into local shelf water or advected away.

A second dye experiment (c.f. 4.3.1) concerned slope current distortion over a *Malin* canyon pair. 100 kg of density-adjusted fluorescein dye was injected at depth 178 m in 626 m water depth (i.e. in near-maximal poleward slope current) at 55.45°N on 12th July 2013 (Fig. 10 "Dye2"). Surveying of the dye patch, as it was tracked northwards, was similar to that in the first dye experiment (section 4.3.1).

As the slope current passed northwards, the relatively shallow canyons here appeared to have a minimal destabilising effect. Based on the separation of iospycnals, the dyed portion of the water column (a density band σ_θ = 27.20–27.24 kg/m^3) stretched vertically by ~ 22% as the slope current failed to follow depth contours and bottom depth increased over the canyons. There is evidence that stretching occurred throughout the upper water column and increased with depth, although estimates for undyed portions of the water column are not demonstrably Lagrangian. This suggests cyclonic relative vorticity over the canyon and a possible overall displacement off-shelf. The degree of downstream recovery was unclear, but overall destabilisation was small. Such behaviour broadly follows model runs by Klinck (1996). Theoretically the effect would be very different for a flow in the opposite direction, in view of the propagation direction of trapped waves (an equatorward flow here could stall propagation and build the amplitude of a canyon perturbation). Canyon mooring SB showed sinking (downslope flow) in a much thicker lower layer than the common "Ekman Drain" (sections 3.1.3, 4.3). At the downstream location SC, a distinct two-day on-shore flow accompanied intensification in poleward, along-slope flow commencing on day 192. Results from the dye release experiment suggest that the slope current, where re-joining the slope, experiences perturbations in the steady flow. These measurements do not enable a transport estimate.

The topography near 55.5°N apparently also causes along-slope Atlantic water to flow onto the Malin shelf (c.f. section 3.2) albeit the precise mechanism is not clear. In July to autumn 2013 about 0.2 Sv of the Atlantic water flowed alongside the Irish Coastal Current (Porter et al. 2018). The Atlantic water mixed with shelf waters as it continued northwards to the Minch and outer Hebridean Shelf [Jones et al. (2020) who also estimate a larger storm-driven transport in December 2013].

Meanders and eddies may cause cross-slope transport and exchange. There are many estimates in the literature of exchange associated with individual eddies. For an overall estimate of exchange from meanders and eddies, we would need their density in space, frequency in time and magnitudes. Satellite remote sensing of sea-surface temperature and fronts can identify such features only when they have a surface signal, and hence does not permit a direct estimate of the exchange involved. Altimetry gives the best prospect for estimating transports: surface slopes imply corresponding surface currents, direct agents of exchange, and identification of eddies via altimetry is well-established, e.g. Chelton et al (2011). For 2010, however, this methodology shows only a few eddies in the Celtic Sea and none on the Malin-Hebrides shelf, despite more being in deep Biscay waters. Identification as in Chelton et al. (2011) filters out eddies with small scales [radius < O(40 km), lifetime < 4 weeks] that probably prevail in shallow, frictional shelf seas. The section 3.3 exchange estimates from altimetry, ~ 1 m^2s^{-1}, account for meanders and eddies at somewhat smaller scales, but still low-pass filtered according to satellite footprint and pass frequency. As the first baroclinic Rossby radius at the shelf break is O(20 km) and greatly reduced on the shelf (LaCasce and Groeskamp, 2020), the eddy field and its associated exchange contribution is most probably under-represented. Counter to this, altimetric estimates (based on geostrophy) include other flows with surface elevation expression. The influence of the large scale is therefore somewhat conflated with mesoscale driven flux. However, the influence of the former is not likely to offset the variance associated with unsampled eddy flux, and so the altimetry-based estimates are likely a lower bound. In addition, some eddy transports might not show a surface signal, though this is less likely if we focus on the shallow shelf break with limited scope for stratification to decouple the flow from the surface slope. For these reasons, we have no firm estimate for eddy contributions to exchange. Comparison with the frequent and much larger Gulf Stream Rings, contributing an average of about 0.25 to 0.6 m^2s^{-1} across the US Atlantic Bight shelf edge (Chaudhuri et al. 2009), would suggest a relatively small value 0.1 m^2s^{-1} or less around the NW European shelf edge.

4.5. Tides, surges, inertial currents

Exchanges on short time scales of order one day or less were often large relative to exchanges from motion on longer time scales (Tables 2, 4, 7) except for the deepest Faroe-Shetland Channel moorings. However, short-term exchange may be ineffective, if it is only movement to-and-fro without constituent transfer to a different water "parcel" or time to change character. Shear dispersion may nevertheless cause longer-term transfer from shorter-period oscillatory motion; shear generates vertical gradients from horizontal gradients and so facilitates vertical diffusion (probably turbulent). To model long-term ^{137}Cs transport on the north-west European continental shelf, Prandle (1984) assumed effective "*x*-" and "*y*-" diffusivities $\alpha U|\boldsymbol{U}|$, $\alpha V|\boldsymbol{U}|$ to represent shear dispersion by largely barotropic tidal currents, $\boldsymbol{U}$ being the predominant M_2 tidal current amplitude; he found a best fit to observed distributions for $\alpha \sim 10^3$ sec. On this basis, and using Table 2 for barotropic tidal contributions, shear dispersion was O(10 m^2s^{-1}) or less *except*: on the Celtic Sea shelf at ST4 and ST5, O(100 m^2s^{-1}); on the Malin and Hebrides shelf at SE, SF, SG and S140, O(20 m^2s^{-1}); on the West Shetland Shelf at H and F, O(20 m^2s^{-1}). Total cross-slope exchange values, labelled $\boldsymbol{u}$ in Tables 2, 4 and 7, take into account tides, surges and inertial currents. However, the caveat remains: short-term displacements may not transfer constituents effectively.

5. Discussion

Variability on short length scales at sub-tidal frequencies, and indeed of internal tides near the Celtic Sea shelf edge, is characteristic of cross-shelf currents in FASTNEt locations and in previous studies (many cited in section 1.3). Such variability questions the representativeness of the measurements made. There is a comparable question of representativeness in time for records not spanning the seasonal cycle (for example). The several short-term moorings, in the respective Celtic Sea

and Malin locations, largely overlap in time and demonstrate spatial variability over distances O(20–30 km). The (relatively few) moorings spanning O(1 year) demonstrate variability on time-scales from days to seasons. As a result, estimates of mean fluxes (from short and long series and drifters) have large confidence intervals or standard errors; however, exchange estimates have relatively small confidence intervals or standard errors (Tables 1-8). Hence the issue is indeed representativeness, given the variations in time and space, rather than determining an estimate from the data obtained. Moorings, drifters and the use of salinity gradients all have their distinct but partly complementary limitations for estimating fluxes and exchanges, as discussed in sections 5.1 and 5.2.

5.1. Reliability of estimates

Mooring-based estimates of fluxes and exchanges appear to be reliable for their specific context, in that (i) different approaches to estimating low-frequency contributions (period > 1–2 days) give consistent results and (ii) there are consistent trends across the slope and in the contributions from different frequencies. Unfortunately, most of the Celtic Sea (2012) and Malin (2013) moorings were of short duration, about two summer weeks, and may represent only a very limited area around their location. Predominance of along-slope flows (greatly exceeding across-slope flow owing to the geostrophic constraint) can make mooring estimates of across-slope flux unrepresentative and uncertain if the flow or depth contours vary in direction. Malin and Faroe-Shetland estimates of cross-slope flux are very sensitive to definition of slope direction. Estimates of cross-slope exchange by smaller-scale processes may be less sensitive to slope direction definition, because their lesser constraint by geostrophy reduces the relative "contamination" by alongslope currents.

Drifters may partly avoid these difficulties of localised moorings and uncertainty in slope direction and representativeness; drifter crossings of depth contours are clear. However, their tracks and hence spatial coverage are not controlled, and indeed are sensitive to conditions during deployment and subsequent interaction with ocean "weather". Response to the 2012 Celtic Sea storm is an example, with initial offshelf crossings into deeper Biscay waters. Deployment location may also introduce biases, e.g. deployment in less than 500 m implies initial crossings of the 500 m contour can only be to deeper water (negative $\overline{u}$). Malin drifters were deployed in more than 600 m but the few crossing the 150 m contour in July 2013 were still within ~ 8 km of each other; their velocities were similar but not widely representative. The 3-hourly interval for drifter locations is also limiting; drifter-based estimates of exchange ½h|u'| only partly include tidal excursions. This is demonstrated by a much smaller increase in exchange estimates from 3-hourly drifter positions (relative to daily positions) than is shown in estimates from moorings' total currents compared with low-frequency currents.

Across-slope transport as internal tides' Stokes Drift may be estimated from moorings with useful accuracy. However, this contribution to transport is a lowest-order difference between Eulerian and Lagrangian approaches. Lagrangian transport onshore is necessarily zero at the coast, so any on– or off-shore Stokes drift tends to be offset by an opposing Eulerian transport (or by along-shore divergence or convergence). Transport estimates depend on appropriate interpretation and distinction between Stokes Drift and its bolus velocity component (section 4.1).

Partition between "flux" and "exchange" depends on (subjective) choices of domain and averaging period. Consider for example a one-month record and variations from week to week. If "flux" is calculated as the average over the month, then weekly departures from that average (as well as within-week variations) will be accounted as "exchange". If "flux" is calculated as the average each week, then only within-week variations will be accounted as "exchange". A similar transfer from "exchange" to "flux" applies if the spatial domain is subdivided. Hence a small domain or short-period averaging favours a time-varying flux and small exchange. A large domain or long-period averaging favours a relatively small or slowly-varying flux but large exchange (with more scope for deviations from the period average, for example). Here, for flux, we have typically averaged over about one month (necessarily less for moorings of shorter duration). Exchange at the long-term Celtic mooring LT1 highlights the effect, being much larger for record-length averaging (Table 2) than for averaging over four M2 periods (Fig. 2e).

Different contributions to exchange are not all detected in all measurements. In particular, drifters do not experience shear dispersion because their depth is constrained, whereas salinity sections, for example, represent the results of all contributions to mixing.

Different seasons were sampled in FASTNEt only by gliders, hydrographic sections, drifters, Faroe-Shetland Channel moorings and a few other moorings. Extension to seasons or years and other shelf sectors, from FASTNEt and other measurements, needs a model validated by such measurements.

5.2. Effective diffusivity and exchange from salinity gradients

The distinctive assumption (limitation), in using a salinity budget to infer effective diffusivity and hence exchange, is that the salinity distribution and large-scale transports controlling it are in a steady state. The inference process then involves (at least) two uncertain factors. (i) Extensive sections are used to estimate the salinity gradient and hence effective diffusivity K; the gradient cannot then be identified with a particular location and depth h. (ii) Equivalence of $-K\partial C/\partial x$ and $\overline{u'C'}$ is used in section 3.5 to estimate exchange as $½h(K/T_d)^{1/2}$; there is uncertainty in the appropriate T_d to use as the time-scale associated with the "eddy" motions presumed to be responsible for the effective diffusivity K. In respect of (i), the estimation of K presumes a salinity maximum which some of the sections (particularly in SSB) do not include. However, in the wider context we know that the maximum exists: salinity values are greater in the slope current than in the adjacent deep ocean and decrease onto the shelf. More uncertainty, most evident in the historical sections (Table 10), lies in the depth range spanned by the sections used to estimate $\partial S/\partial x$; in particular, 35 km from the 500 m depth contour extends to shelf depths ~ 150 m. Confidence in $\partial S/\partial x$ would decrease if shorter sub-sections were used; for alternative locations along the section it is probably better to use instead the dependencies $K \sim h^{-1}$, exchange $\sim h^{½}$. In respect of (ii), the utilized time-scale T_d might partially explain why exchanges estimated in this way consistently exceed the values obtained from moorings and from drifters crossing depth contours. The time-scale T_d is based on the time-integral of the |autocorrelation| of depth integrated flux. T_d is generally evaluated at short-term moorings. Evaluation at long-term moorings gives larger values T_d. At LT1, for example, estimated T_d increases from about 130 h based on 11-day segments to 587 h based on the full-length series u_{res} (712 h based on u_{filt}). It could be argued that the salinity distributions underlying the diffusivity estimates are the result of motions with stochastic character on a wide range of time-scales up to months; the FASTNEt short-term moorings are too short to show relevant autocorrelation over weeks to months. Corresponding reductions in Table 9 values of derived exchange $\sim {T_d}^{-1/2}$ are by factors 0.23 and 0.38 (which bring these estimates closer to those obtained from moorings and drifters).

5.3. Process contributions

We have given (location-specific) estimates for:

- Transports by lenses, O(0.1 m^2s^{-1}) and internal waves, O(0.4 m^2s^{-1}), section 4.1;
- Surface-layer Ekman transport from wind, typically O(0.5 m^2s^{-1}) but up to 5 m^2s^{-1}, section 4.2;

- Bottom Ekman transport for the Malin-Hebrides shelf, from 0.7 m^2s^{-1} to 2.7 m^2s^{-1} as record averages with episodes up to 20 m^2s^{-1}, section 4.3;
- Slope current mis-alignment giving a transport O(0.2 Sv) within 100 km breadth, section 4.4;
- Eddies, possibly less than 0.1 m^2s^{-1}, section 4.4;
- Tides, and wind-driven transports at similarly high frequency, O (5–15 m^2s^{-1}); typically much smaller values resulting from tidal shear dispersion, section 4.5.

As discussed (section 4.5), high-frequency tidal and wind-driven exchanges have large values but effectiveness reduced by the high frequency, perhaps by a factor

(time-scale for transport) / (time-scale for change of water content or characteristics).

Attribution of contributions between tidal and non-tidal motion depends on the tidal analysis. For example, after removing u_{bt}, a harmonic fit of six tidal constituents to the depth mean currents, the long record LT1 still has a significant tidal signal in the residual u_{res} which consequently contributes much exchange. [u_{res} contains the baroclinic tide and depth-mean tidal currents not fitted by the six major constituents analysed.] The (few) longer records have greater scope for an imperfect fit by just six harmonics and hence more scope for exchange from u_{res}.

Additivity of contributions remains a question. If the flow were nearly linear, we would expect separate process contributions to fluxes and exchanges to add to a correct total. However, there are many non-linearities: internal waves and isopycnal displacement amplitudes comparable with layer depths; eddy circulation speeds exceeding translation speeds; currents (tidal, wind-driven and perhaps slope currents) creating turbulence (affecting all motion) and perhaps strong enough to affect propagation of internal waves and eddies. Tidal currents in the Celtic Sea, and their combination with wind-driven flow and storm-driven waves on the Malin-Hebrides and West Shetland shelves, are typically strong enough for their associated turbulence to affect other motion significantly. For example, in a ~ 100 m bottom boundary layer at Celtic Sea mooring ST1, the along-slope flow component decreased to zero near the sea-bed and the off-shelf flow increased. These profiles do not conform to the Ekman spiral and transport that would be expected under an equatorward flow. The bottom 100 m was also where maximum across-shelf exchange took place. Vlasenko et al. (2014) identify a tidal beam originating from the ST1 location and intensified tidal currents in the bottom 100 m which are likely to drive enhanced exchange.

Wind-driven mixing, jointly with (locally-generated) internal waves as in June 2012 near the Celtic Sea shelf break, aids two-way mixing and entrainment between surface and bottom waters. Thereby lateral diffusion is reduced (Palmer et al. 2015), as (i) mixed waters at the shelf break and nearby are in turn helped by the turbulence to break geostrophy, spread laterally and reduce horizontal gradients, (ii) off/on-shelf advection in upper/lower layers leads to some oncoming Atlantic water in the lower layer being mixed upwards and transported back off-shelf, and some shelf water going ocean-wards in the upper layer being mixed deeper and transported back on-shelf. Thus exchange by episodic advection and dispersion is emphasised, rather than linear diffusion.

5.4. Comparison with Huthnance et al. (2009)

The relatively direct estimates of transports (fluxes plus exchanges), from currents at moorings and drifters crossing depth contours, give shelf-break values in the range 1–5 m^2s^{-1} excluding exchanges from tidal currents. The observations are localised (moorings) or spatially indiscriminate (drifters) so that representativeness and resolution by along-shelf sector are problematic. Limited duration also prevents resolution by season from observations alone. There are suggestions of enhanced cross-slope dispersion off-shelf compared with on-shelf, more on the Malin shelf in summer than in winter (from altimetry) but otherwise more in winter than summer (from salinity sections).

Overall along about 5000 km of shelf edge from Biscay to north of Shetland (following the 200 m depth contour closely) fluxes plus exchanges O(2 m^2s^{-1}) amount to O(10 Sv). This exceeds the 2.5 Sv modelled in Huthnance et al. (2009). However, the discussion there suggests processes adding to more than 2 m^2s^{-1} exchange or more than 10 Sv overall in 5000 km. The discrepancy (2.5 *versus* 10 Sv) may be explicable: the Huthnance et al. (2009) exchange estimate is from 1960 to 2004 mean fluxes, onto and off the NW European shelf above and below 150 m depth, in a 12-km-resolution model. Comparably, the total downwelling circulation (a component of exchange based on mean 2012–2013 fluxes) across the north-west European shelf edge (200 m depth contour from Brittany to Norway) is estimated as 1.37 ± 0.24 Sv by a 1.5 km resolution model (Graham et al. 2018b); this is supplemented by lateral exchange (represented by Norwegian Trench outflow) 1.23 ± 0.12 Sv. Much is averaged-out in those estimates: exchanges from time-reversing (e.g. wind-driven) transports; unresolved internal tides and "rough" topography in the coarser-resolution model, for example.

5.5. Implications for shelf-sector budgets

The time-scale to "renew" water on the shelf is proportional to the relevant shelf-sea volume and inversely proportional to the exchange (rate) with the adjacent ocean. Budgeting of transports for a shelf-sector "box" is formalised in Appendix C. Consider along-shelf inflow at the "southern" end, outflow at the "northern" end and exchange across the ocean side. Including shorter-scale processes (in the sense of section 5.4) but excluding tides, indicative exchange is O(2 m^2s^{-1}). For dimensions 500 km along-slope by 100 km across-shelf, typical exchange 1 Sv (2 m^2s^{-1} for 500 km) across the ocean side is large compared with typically 0.1 Sv across each end (inshore of the slope current).

Flux or exchange O(2 m^2s^{-1}) is sufficient to replace the water on an adjacent 400 (or 100) km width of shelf with average depth 100 m in 232 (or 58) days. These shelf widths respectively characterise the broad Celtic Sea (where mean cross-slope transport is weak) and the narrower Malin-Hebrides shelf (which has additional distinct transport tending to reduce the estimate to less than 58 days). Replacement times for the shelf-sea as a whole depend on the penetration of exchange to the interior and the pattern of mean flows. Importance of the interior shelf-sea circulation pattern to transit and flushing times is suggested by large estimates in Hydes et al. (2004): age 400 days for Malin shelf waters at 8°W relative to ocean water crossing the shelf break (but see the caveat in section 2.1); some years for the Celtic Sea (Hydes et al. 2004, c.f. section 2.1) where interior circulation is generally slow and cyclonic (e.g. Brown et al. 2003; Young et al. 2004). The 2014–2015 SSB project in the Celtic Sea (Fig. 1a) found seasonal-scale exchange with the ocean limited to about 100 km of shelf sea nearest the ocean. Velocities in the bottom 40 m of the water column at mooring CCS, 100 km in from the shelf break, were weak (of order 1 km/day) and very varied in direction when averaged over 10.3 days (20 M_2 tidal periods; Ruiz-Castillo et al. 2019). Hence longer-term carbon budgets may depend on episodic events (absent in 2014–2015; Sharples et al. 2019).

Cross-slope transports amount to the volume of NW European shelf seas in about a year (Huthnance, 1991, and references therein relating to the North Sea; Huthnance et al. 2009). In particular, the West Shetland shelf provides inflow to the North Sea with most outflow adjacent to Norway (an exchange viewed on the scale of the whole North Sea). However, much of the northern inflow is confined to the northern North Sea before flowing out again, giving a shorter replacement time there. Large central areas of the North Sea are by-passed and so have time scales of several years for water replacement (Mathis et al. 2013). On such broad shelves – we suggest this includes the Malin-Hebrides shelf – local flushing times can be shorter but the circulation pattern is an important factor in transit times.

Transports of water between deep-ocean and shelf imply transports

of constituents: heat, nutrients, etc. These can be significant. Spingys (2017) estimates net heat input by convergent Celtic Sea eddy transport due to internal waves: O(10 W m^{-2}) over 100 km width of shelf adjacent to the shelf edge, based on eddy transport 0.1 m^2s^{-1} in upper and lower layers and ocean-shelf temperature difference 2.5 °C. [10 W m^{-2} is much less than solar input but over 10^7 s (about 3.8 summer months) can raise the upper 50 m temperature by ~ 0.5° C and is significant in a long-term heat balance.] Stokes' transport contributions to on-/off-shelf transports of other constituents are discussed in Spingys et al. (2020). Typically the Stokes' transport in a 3-layer system is onto-shelf in top and bottom layers and off-shelf between. Thereby a shelf source will typically cause an off-shelf transport (at mid-depth), and a shelf sink will be supplied by on-shelf transport in the top and bottom layers, as the source/sink induces different concentrations in the respective "upstream"/"downstream" layers.

Nitrogen budgeting for the North-West European shelf sea is modelled in Holt et al. (2012; see their Table 3). Specifically, inorganic nitrogen is in approximate long-term balance. Fluxes from and to the ocean for this shelf sea as a whole are about 10 times the advective divergence of inorganic nitrogen in the northern and southern domains, and exceed their combined pelagic phytoplankton uptake – recycling. Hence ocean-shelf exchange, O(1.4 m^2s^{-1}) for Brittany to the Norwegian Trench in Holt et al. (2012), can be important for shelf-sea nutrient budgeting, even on this broad shelf with substantial along-shelf flow. For the Celtic Sea to maintain a pool of nutrient-rich oceanic-origin water, Ruiz-Castillo et al. (2022) estimate that the shelf must be flushed by large episodic events on average every 2–3 years (range of 1.5–6 years).

5.6. Global perspective

Two aspects are considered here: (i) Comparison with other ocean-shelf exchanges around the world, in terms of volume transport and the character of its impact; (ii) significance of the exchanges for global ocean transports. There is a *prima facie* case for (ii) as O(1 m^2s^{-1}) amounts to O(500 Sv) in aggregate around the global ocean margin, far exceeding the transport of any gyre, overturning circulation or the Antarctic Circumpolar Current.

5.6.1. NW European shelf in comparison

Large cross-slope transport contributions have been estimated in various locations for: boundary current meanders, along-shelf flows that converge or are deflected by topography, dense water flowing downslope, Ekman transports from along-shelf winds and below along-slope currents, adjacent eddies. Examples of these are taken in turn in the following.

Western boundary currents partly excurse onto the shelf in some places (and off-shelf elsewhere, implying an exchange when viewed broadly). In the East China Sea, a flux 0.5–3 Sv (mean 1.53 Sv) of the Kuroshio across about 1300 km of 200 m depth contour was found by Zhao and Guo (2011); within this were much larger values of exchange. Ding et al. (2016, 2019) found an on-shelf 1993–2014 mean 1.6 Sv plus comparable exchange and inter-annual variability across the 200 m depth contour. This is a small fraction of the Kuroshio transport but important to the shelf nutrient budget (Ding et al. 2019).

Confluence of the Brazil and Malvinas Currents off the mouth of the La Plata River creates intense mesoscale variability and off shelf transport (Matano et al. 2010). Several currents converging towards Elephant Island off the Antarctic Peninsula lead to localised off-shelf transports totalling O(10 Sv) near and north-east of Elephant Island, with flows towards the shelf between; non-linearity enables crossing of depth contours (Jiang et al. 2013). Modelled South Georgia flushing times for the shelf to depth 300 m are typically 80 days but vary from ~ 20 to 180 days (depending on meltwater, winds and the relative configuration of the Antarctic Circumpolar Current; Young et al. 2014); they suggest transports typically O(1 m^2s^{-1}) but occasionally up to 4 m^2s^{-1}.

Local exchanges O(20 m^2s^{-1}) in 900 m over a canyon in the Gulf of Lions (NW Mediterranean) are indicated in Durrieu de Madron et al. (1999), associated with cross-slope fluctuations of the Liguro-Provençal or Northern Current. However, the aggregate exchange is limited to the Current's total transport O(2 Sv). Estimates by Ulses et al. (2008a, b) for winter storm-enhanced dense water transport down Gulf of Lions canyons are much smaller.

Adriatic Dense Water transports through the Otranto Strait were reviewed and estimated by Vilibić and Orlić (2002) as O(0.3 Sv); they derive from cooling on a northern Adriatic shelf area O(3.10^4 km^2). Carniel et al. (2016) found a similar transport further "upstream" (across a section from Gargano) as a 4-month average after a severe winter (2012), but with a peak of 2 Sv on a time-scale less than 1 day; their average across the 450 m depth contour (length ~ 250 km) just downstream was ~ 0.2 Sv.

Dense Antarctic shelf water export as a whole has been estimated as 5.4 ± 1.7 Sv (Orsi et al. 2002), distributed very unevenly around the Antarctic perimeter O(2.10^4 km). Annual-averaged export of dense High Salinity Shelf Water and Ice Shelf Water from the Ross Sea, ice shelf front length O(1000 km), is estimated as 1 Sv or more (Gordon et al. 2009b). Rickard et al. (2010) find a model estimate ~ 4 Sv for dense Antarctic Bottom Water export from the Ross Sea as a whole across the 1000 m depth contour, length O(1500 km). Overflow at the Filchner sill of Ice Shelf Water from the Filchner–Ronne Ice Shelf, with ice front length O (1000 km), has been estimated as 1.6 ± 0.5 Sv (Foldvik et al. 2004) or perhaps 2.2 Sv with localised transports up to 34 m^2s^{-1} (Daae et al. 2019).

Antarctic exchanges are important for heat transfer and melting ice, albeit moderate in terms of volume replacing shelf water. In modelling and analysing heat transport to the Antarctic shelf, Palóczy et al. (2018) emphasise topography-related local variability of cross-slope transports and the role of eddies. According to the sense of zonal flow over the shelf and slope, bottom Ekman transport may be off-shelf in the Ross Sea or onto-shelf further east adjacent to the Bellingshausen Sea and the West Antarctic Peninsula; Klink and Dinniman (2010) estimate 0.5 m^2s^{-1}. They also estimate 100 m vertical excursions of "warm" Circumpolar Deep Water as the Antarctic Circumpolar Current varies; we infer an associated exchange O(0.5–1 m^2s^{-1}), much influenced by topography, from a lateral Rossby deformation scale ~ 5 km and associated eddies with a time-scale of order 1 week (Moffat and Meredith, 2018; Henley et al. 2019). Transports O(0.5 Sv) warming Belgica Trough and Marguerite Trough, West Antarctic Peninsula, are suggested by Graham et al. (2016).

Mean bottom boundary layer transports off the east Greenland shelf in 248 m near 65.6°N were O(5 m^2s^{-1}) for September 2007 to October 2008, more in winter (Harden et al. 2014, Fig. 5). Additional nearly-barotropic on–off-shelf fluctuations were O(10 m^2s^{-1}). These transports are attributed to winds (local and possibly remote via coastal trapped waves) and off-shelf cyclones. Such large values are probably localised; such transports off the whole east Greenland shelf and amplified by mixing over the slope would lead to along-slope flows greater than observed.

Modelled total transports across the 1500 km-long 100 m contour bounding the Bering Sea were O(1.5 Sv) (Danielson et al. 2012) with strong westward intensification in summer. They depend on Bering Strait through-flow and in winter on wind direction.

Regional upwelling implies ocean-shelf exchange directly related to wind stress in the early stages. Surface Ekman transports of 1 m^2s^{-1} correspond to winds O(10 m s^{-1}; less at low latitudes). Equal correspondence applies to downwelling. In the Benguela upwelling system, Veitch et al. (2009) find strong time-mean upwelling transports, spatially-varying with wind-coast relative orientation; values are typically 2 m^2s^{-1} but 4 m^2s^{-1} in 26°–28°S. Smaller climatological values across the 300 m depth contour were modelled by Muller et al. (2014): less than 1 m^2s^{-1} except for ~ 1.5 m^2s^{-1} off-shelf summer transport in 25°–28°S. Associated along-shelf flow may develop instabilities, eddies

and filaments enhancing cross-slope flows and ocean-shelf exchange. Mesoscale eddies in the southern Benguela upwelling system, some coming from the Agulhas Retroflection (Veitch et al. 2009), may transport as much as 10 m^2s^{-1} oceanward over the deeper slope, based on volumes and probabilities in Rubio et al. (2009), but are much reduced nearer the coast.

Shelf water transported offshore by Gulf Stream Warm Core Rings is estimated as about 0.25 to 0.6 m^2s^{-1} (varying by sector within 50°-75°W; Chaudhuri et al. 2009; 1978–1999 averages). However, annual transports over the whole 25° longitude varied from 2000 km^3 in 1996 to 74000 km^3 in 1990 (~ 0.03 to 1.2 m^2s^{-1}) according to Warm Core Ring intensity.

5.6.2. *Significance for ocean-wide and constituent transports*

Minimal normal transport at the coast is strongly contrasted by hundreds of Sv crossing the shelf break and needing account in any ocean transport budget. By continuity, almost all the water crossing the shelf break must return, but this will generally be at a different depth or horizontal location and after some time during which its properties or contents may have changed. We consider some representative characteristics from shelf-sea and open-ocean perspectives.

Shelf-sea salinity is broadly 95% or more of open-ocean values. [Exceptions are areas under the influence of melting ice and river outflows. However, even the latter have typical salinities exceeding 90% of oceanic values, except where confined as in the Baltic for example.] This usual "flooding" of shelf seas by water with oceanic characteristics illustrates the large factor by which ocean-shelf exchanges typically exceed riverine inputs. There is correspondingly little (short-term) effect on off-shelf oceanic salinity. Freshwater transport 0.21–0.45 Sv during August 2014 to April 2016 by the northern North Atlantic meridional overturning circulation (AMOC; Lozier et al. 2019) greatly exceeds freshwater inputs (0.03 Sv) from north-European shelf seas. However, river discharges totalling O(0.08 Sv) to the Arctic almost all enter the Atlantic via Arctic shelves and make a significant contribution to the AMOC freshwater transport.

Heat input to broad shelf seas is dominated by radiation and exchange with the atmosphere, of order 200 W/m^2 considering the seasonal heating and cooling cycle. For a shelf width 100 km this equates to 2.10^4 kW/m to be compared with a shelf-edge exchange contribution ~ 4.10^3 kW/m from exchange 1 m^2s^{-1} with 1 °C temperature difference (for example, or 10^3 kW/m from the Celtic Sea eddy transport due to internal waves; Spingys (2017) as in section 5.5). The comparison could be reversed for a narrow shelf with large exchange and ocean-shelf temperature difference (albeit the combination would work to reduce the temperature difference). Persistent heat import or export could affect long-term shelf-sea heat balance. On the other hand, these heat transports are tiny compared with open-ocean values. For example, from 26° to 56°N the above transport across ~ 4000 km shelf edge might amount to 16 GW, much less than the 0.8 PW AMOC heat transport convergence between 26° and 56°N (e.g. McCarthy et al. 2015, Holliday et al. 2018).

Dense water formed via cooling and ice formation on high-latitude shelves descends the adjacent slope with some entrainment and consequent increase of transport to form bottom waters. The Orsi et al. (2002) estimate 5.4 ± 1.7 Sv for dense *Antarctic* shelf water export becomes 18 to 20 Sv for the maximum deep meridional circulation integrated around Antarctica with Antarctic Bottom Water forming the lower limb (Kusahara et al. 2017). This bottom water extends through much of the deep global ocean. Its significance derives not so much from the moderate transport (in global terms) as from its distinctiveness: maximum density in the water column, inhibiting mixing and so maintaining identity. *Arctic* Mediterranean dense water (mostly from Atlantic water cooled in the Nordic Seas and on Eurasian shelves) flows over the Greenland-Scotland Ridge. Its ~ 6 Sv (Østerhus et al. 2019) contributes to the lower limb of the AMOC (total 14 – 21 Sv at 26°N, Moat et al. 2020; 8-24 Sv at 56°N, Lozier et al. 2019). Compared with Antarctic Bottom Water its transport is less and it is distinct only in the Atlantic Ocean. *Mediterranean Outflow Water* has been estimated to include just 0.4 Sv of "pure" Mediterranean Water but increases by entrainment to ~ 2 Sv within the Eastern Gulf of Cadiz (Baringer and Price, 1997). It remains distinctive northwards to Rockall Trough (McGrath et al. 2012) and in the North Atlantic sub-tropical gyre.

Densification also takes place on the NW European shelf. Intermediate-density on-shelf flow, 1.5 Sv in 1025.7 to 1027.1 kg m^{-3}, is found to be transformed by seasonal heating and cooling to off-shelf flows of 0.5 Sv in 1023.9 to 1025.7 kg m^{-3} and 1 Sv in 1027.1 to 1027.9 kg m^{-3} (Spingys 2017). These quantities are comparable with those of Mediterranean Outflow Water and probably exceed the Gulf of Lions and Adriatic dense water flows. However, the resulting denser water is not so distinctive relative to the adjacent Atlantic sub-thermocline waters with which it merges. Much of the lighter water is more "visible" as North Sea outflow joining the Norwegian Coastal Current. The quantity transformed on the NW European shelf relates primarily to the shelf-sea area via the seasonal heating and cooling cycle. Extrapolation to the global temperate shelf-sea area suggests perhaps O(10 Sv) of such moderate transformation.

Dense water flow is a potentially important factor in sediment transport (along with sediment supply and other currents disturbing the sea bed), for example in the Gulf of Lions (e.g. Durrieu de Madron et al. 1999) and Adriatic (e.g. Carniel et al. 2016).

Nitrogen cycling in the ocean has large shelf-sea components as reviewed by Voss et al. (2013). 20% of the primary input is from rivers (mainly) and groundwater via shelf seas. A third of marine denitrification is in shelf seas. Shelf-ocean exchange ~ 400.10^{12} g N/yr is about half of the total marine cycle; nitrate from the deep ocean fuels shelf sea production resulting in organic nitrogen passing from shelf sea to ocean. This exchange is most apparent in upwelling regions. The integrated input of upwelled nutrients for primary production is related to the length of shelf with upwelling-favourable winds. Nevertheless, nearly 80% of the fixed water-borne nitrogen supply to the NW European shelf, a downwelling region overall, is estimated to come from the adjacent Atlantic (Holt et al. 2012). This nitrogen supply enables the region to act as a CO_2 "pump", taking up a net 1.3 to 3.3 × 10^{12} mol C/yr from the atmosphere (Wakelin et al. 2012, Kitidis et al. 2019, Legge et al. 2020). Carbon transport off the northwest European shelf is estimated to account for 4.9 to 12% of global shelf carbon fluxes (Legge et al. 2020) in about 3.5% of total global continental shelf area. Uptake 2. 10^{12} mol C/yr from the atmosphere (a "central" estimate above) is about 12% of the global coastal seas' CO_2 sink, ~0.20 Pg C/yr, which in turn is about 12% of global ocean net CO_2 uptake ~ 1.7 Pg C/yr (Roobaert et al. 2019). These substantial proportions considerably exceed the proportions of ocean boundary and ocean area respectively; the NW European shelf breadth enables enough CO_2 uptake within its area to fully utilise the fixed-nitrogen supply. In this case the "pump" is aided by overall downwelling with its associated off-shelf lower-layer transport of organic carbon. In some regions, especially with well-developed upwelling, entrainment of shelf water by meanders and eddies over the slope conveys some shelf-sea production to the open ocean.

Climate change may potentially affect ocean – shelf-sea interaction. Changed wind patterns and storminess may affect up-/down-welling and higher-frequency wind-forced exchange. Overall warming is expected to increase stratification which may inhibit up-/down-welling, nutrient supply to shelf seas and hence their primary production and carbon cycling – but perhaps not for the north-west European shelf (Mathis and Mikolajewicz, 2020). Some future model scenarios alter the oceanic density gradient along-side the NW European shelf to reduce the slope current and North Sea circulation (Holt et al. 2018). Investigation of these possibilities is for future study.

In summary, the volume transports found for the NW European shelf are relatively large in comparison with elsewhere, excepting localised transports from diverted boundary currents and dense bottom currents. However, the significance of transports between ocean and shelf sea

depends more on water properties or its contents, notably nutrients and carbon (organic and inorganic) – and pollutants, not discussed here. The NW European shelf CO_2 "pump" is strong.

5.7. Future work

This overview of FASTNEt and related projects has emphasised the observations and their analysis for transports (categorised as fluxes, i.e. averages over a month or mooring duration, and exchanges from shorter-period variations). This leaves much potential for numerical modelling to develop understanding, resolution and extension in time and space, and projections for alternative scenarios.

Models need to resolve the context and process scales, yet be extensive enough for their results to depend on internal dynamics as well as open boundary conditions, to compare different ocean margin sectors and to compare different seasons. Models enable interpolation and extrapolation, and inherently budget any constituents represented.

In turn, sufficient observations are needed to help formulate and to validate such models for their representation of involved processes. Moreover, conditions must be known at open boundaries (except where flow or any propagating features leave the model), or such boundaries should be far enough away for inputs and boundary influence to decay before reaching the location of interest. The shelf edge is particularly challenging in the need for extensive knowledge (as effects of distant forcing can propagate along-slope to the region of interest) combined with intensive knowledge (because much cross-slope transport is attributable to processes of short scale in length and/or time and measurements show short correlation scales).

Satellite remote sensing can provide extensive contextual information with temporal and spatial coverage of surface conditions: radiance for temperature, colour and (with limited sensitivity) salinity; altimetry for surface slopes from which surface currents may be inferred. However, coarse resolution (in space and time) hitherto probably results in an under-estimate of velocity variance (for example; section 3.3). Future potential Earth observation technologies, such as SEASTAR (Gommenginger et al., 2019), may serve to address this limitation.

Spatially "intensive" means resolving topographic and internal deformation scales as well as those of any particular process of interest, whichever is shorter. This might be achieved with many moorings, which can certainly provide the associated temporal resolution, but may be more practically addressed by repeated survey of the nearby context with towed or autonomous undulating vehicles. Surveys' temporal resolution is relatively coarse but their spatial coverage can address a mooring's limitation of only providing measurements at a possibly unrepresentative point (in horizontal dimensions).

Specifically for transports across depth contours, drogued drifters show promise via frequent location relative to known bathymetry. If this is to take account of depth-varying flow, then drogues are needed at various depths to cover the water column. The lack of control of drifter tracks (and hence where and when they cross depth contours) may be addressed by successive deployments, perhaps guided by some knowledge of currents from contemporary measurements and operational forecasts as increasingly available.

Given a model, individual process contributions to fluxes and exchanges, discussed in section 5.3, may be assessed by (i) differencing results of otherwise "full" numerical model runs with and without any individual process, or (ii) a run for that process alone. Additivity of processes may be assessed by comparing (i) and (ii): for example, comparing "full" – "no winds" with a run having only winds. Deriving such process attribution directly from observations with (statistical) confidence depends on multiple occurrences of identified processes in varying proportions, entailing long (months-years?) time series.

To the extent to which FASTNEt and other measurements validate models, model runs may provide much more systematic coverage. In practice, as exemplified by the Atlantic margin models AMM60 (section 2.4; Guihou et al. 2018) and AMM15 (Graham et al. 2018a), there is coverage of the north-west European shelf and closely-adjacent deep Atlantic with resolution ~ 1.8 km, 1.5 km respectively. With such coverage and a span of some years, ocean-shelf exchange may be diagnosed by sector and time-scale, e.g. for seasonal contributions, and subareas budgeted for salinity, heat and tracers. Such diagnosis is exemplified on a coarse scale in Huthnance et al. (2009) by a run spanning 1960–2004, but only contrasting summer and winter. Budgeting is described in Holt et al. (2009, 2012) and Wakelin et al. (2012). Finer spatial resolution makes little change to upper-layer fluxes but increases exchange estimates, especially in summer, suggesting significant contributions from processes and perhaps topography at scales of a few km (Graham et al. 2018b). There remains scope for more refined analysis by season and sector.

A natural follow-on is for modelling to investigate sensitivities of (shelf-wide) salinity, heat and tracers to ocean-shelf exchange and its variability, in relation to the North Atlantic Oscillation (NAO, for example) and climate change. Indeed, the latter has been investigated using northwest European shelf models run with wider conditions supplied by global climate model projections. Holt et al. (2018) found much reduced 2080–2100 North Sea circulation associated with a few projections. Mathis and Mikolajewicz (2020) projected nutrient supply to the northwest European shelf in 2101–2150 sustained by mixing up of nutrient-enriched Atlantic sub-pycnocline water at the shelf edge. A parallel approach to such sensitivities may be to perturb present-day forcing with principal components of its variability (which may be expected to include a form of NAO).

Shelf-wide sensitivities are mediated by more local shelf-edge exchange and process sensitivities (to climate change in particular) which form another topic to investigate with (especially) fine-resolution models of this demanding context.

In the meantime, the configuration developments in AMM60, under FASTNEt, have been "pulled through" to the UK Met Office operational suite (with resolution ~ 1.5 km; Graham et al. 2018a; Tonani et al. 2019) and benefit the UK Environmental Prediction system (UKEP; Lewis et al. 2018).

6. Conclusions

Overall, exchange values from moorings and drifters are encouragingly consistent, and large, in two senses. (i) Around the British Isles the shelf-break values, O(1 m^2s^{-1} or more) from motion with time-scale exceeding a day, are relatively large in comparison with most regions for which there are estimates, excepting localised transports from diverted boundary currents and dense bottom currents (section 5.6). Strong wind forcing and along-slope flow typically reinforce each other around the NW European shelf edge. Tidal exchanges are larger, several m^2s^{-1}, but their reversals every ~ 6.2 h imply much reduced effectiveness in longer-term transport of constituents that only evolve in days or longer (sections 4.5, 5.3). (ii) Globally, exchanges of order 1 m^2s^{-1} and shelf-edge extent of order 500,000 km imply transports amounting to 500 Sv or more. This greatly exceeds any ocean current transport, albeit the significance varies markedly with shelf sector, depending on distinctive properties of the water or its contents (e.g. nutrients, carbon; section 5.6). Transports across the NW European shelf edge enable this shelf sea to greatly exceed its area-based proportion of the global marine CO_2 "pump".

Effective cross-slope diffusivities from drifters and salinity sections are related to exchanges, but the relation is sensitive to an uncertain estimate of time-scale. FASTNEt values in the wide range 50–700 m^2s^{-1} (sections 3.4, 3.5) were consistent with previous estimates; some smaller estimates were derived from long-term salinity sections across the Hebrides shelf.

The observed cross-slope transports are such as to replace the water on an adjacent 100 km – wide shelf (e.g. Malin-Hebrides shelf) in about 2 months, and would suggest about a year for the broad Celtic Sea and the NW European shelf as a whole. However, on such broad shelves – we

suggest this includes the Malin-Hebrides shelf – the circulation pattern is also an important factor. Flushing times can be shorter locally but large central areas of the Celtic Sea and North Sea are believed to have time scales of several years for water replacement (section 5.5).

Processes of small scale (in space or time), and friction, enable cross-slope transports via relaxation of geostrophic constraints. However, small scales, the complex context (irregular topography) and numerous processes contributing to transports imply a need for models (section 5.7).

FASTNEt measurements were inevitably limited in space and time, disappointingly so in the dearth of longer-duration measurements in the Celtic and Malin contexts. This has rendered the findings susceptible to the particular conditions where and when the measurements took place, especially:

- strong winds and mixing during the June 2012 Celtic Sea deployments (sections 3.1.1, 3.2, 4.1);
- moderate Malin topographic variations (shelf-edge depth and shallow slope canyon; sections 3.2, 3.4, 4.1, 4.4).

The February 1996 (SES) slope current reversal and bottom flow is another "event" (section 3.1.4).

The variability renders FASTNet and other observations insufficient for stable estimates of transports and exchanges, especially if partitioned by sector and season. Indeed, observations suggest that much variability cannot be attributed to season and sector but is related to particular locations and events which may cause significant inter-annual differences (see also sections 2.1, 3.1.3, 5.5).

Nevertheless, FASTNEt has accumulated a wide variety of behaviours and events (Table 15) valuable for model validation. Validated fine-resolution models, as already implemented in UKEP, give the best prospect of fuller space/time coverage, distinguishing shelf sectors and seasons, and of estimating sensitivities of shelf-sea properties to oceanic conditions and ocean-shelf exchange.

CRediT authorship contribution statement

John Huthnance: Conceptualization, Methodology, Writing – original draft, Writing – review & editing. **Jo Hopkins:** Methodology, Formal analysis, Writing – original draft, Writing – review & editing, Visualization. **Bee Berx:** Formal analysis, Investigation. **Andy Dale:** Methodology, Investigation, Writing – original draft. **Jason Holt:** Methodology, Writing – review & editing. **Philip Hosegood:** Methodology, Investigation, Writing – original draft. **Mark Inall:** Conceptualization, Writing – original draft, Investigation, Supervision, Funding acquisition. **Sam Jones:** Formal analysis, Investigation, Writing – original draft. **Benjamin R. Loveday:** Formal analysis, Writing – review & editing. **Peter I. Miller:** Methodology, Writing – review & editing. **Jeff Polton:** Investigation. **Marie Porter:** Methodology, Formal analysis, Investigation. **Carl Spingys:** Methodology, Investigation, Writing – review & editing.

Declaration of Competing Interest

The authors declare that they have no known competing financial interests or personal relationships that could have appeared to influence the work reported in this paper.

Acknowledgements

This work was funded by the UK Natural Environment Research Council FASTNEt consortium grant NE/1030224/1; support also received from NERC National Capability programme CLASS (Climate Linked Atlantic Sector Science), grant number NE/R015953/1. We thank the referees for many constructive comments.

Data Access

All FASTNEt data are managed by the British Oceanographic Data Centre, see https://www.bodc.ac.uk/projects/data_management/uk/fastnet/data_inventories/.

Appendix A. Surface and bottom layers

Surface layer depths $h(t)$ vary through internal tidal and high-frequency wave activity, wind-driven mixing and seasonal stratification, posing a challenge for specifying $h(t)$ as listed in Table S2.

Celtic Sea ADCPs at ST1, ST2, ST4 and ST5 were accompanied by temperature chains through most of the water column. At ST4 and ST5 salinity measurements were also available at four or five depths allowing a potential density time series to be constructed. Modal analysis was performed at ST4 and ST5 using a smooth least-squares approximation of form $a + b\,tanh((z + c)/d)$ to the density profiles. [This form allows any intensity and thickness of pycnocline; the main constraint is anti-symmetry about the mid-density.] On average the 1027.05 kg m^{-3} isopycnal best represented the mode-1 zero crossing point and therefore the division between the surface and bottom layers at ST4 and ST5. This limited density information was converted into a representative isotherm, 12.9 °C, to define a time series $h(t)$. CTD casts near ST1 and ST2 were used to identify the isotherm that best represented the 1027.05 kg m^{-3} isopycnal at these locations, likewise to construct a time series $h(t)$. There was no temperature chain at ST3; fixed $h(t) = 75$ m was therefore chosen based on locating the 1027.05 kg m^{-3} isopycnal from nearby CTD casts. For the deep long-term mooring LT1, monthly climatology – World Ocean Atlas 2013 temperature and salinity (https://www.nodc.noaa.gov/OC5/WOD13/) – suggests 500 m as the maximum depth of the winter mixed layer. The base of the surface layer was therefore taken as 500 m at LT1.

On the *Malin Shelf*, a full water column temperature chain (with salinity also recorded at four or five depths) was deployed at SE and SG. Modal analysis performed on smoothed density profiles was used to determine the isopycnal, and subsequently the isotherm, of the mode-1 zero crossing point, to construct $h(t)$. A fixed $h(t) = 50$ m was chosen for the other sites LA, LB, SB, SD, SC, and 45.5 m at SF, based on three across-shelf CTD sections passing through the moorings.

For the *Hebrides* moorings in 1995–96, limited ADCP data for the upper layer led to the water column being split at 50 m, for S140 only. A depth of 50 m was chosen to be consistent with the Malin shelf moorings slightly further south. It is a reasonable choice for the depth of the surface mixed layer during the summer months. S400 only recorded below 75 m depth, so it was not split into upper and lower layers. For the *Faroe-Shetland Channel*, a constant surface-layer depth was chosen for each mooring location, based on ship-based water column CTD profiles from the Fair Isle-Munken (Faroes) section (lacking fine-resolution water column hydrography during mooring deployments).

Appendix B. "Along-slope" definition, compass error and sensitivities thereto

Potentially large errors in calculated across-slope flux could arise through (a) poorly calibrated ADCP compasses or (b) the definition of along-slope

direction described below and listed in Table S3.

For the *Celtic Sea* moorings, along-slope direction was determined from the long-term mooring LT1 in 1500 m depth on the slope. The average flow direction between 500 and 1000 m was 302°. This is assumed to be near geostrophic and parallel with isobaths, and in fact agrees with the orientation of the local bathymetry. "Along-slope" was therefore taken as 302° at all moorings (short and long term). However, results are sensitive to this definition. At ST3, for example, the calculated across shelf flux, $-4.13\ m^2s^{-1}$, would increase / decrease by $0.4\ m^2s^{-1}$ if the angle of rotation varied by ± 10° (i.e. a sensitivity of 9.9% per 10°). At the other extreme, ST1 and LT1 have sensitivities of 71.7% and 88.6% per 10° respectively. This is mainly due to the prevalent along-slope current at these locations. [The choice of along-slope orientation is just 10° away from maximising the along-slope flux at ST1 and LT1.]

At each *Malin* shelf mooring site, more than one ADCP was deployed to ensure full water column coverage. Adjustments were therefore necessary to correct for compass misalignment. "Along-slope" was chosen (as for the Celtic Sea) as the direction of the mid-depth deployment-mean current, assumed to be near-geostrophic and therefore parallel with the isobaths. There was about 8° difference between mean current directions at sites LA and LB upstream of the canyon. Directions at sites (SD, SC) downstream of the canyon agree more closely. Signs and magnitudes of across-shelf fluxes are very sensitive to the defined "along-shelf" direction and to any ADCP compass errors, (much) more than 100% per 10° except at SF and SG. This is a consequence of strong along-slope fluxes at LA, LB, SB, SC, SD.

At *Hebrides* 1995–1996 (SES) moorings S140, S400, across-slope flux estimates are very sensitive to the definition of "along-shelf" direction and to compass errors, again much more than 100% per 10°. Moreover, identifying the "along-shelf" direction for the SES ADCPs was problematic. The mean direction of flow was assessed for each deployment; estimates varied between −5° and 51° clockwise from North; one outlier was 168° at S140. It was concluded that S400 had a different compass bias for each deployment, corroborated by independent current meter data during deployments 1 and 5. S140 directions were confirmed by independent current meter data. To ameliorate the S400 compass errors, "corrections" were applied so that for each deployment the mean direction in the mid-depth range 100–250 m was N10°E; this chosen "along-shelf" direction is between the mean current-meter direction at S400 (N8.2°E) and the mean direction (N12.1°E) from ADCP and current meter deployments at S140. The realignment of S400 data should provide more realistic cross-shelf estimates, possibly at the expense of real seasonal variability in flux estimates (this procedure minimises net "cross-slope" flow through much of the depth range).

For the *Faroe-Shetland Channel*, using the same approach as for the Celtic Sea, an along-slope direction N 38° E was adopted.

Appendix C. Budgeting

We budget transport estimates in a shelf-sector "box" (Figure S5) with open "south" (S) and "north" (N) ends, coastal and ocean sides, top and bottom (collective index *i*). The ends and sides are fixed, the top is typically a moving isopycnal (notably the free surface) and the bottom may be a moving isopycnal or fixed (the sea floor).

Following Huthnance et al. (2002, *q.v.* for more detail) consider a budget over time T long enough to neglect the rate of change of "box" contents. The inflow *flux* (net transport) at the southern end is $q_S \equiv \iint \boldsymbol{u}.\boldsymbol{n}\, dl\, dz$, averaged over T, where $\boldsymbol{u}$ is the velocity vector, $\boldsymbol{n}$ the inward normal at the southern end, l is the coordinate along the box boundary and z is the vertical coordinate. Define respective outward fluxes (net transports) q_N, q_i likewise. Water conservation gives

$$q_S = q_N + \sum_i q_i \tag{C1}$$

For a box size 500 km (N-S) × 100 km (length of N and S ends), a 1% imbalance in moderate transports O($1\ m^2s^{-1}$) across the open sides (500 + 100 + 100 km) amounts to about 0.35 m per month change in surface elevation. This greatly exceeds observed (non-tidal) variability in surface elevation. Hence over ($T =$) one month the lack of change in surface elevation implies a very close balance in volume transports. Typical exchange 0.5 to 1 Sv across the ocean side is clearly important compared with typically 0.1 Sv across the S and N ends (on the shelf).

Let C_S, C_N and C_i be respective constituent concentrations (C_i is for *inflows* to the box from adjacent waters or the coast); let $\widehat{C} \equiv (C_S + C_N)/2$ be the average concentration for ocean-side outflows; it is assumed that an average salinity can be ascribed to the inflow or outflow on each side. If $\overline{u} \equiv q_i/$(*area of side i*) and $u' = u - \overline{u}$, the transport across side *i* additional to q_i is $\iint |\boldsymbol{u}'.\boldsymbol{n}|\, dl\, dz$ (averaged over T); the equal amounts in and out form *exchange* transport $q_i' \equiv \iint |\boldsymbol{u}'.\boldsymbol{n}|\, dl\, dz/2$. Then constituent conservation gives

$$(C_S - C_N)(q_S + q_N)\Big/2 = \sum_{inflows} |q_i|(\widehat{C} - C_i) + \left[\sum_i q_i' C_i' = -\sum_i Lh_iK_i\partial C\Big/\partial n_i\right] \tag{C2}$$

where $C_i' \equiv \widehat{C} - C_i$, L is the box length, h_i the depth of the side *i*, K_i the diffusion coefficient across side *i* and n_i the outward normal to side *i*. Because fluxes of water add to zero, an arbitrary change of "zero" for constituent concentrations has no effect; only concentration differences are significant. Estimates of terms in (C2) thus depend on (a) measured mean concentration differences for chosen constituents, and (b) averaged statistics for the measured currents.

Appendix D. Supplementary material

Supplementary data to this article can be found online at https://doi.org/10.1016/j.pocean.2022.102760.

References

Aagaard, K., Roach, A.T., 1990. Arctic-Ocean shelf exchange – measurements in Barrow Canyon. J. Geophys. Res. 95 (C10), 18163–18175. https://doi.org/10.1029/JC095iC10p18163.

Allen, S.E., Durrieu de Madron, X., 2009. A review of the role of submarine canyons in deep-ocean exchange with the shelf. Ocean Sci. 5 (4), 607–620.

Amaro, T., Huvenne, V.A.I., Allcock, A.L., Aslam, T., Davies, J.S., Danovaro, R., De Stigter, H.C., Duineveld, G.C.A., Gambi, C., Gooday, A.J., Gunton, L.M., Hall, R., Howell, K.L., Ingels, J., Kiriakoulakis, K., Kershaw, C.E., Lavaleye, M.S.S., Robert, K., Stewart, H., Van Rooij, D., White, M., Wilson, A.M., 2016. The Whittard Canyon – A case study of submarine canyon processes. Prog. Oceanogr. 146, 38–57.

Barber, R.T., 2001. Upwelling ecosystems. In: Steele, J.H., Thorpe, S.A., Turekian, K.K. (Eds.), Encyclopedia of Ocean Sciences. Academic Press, London, pp. 3128–3135. ISBN 0-12-227430-X.

Baringer, M.O., Price, J.F., 1997. Mixing and Spreading of the Mediterranean Outflow. J. Phys. Oceanogr. 27 (8), 1654–1677. https://doi.org/10.1175/1520-0485(1997)027%3C1654:MASOTM%3E2.0.CO;2.

Batchelor, G.K., 1952. Diffusion in a field of homogeneous turbulence. Math. Proc. Camb. Philos. Soc. 48 (2), 345–362.

Beardsley, R.C., Lentz, S.J., 1987. The coastal ocean dynamics experiment collection: an introduction. J. Geophys. Res. 92 (C2), 1455–1463.

Berx, B., Hansen, B., Østerhus, S., Larsen, K.M., Sherwin, T., Jochumsen, K., 2013. Combining in situ measurements and altimetry to estimate volume, heat and salt transport variability through the Faroe-Shetland Channel. Ocean Sci. 9 (4), 639–654.

Biscaye, P.E., Flagg, C.N., Falkowski, P.G., 1994. The Shelf Edge Exchange Processes experiment, SEEP-II: an introduction to hypotheses, results and conclusions. Deep-Sea Res. II 41 (2-3), 231–252.

Brink, K.H., Cowles, T.J., 1991. The coastal transition zone program. J. Geophys. Res. (Oceans) 96, 14637–14647. https://doi.org/10.1029/91JC01206.

Brink, K.H., 2016. Cross-shelf exchange. Ann. Rev. Mar. Sci. 8 (1), 59–78.

Brown, J., Carrillo, L., Fernand, L., Horsburgh, K.J., Hill, A.E., Young, E.F., Medler, K., 2003. Observations of the physical structure and seasonal jet-like circulation of the Celtic Sea and St. George's Channel of the Irish Sea. Cont. Shelf Res. 23 (6), 533–561. https://doi.org/10.1016/S0278-4343(03)00008-6.

Carniel, S., Bonaldo, D., Benetazzo, A., Bergamasco, A., Boldrin, A., Falcieri, F.M., Sclavo, M., Trincardi, F., Langone, L., 2016. Off-shelf fluxes across the southern Adriatic margin: Factors controlling dense-water-driven transport phenomena. Mar. Geol. 375, 44–63.

Chafik, L., Hátún, H., Kjellsson, J., Larsen, K.M.H., Rossby, T., Berx, B., 2020. Discovery of an unrecognized pathway carrying overflow waters toward the Faroe Bank Channel. Nat. Commun. 11, 3721. https://doi.org/10.1038/s41467-020-17426-8.

Chaudhuri, A.H., Bisagni, J.J., Gangopadhyay, A., 2009. Shelf water entrainment by Gulf Stream warm-core rings between 75°W and 50°W during 1978–1999. Continental Shelf Res. 29 (2), 393–406. https://doi.org/10.1016/j.csr.2008.10.001.

Chelton, D.B., Schlax, M.G., Samelson, R.M., 2011. Global observations of nonlinear mesoscale eddies. Prog. Oceanogr. 91 (2), 167–216.

Cooper, L.H.N., Vaux, D., 1949. Cascading over the continental slope of water from the Celtic Sea. J. Mar. Biol. Assoc. UK 28 (3), 719–750.

Corrado, R., Lacorata, G., Palatella, L., Santoleri, R., Zambianchi, E., 2017. General characteristics of relative dispersion in the ocean. Nature Sci. Rep. 7, 46291. https://doi.org/10.1038/srep46291.

Daae, K., Fer, I., Darelius, E., 2019. Variability and mixing of the Filchner Overflow Plume on the continental slope, Weddell Sea. J. Phys. Oceanogr. 49, 3–20.

Daniault, N., Mazé, J.P., Arhan, M., 1994. Circulation and mixing of Mediterranean Water west of the Iberian Peninsula. Deep-Sea Res. 41 (11-12), 1685–1714.

Danielson, S., Hedstrom, K., Aagaard, K., Weingartner, T., Curchitser, E., 2012. Wind-induced reorganization of the Bering shelf circulation. Geophys. Res. Lett. 39 (8), n/a–n/a. https://doi.org/10.1029/2012GL051231.

Davies, A.M., Xing, J., 2005. Modelling processes influencing shelf edge exchange of water and suspended sediment. Continental Shelf Res. 25 (7-8), 973–1001. https://doi.org/10.1016/j.csr.2004.12.006.

Dee, D.P., Uppala, S.M., Simmons, A.J., Berrisford, P., Poli, P., Kobayashi, S., Andrae, U., Balmaseda, M.A., Balsamo, G., Bauer, P., Bechtold, P., Beljaars, A.C.M., van de Berg, L., Bidlot, J., Bormann, N., Delsol, C., Dragani, R., Fuentes, M., Geer, A.J., Haimberger, L., Healy, S.B., Hersbach, H., Hólm, E.V., Isaksen, L., Kållberg, P., Köhler, M., Matricardi, M., McNally, A.P., Monge-Sanz, B.M., Morcrette, J.-J., Park, B.-K., Peubey, C., de Rosnay, P., Tavolato, C., Thépaut, J.-N., Vitart, F., 2011. The ERA-interim reanalysis: configuration and performance of the data assimilation system. Q. J. R. Meteorol. Soc. 137 (656), 553–597.

Ding, R., Huang, D., Xuan, J., Mayer, B., Zhou, F., Pohlmann, T., 2016. Cross-shelf water exchange in the East China Sea as estimated by satellite altimetry and in situ hydrographic measurement. J. Geophys. Res. Oceans 121 (9), 7192–7211. https://doi.org/10.1002/2016JC011972.

Ding, R., Huang, D., Xuan, J., Zhou, F., Pohlmann, T., 2019. Temporal and spatial variations of cross-shelf nutrient exchange in the East China Sea, as estimated by satellite altimetry and in situ measurements. J. Geophys. Res Oceans 124 (2), 1331–1356. https://doi.org/10.1029/2018JC014496.

Dinniman, M.S., Klinck, J.M., Smith, W.O., 2011. A model study of Circumpolar Deep Water on the West Antarctic Peninsula and Ross Sea continental shelves. *Deep-Sea Res.* II 58 (13-16), 1508–1523. https://doi.org/10.1016/j.dsr2.2010.11.013.

Durrieu de Madron, X., Radakovitch, O., Heussner, S., Loye-Pilot, M.D., Monaco, A., 1999. Role of the climatological and current variability on shelf-slope exchanges of particulate matter: evidence from the Rhone continental margin (NW Mediterranean). *Deep-Sea Res.* I 46, 1513–1538.

Fennel, K., 2010. The role of continental shelves in nitrogen and carbon cycling: Northwestern North Atlantic case study. Ocean Sci. 6 (2), 539–548.

Fiúza, A.F.G., Hamann, M., Ambar, I., Díaz del Río, G., González, N., Cabanas, J.M., 1998. Water masses and their circulation off western Iberia during May 1993. Deep-Sea Res. I 45 (7), 1127–1160.

Foldvik, A., Gammelsrød, T., Østerhus, S., Fahrbach, E., Rohardt, G., Schröder, M., Nicholls, K.W., Padman, L., Woodgate, R.A., 2004. Ice shelf water overflow and bottom water formation in the southern Weddell Sea. J. Geophys. Res. Oceans 109, C02015. https://doi.org/10.1029/2003JC002008.

Gommenginger, C., Chapron, B., Hogg, A., Buckingham, C., Fox-Kemper, B., Eriksson, L., Soulat, F., Ubelmann, C., Ocampo-Torres, F., Nardelli, B.B., Griffin, D., Lopez-Dekker, P., Knudsen, P., Andersen, O., Stenseng, L., Stapleton, N., Perrie, W., Violante-Carvalho, N., Schulz-Stellenfleth, J., Woolf, D., Isern-Fontanet, J., Ardhuin, F., Klein, P., Mouche, A., Pascual, A., Capet, X., Hauser, D., Stoffelen, A.d., Morrow, R., Aouf, L., Breivik, Ø., Fu, L.-L., Johannessen, J.A., Aksenov, Y., Bricheno, L., Hirschi, J., Martin, A.C.H., Martin, A.P., Nurser, G., Polton, J., Wolf, J., Johnsen, H., Soloviev, A., Jacobs, G.A., Collard, F., Groom, S., Kudryavtsev, V., Wilkin, J., Navarro, V., Babanin, A., Martin, M., Siddorn, J., Saulter, A., Rippeth, T., Emery, B., Maximenko, N., Romeiser, R., Graber, H., Azcarate, A.A., Hughes, C.W., Vandemark, D., Silva, J.d., Leeuwen, P.J.V., Naveira-Garabato, A., Gemmrich, J., Mahadevan, A., Marquez, J., Munro, Y., Doody, S., Burbidge, G., 2019. SEASTAR: a mission to study ocean submesoscale dynamics and small-scale atmosphere-ocean processes in coastal, shelf and polar seas. Front. Mar. Sci. 6 https://doi.org/10.3389/fmars.2019.00457.

Gordon, A.L., Padman, L., Bergamasco, A., 2009a. Southern Ocean shelf slope exchange: Preface. *Deep-Sea Res.* II 56 (13-14), 775–777. https://doi.org/10.1016/j.dsr2.2008.11.002.

Gordon, A.L., Orsi, A.H., Muench, R., Huber, B.A., Zambianchi, E., Visbeck, M., 2009b. Western Ross Sea continental slope gravity currents. *Deep-Sea Res.* II 56 (13-14), 796–817. https://doi.org/10.1016/j.dsr2.2008.10.037.

Graham, J.A., Dinniman, M.S., Klinck, J.M., 2016. Impact of model resolution for on-shelf heat transport along the West Antarctic Peninsula. J. Geophys. Res. Oceans 121 (10), 7880–7897. https://doi.org/10.1002/2016JC011875.

Graham, J.A., O'Dea, E., Holt, J., Polton, J., Hewitt, H.T., Furner, R., Guihou, K., Brereton, A., Arnold, A., Wakelin, S., Sanchez, J.M.C., Mayorga Adame, C.G., 2018a. AMM15: a new high-resolution NEMO configuration for operational simulation of the European north-west shelf. Geosci. Model Dev. 11, 681–696. https://doi.org/10.5194/gmd-11-681-2018.

Graham, J.A., Rosser, J.P., O'Dea, E., Hewitt, H.T., 2018b. Resolving shelf break exchange around the European Northwest Shelf. Geophys. Res. Lett. 45 (22), 12,386–12,395. https://doi.org/10.1029/2018GL079399.

Gröger, M., Maier-Reimer, E., Mikolajewicz, U., Moll, A., Sein, D., 2013. NW European shelf under climate warming: implications for open ocean - shelf exchange, primary production, and carbon absorption. Biogeosciences 10 (6), 3767–3792. https://doi.org/10.5194/bg-10-3767-201310.5194/bg-10-3767-2013-supplement.

Guarracino, M., Barnier, B., Marsaleix, P., Durrieu de Madron, X., Monaco, A., Escoubeyrou, K., Marty, J.-C., 2006. Transfer of particulate matter from the northwestern Mediterranean continental margin: Variability and controlling factors. J. Mar. Res. 64 (2), 195–220.

Guihou, K., Polton, J., Harle, J., Wakelin, S., O'Dea, E., Holt, J., 2018. Kilometric scale modeling of the North West European shelf seas: Exploring the spatial and temporal variability of internal tides. J. Geophys. Res. (Oceans) 123 (1), 688–707. https://doi.org/10.1002/2017JC012960.

Harden, B.E., Pickart, R.S., Renfrew, I.A., 2014. Offshore transport of dense water from the east Greenland shelf. J. Phys. Oceanogr. 44 (1), 229–245. https://doi.org/10.1175/JPO-D-12-0218.1.

Henley, S.F., Schofield, O.M., Hendry, K.R., et al., 2019. Variability and change in the west Antarctic Peninsula marine system: Research priorities and opportunities. Prog. Oceanogr. 173, 208–237.

Heussner, S., Durrieu de Madron, X., Radakovitch, O., Beaufort, L., Biscaye, P.E., Carbonne, J., Delsaut, Nicole, Etcheber, H., Monaco, A., 1999. Spatial and temporal patterns of downward particle fluxes on the continental slope of the Bay of Biscay (northeastern Atlantic). Deep-Sea Res. II 46 (10), 2101–2146.

Hill, A.E., Mitchelson-Jacob, E.G., 1993. Observations of a poleward-flowing saline core on the continental slope west of Scotland. Deep-Sea Res. 40 (7), 1521–1527.

Hill, A.E., Horsburgh, K.J., Garvine, R.W., Gillibrand, P.A., Slesser, G., Turrell, W.R., Adams, R.D., 1997. Observations of a density-driven recirculation of the Scottish coastal current in the Minch. Estuar. Coast. Shelf Sci. 45 (4), 473–484.

Hill, A.E., Souza, A.J., Jones, K., Simpson, J.H., Shapiro, G.I., McCandliss, R., Wilson, H., Leftley, J., 1998. The Malin cascade in winter 1996. J. Mar. Res. 56 (1), 87–106.

Holliday, N.P., Cunningham, S.A., Johnson, C., Gary, S.F., Griffiths, C., Read, J.F., Sherwin, T., 2015. Multi-decadal variability of potential temperature, salinity and transport in the eastern sub-polar North Atlantic. J. Geophys. Res. (Oceans) 120, 5945–5967.

Holliday, N.P., Bacon, S., Cunningham, S.A., Gary, S.F., Karstensen, J., King, B.A., Li, F., Mcdonagh, E.L., 2018. Subpolar North Atlantic overturning and gyre-scale circulation in the summers of 2014 and 2016. J. Geophys. Res. (Oceans) 123 (7), 4538–4559.

Holt, J., Wakelin, S., Huthnance, J., 2009. Down-welling circulation of the northwest European continental shelf: A driving mechanism for the continental shelf carbon pump. Geophys. Res. Lett. 36, L14602.

Holt, J., Butenschoen, M., Wakelin, S.L., Artioli, Y., Allen, J.I., 2012. Oceanic controls on the primary production of the northwest European continental shelf: model experiments under recent past conditions and a potential future scenario. Biogeosciences 9, 97–117. https://doi.org/10.5194/bg-9-97-2012.

Holt, J., Allen, J.I., Anderson, T.R., Brewin, R., Butenschon, M., Harle, J., Huse, G., Lehodey, P., Lindemann, C., Memery, L., Salihoglu, B., Senina, I., Yool, A., 2014. Challenges in integrative approaches to modelling the marine ecosystems of the North Atlantic: Physics to Fish and Coasts to Ocean. Prog. Oceanogr. 129, 285–313. https://doi.org/10.1016/j.pocean.2014.04.024.

Holt, J., Polton, J., Huthnance, J., Wakelin, S., O'Dea, E., Harle, J., Yool, A., Artioli, Y., Blackford, J., Siddorn, J., Inall, M., 2018. Climate-driven change in the North Atlantic and Arctic Oceans can greatly reduce the circulation of the North Sea. Geophys. Res. Lett. 45 (21), 11,827–11,836.

Hopkins, J., Sharples, J., Huthnance, J.M., 2012. On-shelf transport of slope water lenses within the seasonal pycnocline. Geophys. Res. Lett. 39 (8), n/a–n/a. https://doi.org/10.1029/2012GL051388.

Hopkins, J.E., Stephenson, G.R., Green, J.A.M., Inall, M.E., Palmer, M.R., 2014. Storms modify baroclinic energy fluxes in a seasonally stratified shelf sea: Inertial-tidal interaction. J. Geophys. Res. (Oceans) 119 (10), 6863–6883.
Houghton, R.W., Aikman, F., Ou, H.W., 1988. Shelf-slope frontal structure and cross-shelf exchange at the New-England shelf-break. Cont. Shelf Res. 8 (5-7), 687–710.
Houghton, R.W., 1995. The bottom boundary-layer structure in the vicinity of the Middle Atlantic Bight shelfbreak front. Cont. Shelf Res. 15 (10), 1173–1194.
Huthnance, J.M., 1986. The Rockall slope current and shelf-edge processes. Proc. Roy. Soc. Edinburgh 88, 83–101.
Huthnance, J., 1991. Physical oceanography of the North Sea. Ocean and Shoreline Management 16 (3-4), 199–231.
Huthnance, J.M., 1995. Circulation, exchange and water masses at the ocean margin: the role of physical processes at the shelf edge. Prog. Oceanogr. 35 (4), 353–431.
Huthnance, J.M., Coelho, H., Griffiths, C.R., Knight, P.J., Rees, A.P., Sinha, B., Vangriesheim, A., White, M., Chatwin, P.G., 2001. Physical structures, advection and mixing in the region of Goban Spur. Deep-Sea Res. II 48 (14-15), 2979–3021.
Huthnance, J.M., Van Aken, H.M., White, M., Barton, E.D., Le Cann, B., Coelho, E.F., Alvarez Fanjul, E., Miller, P., Vitorino, J., 2002. Ocean margin exchange – water flux estimates. J. Marine Systems 32 (1-3), 107–137.
Huthnance, J.M., Holt, J.T., Wakelin, S.L., 2009. Deep ocean exchange with west-European shelf seas. Ocean Sci. 5 (4), 621–634.
Huthnance, J.M., Inall, M.E., Fraser, N.J., 2020. Oceanic density/pressure gradients and slope currents. J. Phys. Oceanogr. 50, 1643–1654.
Hydes, D.J., Gowen, R.J., Holliday, N.P., Shammon, T., Mills, D., 2004. External and internal control of winter concentrations of nutrients (N, P and Si) in north-west European shelf seas. Estuarine Coastal and Shelf Sci. 59 (1), 151–161.
Inall, M.E., Rippeth, T.P., Sherwin, T.J., 2000. Impact of nonlinear waves on the dissipation of internal tidal energy at a shelf break. J. Geophys. Res. (Oceans) 105 (C4), 8687–8705.
Inall, M.E., Shapiro, G.I., Sherwin, T.J., 2001. Mass transport by non-linear internal waves on the Malin Shelf. Cont. Shelf Res. 21 (13-14), 1449–1472.
Inall, M., Gillibrand, P., Griffiths, C., MacDougal, N., Blackwell, K., 2009. On the oceanographic variability of the North-West European Shelf to the West of Scotland. J. Marine Systems 77 (3), 210–226.
Inall, M., Aleynik, D., Boyd, T., Palmer, M., Sharples, J., 2011. Internal tide coherence and decay over a wide shelf sea. Geophys. Res. Lett. 38 (23), n/a–n/a. https://doi.org/10.1029/2011GL049943.
Jiang, M., Charette, M.A., Measures, C.I., Zhu, Y., Zhou, M., 2013. Seasonal cycle of circulation in the Antarctic Peninsula and the off-shelf transport of shelf waters into southern Drake Passage and Scotia Sea. Deep-Sea Res. II 90, 15–30.
Johnson, J., Chapman, P., 2011. Preface "Deep Ocean Exchange with the Shelf (DOES)". Ocean Sci. 7, 101–109. https://doi.org/10.5194/os-7-101-2011.
Jones, S.C., 2016. Shelf Edge Exchange and the Influence on Coastal Oceanography. University of Aberdeen. PhD dissertation.
Jones, S., Cottier, F., Inall, M., Griffiths, C., 2018. Decadal variability on the Northwest European continental shelf. Prog. Oceanogr. 161, 131–151.
Jones, S., Inall, M., Porter, M., Graham, J.A., Cottier, F., 2020. Storm-driven across-shelf oceanic flows into coastal waters. Ocean Sci. 16, 389–403. https://doi.org/10.5194/os-16-389-2020.
Jordi, A., Orfila, A., Basterretxea, G., Tintoré, J., 2005. Shelf-slope exchanges by frontal variability in a steep submarine canyon. Prog. Oceanogr. 66 (2-4), 120–141.
Jordi, A., Basterretxea, G., Orfila, A., Tintoré, J., 2006. Analysis of the circulation and shelf-slope exchanges in the continental margin of the northwestern Mediterranean. Ocean Sci. 2 (2), 173–181.
Kitidis, V., Shutler, J.D., Ashton, I., Warren, M., Brown, I., Findlay, H., Hartman, S.E., Sanders, R., Humphreys, M., Kivimäe, C., Greenwood, N., Hull, T., Pearce, D., McGrath, T., Stewart, B.M., Walsham, P., McGovern, E., Bozec, Y., Gac, J.-P., van Heuven, S.M.A.C., Hoppema, M., Schuster, U., Johannessen, T., Omar, A., Lauvset, S. K., Skjelvan, I., Olsen, A., Steinhoff, T., Körtzinger, A., Becker, M., Lefevre, N., Diverrès, D., Gkritzalis, T., Cattrijsse, A., Petersen, W., Voynova, Y.G., Chapron, B., Grouazel, A., Land, P.E., Sharples, J., Nightingale, P.D., 2019. Winter weather controls net influx of atmospheric CO_2 on the north-west European shelf. Nature Scientific Reports 9 (1). https://doi.org/10.1038/s41598-019-56363-5.
Klinck, J.M., 1996. Circulation near submarine canyons: A modeling study. J. Geophys. Res. (Oceans) 101 (C1), 1211–1223. https://doi.org/10.1029/95JC02901.
Kusahara, K., Williams, G.D., Tamura, T., Massom, R., Hasumi, H., 2017. Dense shelf water spreading from Antarctic coastal polynyas to the deep Southern Ocean: A regional circumpolar model study. J. Geophys. Res. Oceans 122 (C8), 6238–6253. https://doi.org/10.1002/2017JC012911.
LaCasce, J.H., Bower, A., 2000. Relative dispersion in the subsurface North Atlantic. J. Mar. Res. 58 (6), 863–894.
LaCasce, J.H., Groeskamp, S., 2020. Baroclinic modes over rough bathymetry and the surface deformation radius. J. Phys. Oceanogr. 50 (10), 2835–2847.
Lee, C.M., Brink, K.H., 2010. Observations of storm-induced mixing and Gulf Stream Ring incursion over the southern flank of Georges Bank: Winter and summer 1997. J. Geophys. Res. 115 (C8), C08008. https://doi.org/10.1029/2009JC005706.
Legge, O., Johnson, M., Hicks, N., Jickells, T., Diesing, M., Aldridge, J., Andrews, J., Artioli, Y., Bakker, D.C.E., Burrows, M.T., Carr, N., Cripps, G., Felgate, S.L., Fernand, L., Greenwood, N., Hartman, S., Kröger, S., Lessin, G., Mahaffey, C., Mayor, D.J., Parker, R., Queirós, A.M., Shutler, J.D., Silva, T., Stahl, H., Tinker, J., Underwood, G.J.C., Van Der Molen, J., Wakelin, S., Weston, K., Williamson, P., 2020. Carbon on the northwest European shelf: contemporary budget and future influences. Front. Mar. Sci. 7, 143. https://doi.org/10.3389/fmars.2020.00143.
Lewis, H.W., Castillo Sanchez, J.M., Graham, J., Saulter, A., Bornemann, J., Arnold, A., Fallmann, J., Harris, C., Pearson, D., Ramsdale, S., Martínez-de la Torre, A., Bricheno, L., Blyth, E., Bell, V.A., Davies, H., Marthews, T.R., O'Neill, C., Rumbold, H., O'Dea, E., Brereton, A., Guihou, K., Hines, A., Butenschon, M., Dadson, S.J., Palmer, T., Holt, J., Reynard, N., Best, M., Edwards, J., Siddorn, J., 2018. The UKC2 regional coupled environmental prediction system. Geosci. Model Dev. 11 (1), 1–42. https://doi.org/10.5194/gmd-11-1-201810.5194/gmd-11-1-2018-supplement.
Lo Iacono, C., Guillén, J., Guerrero, Q., Durán, R., Wardell, C., Hall, R.A., Aslam, T., Carter, G.D.O., Gales, J.A., Huvenne, V.A.I., 2020. Bidirectional bedform fields at the head of a submarine canyon (NE Atlantic). Earth Planet. Sci. Letters 542, 116321. https://doi.org/10.1016/j.epsl.2020.116321.
Lozier, M.S., Li, F., Bacon, S., Bahr, F., Bower, A.S., Cunningham, S.A., de Jong, M.F., de Steur, L., deYoung, B., Fischer, J., Gary, S.F., Greenan, B.J.W., Holliday, N.P., Houk, A., Houpert, L., Inall, M.E., Johns, W.E., Johnson, H.L., Johnson, C., Karstensen, J., Koman, G., Le Bras, I.A., Lin, X., Mackay, N., Marshall, D.P., Mercier, H., Oltmanns, M., Pickart, R.S., Ramsey, A.L., Rayner, D., Straneo, F., Thierry, V., Torres, D.J., Williams, R.G., Wilson, C., Yang, J., Yashayaev, I., Zhao, J., 2019. A sea change in our view of overturning in the subpolar North Atlantic. Science 363 (6426), 516–521.
Liu, K.K., Atkinson, L., Quiñones, R.A., Talaue-McManus, L., 2010. Biogeochemistry of Continental Margins in a Global Context. In: Liu, K.K., Atkinson, L., Quiñones, R.A., Talaue-McManus, L., Liu, K.K., Atkinson, L., Quiñones, R.A., Talaue-McManus, L. (Eds.), Carbon and Nutrient Fluxes in Continental Margins: A Global Synthesis. Springer.
Luneva, M.V., Ivanov, V.V., Tuzov, F., Aksenov, Y., Harle, J.D., Kelly, S., Holt, J.T., 2020. Hotspots of dense water cascading in the Arctic Ocean: Implications for the Pacific Water pathways. *J. Geophys. Res.* (Oceans) online. 125 (10) https://doi.org/10.1029/2020JC016044.
McCarthy, G.D., Smeed, D.A., Johns, W.E., Frajka-Williams, E., Moat, B.I., Rayner, D., Baringer, M.O., Meinen, C.S., Collins, J., Bryden, H.L., 2015. Measuring the Atlantic Meridional Overturning Circulation at 26°N. Prog. Oceanogr. 130, 91–111.
McDougall, T.J., McIntosh, P.C., 2001. The temporal-residual-mean velocity. ii: Isopycnal interpretation and the tracer and momentum equations. J. Phys. Oceanogr. 31, 1222–1246.
McGrath, T., Nolan, G., McGovern, E., 2012. Chemical characteristics of water masses in the Rockall Trough. Deep-Sea Res. I 61, 57–73.
McPhee-Shaw, E., 2006. Boundary-interior exchange: Reviewing the idea that internal-wave mixing enhances lateral dispersal near continental margins. Deep-Sea Res. II 53 (1-2), 42–59.
Madec G, the NEMO team, 2016. NEMO reference manual 3_6_STABLE: "NEMO ocean engine". Note du Pôle de modélisation, Institut Pierre-Simon Laplace (IPSL), France, No 27 ISSN No 1288-1619.
Marsh, R., Haigh, I.D., Cunningham, S.A., Inall, M.E., Porter, M., Moat, B.I., 2017. Large-scale forcing of the European Slope Current and associated inflows to the North Sea. Ocean Sci. 13 (2), 315–335.
Matano, R.P., Palma, E.D., Piola, A.R., 2010. The influence of the Brazil and Malvinas Currents on the Southwestern Atlantic Shelf circulation. Ocean Sci. 6, 983–995. https://doi.org/10.5194/os-6-983-2010.
Mathis, M., Mikolajewicz, U., 2020. The impact of meltwater discharge from the Greenland ice sheet on the Atlantic nutrient supply to the northwest European shelf. Ocean Sci. 16 (1), 167–193.
Mathis, M., Mayer, B., Pohlmann, T., 2013. An uncoupled dynamical downscaling for the North Sea: method and evaluation. Ocean Model. 72, 153–166. https://doi.org/10.1016/j.ocemod.2013.09.004.
Mienert, J., Abrantes, F., Auffret, G., Evans, D., Kenyon, N., Kuijpers, A., Sejrup, H.P., van Weering, T., 1998. European North Atlantic Margin (ENAM I): Sediment pathways, processes, and fluxes - an introduction. Marine Geol. 152 (1-3), 3–6.
Moat, B.I., Smeed, D.A., Frajka-Williams, E., Desbruyères, D.G., Beaulieu, C., Johns, W. E., Rayner, D., Sanchez-Franks, A., Baringer, M.O., Volkov, D., Jackson, L.C., Bryden, H.L., 2020. Pending recovery in the strength of the meridional overturning circulation at 26° N. Ocean Sci. 16 (4), 863–874. https://doi.org/10.5194/os-16-863-2020.
Moffat, C., Meredith, M., 2018. Shelf–ocean exchange and hydrography west of the Antarctic Peninsula: a review. Phil. Trans. R. Soc. A 376 (2122), 20170164. https://doi.org/10.1098/rsta.2017.0164.
Monaco, A., Biscaye, P., Soyer, J., Pocklington, R., Heussner, S., 1990. Particle fluxes and ecosystem response on a continental margin – the 1985–1988 Mediterranean ECOMARGE experiment. Continental Shelf Res. 10 (9-11), 809–839.
Monteiro, P.M.S., Dewitte, B., Scranton, M.I., Paulmier, A., van der Plas, A.K., 2011. The role of open ocean boundary forcing on seasonal to decadal-scale variability and long-term change of natural shelf hypoxia. Environmental Res. Lett. 6 (2), 025002. https://doi.org/10.1088/1748-9326/6/2/025002.
Moseidjord, H., Svendsen, H., Slagstad, D., 1999. Sensitivity studies of circulation and ocean-shelf exchange off northern Norway. Sarsia 84, 191–198.
Muller, A.A., Reason, C.J.C., Schmidt, M., Mohrholz, V., Eggert, A., 2014. Computing transport budgets along the shelf and across the shelf edge in the northern Benguela during summer (DJF) and winter (JJA). J. Marine Systems 140, 82–91.
Muller-Karger, F.E., Varela, R., Thunell, R., Luerssen, R., Hu, C., Walsh, J.J., 2005. The importance of continental margins in the global carbon cycle. Geophys. Res. Lett. 32, L01602.
O'Dea, E.J., Arnold, A.K., Edwards, K.P., Furner, R., Hyder, P., Martin, M.J., Siddorn, J. R., Storkey, D., While, J., Holt, J.T., Liu, H., 2012. An operational ocean forecast system incorporating NEMO and SST data assimilation for the tidally driven European North-West shelf. Journal of Operational Oceanography 5, 3–17. https://doi.org/10.1080/1755876X.
Østerhus, S., Woodgate, R., Valdimarsson, H., Turrell, B., de Steur, L., Quadfasel, D., Olsen, S.M., Moritz, M., Lee, C.M., Larsen, K.M.H., Jónsson, S., Johnson, C., Jochumsen, K., Hansen, B., Curry, B., Cunningham, S., Berx, B., 2019. Arctic

Mediterranean exchanges: a consistent volume budget and trends in transports from two decades of observations. Ocean Sci. 15 (2), 379–399. https://doi.org/10.5194/os-15-379-201910.5194/os-15-379-2019-supplement.
Orsi, A.H., Smethie, W.M., Bullister, J.L., 2002. On the total input of Antarctic waters to the deep ocean: A preliminary estimate from chlorofluorocarbon measurements. *J. Geophys. Res.* (*Oceans)* 107 (C8), 3122. https://doi.org/10.1029/2001JC000976.
Painter, S.C., Hartman, S.E., Kivimäe, C., Salt, L.A., Clargo, N.M., Bozec, Y., Daniels, C.J., Jones, S.C., Hemsley, V.S., Munns, L.R., Allen, S.R., 2016. Carbon exchange between a shelf sea and the ocean: The Hebrides Shelf, west of Scotland. *J. Geophys. Res.* (*Oceans)* 121 (7), 4522–4544.
Palmer, M.R., Stephenson, G.R., Inall, M.E., Balfour, C., Düsterhus, A., Green, J.A.M., 2015. Turbulence and mixing by internal waves in the Celtic Sea determined from ocean glider microstructure measurements. J. Mar. Systems 144, 57–69.
Palóczy, A., Gille, S.T., McClean, J.L., 2018. Oceanic heat delivery to the Antarctic continental shelf: Large-scale, low-frequency variability. J. Geophys. Res. Oceans 123 (11), 7678–7701. https://doi.org/10.1029/2018JC014345.
Pauly, D., Christensen, V., Guenette, S., et al., 2002. Towards sustainability in world fisheries. Nature 418, 689–695.
Pingree, R.D., 1979. Baroclinic eddies bordering the Celtic Sea in late summer. J. Mar. Biol. Assoc. UK 59 (3), 689–703.
Pingree, R.D., Le Cann, B., 1989. Celtic and Armorican slope and shelf residual currents. Prog. Oceanogr. 23 (4), 303–338.
Pingree, R.D., Le Cann, B., 1990. Structure, strength and seasonality of the slope currents in the Bay of Biscay region. J. Mar. Biol. Assoc. UK 70 (4), 857–885.
Pingree, R.D., New, A.L., 1995. Structure, seasonal development and sunglint spatial coherence of the internal tide on the Celtic and Armorican Shelves and in the Bay of Biscay. Deep Sea Res. I 42 (2), 245–284. https://doi.org/10.1016/0967-0637(94)00041-P.
Pingree, R.D., Sinha, B., Griffiths, C.R., 1999. Seasonality of the European slope current (Goban Spur) and ocean margin exchange. Cont. Shelf. Res. 19 (7), 929–975. https://doi.org/10.1016/S0278-4343(98)00116-2.
Porter, M., Inall, M.E., Green, J.A.M., Simpson, J.H., Dale, A.C., Miller, P.I., 2016a. Drifter observations in the summer time Bay of Biscay slope current. J. Mar. Systems 157, 65–74.
Porter, M., Inall, M.E., Hopkins, J., Palmer, M.R., Dale, A.C., Aleynik, D., Barth, J.A., Mahaffey, C., Smeed, D.A., 2016b. Glider observations of enhanced deep water upwelling at a shelf break canyon: A mechanism for cross-slope carbon and nutrient exchange. *J. Geophys. Res. (Oceans)* 121 (10), 7575–7588.
Porter, M., Dale, A.C., Jones, S., Siemering, B., Inall, M.E., 2018. Cross-slope flow in the Atlantic Inflow Current driven by the on shelf deflection of a slope current. Deep-Sea Research I 140, 173–185.
Prandle, D., 1984. A modelling study of the mixing of ^{137}Cs in the seas of the European continental shelf. *Phil. Trans. Roy. Soc. Lond.* A 310, 407–436.
Proctor, R., Chen, F., Tett, P., 2003. Carbon and nitrogen fluxes across the Hebridean shelf break, estimated by a 2D coupled physical-microbiological model. Sci. Total Environ. 314-316, 787–800.
Rickard, G., Roberts, M., Williams, M., Dunn, A., Smith, M., 2010. Mean circulation and hydrography in the Ross Sea sector, Southern Ocean: Representation in numerical models. Antarct. Sci. 22 (5), 533–558. https://doi.org/10.1017/S0954102010000246.
Robinson, A.R., Brink, K.H., Ducklow, H.W., Jahnke, R.A., Rothschild, B.J., 2005. Interdisciplinary multiscale coastal dynamical processes and interaction. Robinson, A.R., Brink, K.H., (Eds.), The Sea 13, pp. 3–35.
Roobaert, A., Laruelle, G.G., Landschützer, P., Gruber, N., Chou, L., Regnier, P., 2019. The spatiotemporal dynamics of the sources and sinks of CO_2 in the global coastal ocean. Global Biogeochem. Cycles 33 (12), 1693–1714.
Rubio, A., Blanke, B., Speich, S., Grima, N., Roy, C., 2009. Mesoscale eddy activity in the southern Benguela upwelling system from satellite altimetry and model data. Prog. Oceanogr. 83 (1-4), 288–295.
Ruiz-Castillo, E., Sharples, J., Hopkins, J., Woodward, M., 2019. Seasonality in the cross-shelf physical structure of a temperate shelf sea and the implications for nitrate supply. Prog. Oceanogr. 177, 101985. https://doi.org/10.1016/j.pocean.2018.07.006.
Ruiz-Castillo, E, Hopkins, J, Sharples, J, 2022. Wind and internal tide drive on-shelf nutrient transport in a temperate shelf sea. J. Geophys. Res. Oceans, revised.
Savidge, D.K., Bane, J.M., 2001. Wind and Gulf Stream influences on along-shelf transport and off-shelf export at Cape Hatteras, North Carolina. J. Geophys. Res. 106 (C6), 11505–11527. https://doi.org/10.1029/2000JC000574.
Schauer, U., Muench, R.D., Rudels, B., Timokhov, L., 1997. Impact of eastern Arctic shelf waters on the Nansen Basin intermediate layers. J. Geophys. Res. Oceans 102 (C2), 3371–3382.
Serpette, A., Le Cann, B., Colas, F., 2006. Lagrangian circulation of the North Atlantic Central Water over the abyssal plain and continental slopes of the Bay of Biscay: description of selected mesoscale features. Scientia Marina 70 (Suppl. S1), 27–42.
Shapiro, G.I., Hill, A.E., 1997. Dynamics of Dense Water Cascades at the Shelf Edge. J. Phys. Oceanogr. 27 (11), 2381–2394.
Sharples, J., Mayor, D.J., Poulton, A.J., Rees, A.P., Robinson, C., 2019. Shelf Sea Biogeochemistry: Nutrient and carbon cycling in a temperate shelf sea water column. Prog. Oceanogr. 177, 102182. https://doi.org/10.1016/j.pocean.2019.102182.
Sherwin, T.J., Williams, M.O., Turrell, W.R., Hughes, S.L., Miller, P.I., 2006. A description and analysis of mesoscale variability in the Faroe-Shetland Channel. J. Geophys. Res. 111 (C3), 17 pp. https://doi.org/10.1029/2005JC002867.
Sherwin, T.J., Aleynik, D., Dumont, E., Inall, M.E., 2015. Deep drivers of mesoscale circulation in the central Rockall Trough. Ocean Sci. 11 (3), 343–359. https://doi.org/10.5194/os-11-343-201510.5194/os-11-343-2015-supplement.
Siedlecki, S.A., Archer, D.E., Mahadevan, A., 2011. Nutrient exchange and ventilation of benthic gases across the continental shelf break. J. Geophys. Res. (Oceans) 116, C06023.
Simpson, J.H., McCandliss, R.R., 2013. "The Ekman Drain": a conduit to the deep ocean for shelf material. Ocean Dyn. 63 (9-10), 1063–1072. https://doi.org/10.1007/s10236-013-0644-y.
Skliris, N., Hecq, J.H., Djenidi, S., 2002. Water fluxes at an ocean margin in the presence of a submarine canyon. J. Mar. Syst. 32 (1-3), 239–251.
Smagorinsky, J., 1963. General circulation experiments with the primitive equations. Mon. Weather Rev. 91 (3), 99–164.
Smilenova, A., Gula, J., Le Corre, M., Houpert, L., Reecht, Y., 2020. A persistent deep anticyclonic vortex in the Rockall Trough sustained by anticyclonic vortices shed from the slope current and wintertime convection. J. Geophys. Res. Oceans) 125. https://doi.org/10.1029/2019JC015905.
Smith, P.C., 1978. Low-frequency fluxes of momentum, heat, salt, and nutrients at the edge of the Scotian shelf. J. Geophys. Res. 83 (C8), 4079. https://doi.org/10.1029/JC083iC08p04079.
Souza, A.J., Simpson, J.H., Harikrishnan, M., Malarkey, J., 2001. Flow and seasonality in the Hebridean slope current. Oceanol. Acta 24 (Suppl. 1), S63–S76. https://doi.org/10.1016/S0399-1784(00)01103-8.
Spingys, C., 2017. Volume exchange across the shelf edge: the role of the internal tide and other physical processes. PhD Thesis, University of Liverpool. xxvi + 198 pp.
Spingys, C.P., Williams, R.G., Hopkins, J.E., Hall, R.A., Green, J.A.M., Sharples, J., 2020. Internal tide-driven tracer transport across the continental slope. J. Geophys. Res. Oceans 125 (9). https://doi.org/10.1029/2019JC015530.
Stashchuk, N., Vlasenko, V., 2017. Bottom trapped internal waves over the Malin Sea continental slope. Deep-Sea Research I 119, 68–80.
Stashchuk, N., Vlasenko, V., Hosegood, P., Nimmo-Smith, W.A.M., 2017. Tidally induced residual current over the Malin Sea continental slope. Cont. Shelf Res. 139, 21–34.
Stephenson, G.R., Hopkins, J.E., Mattias Green, J.A., Inall, M.E., Palmer, M.R., 2015. Baroclinic energy flux at the continental shelf edge modified by wind-mixing. Geophys. Res. Lett. 42 (6), 1826–1833.
Stevens, I., Hamann, M., Johnson, J.A., Fiúza, A.F.G., 2000. Comparisons between a fine resolution model and observations in the Iberian shelf-slope region. J. Mar. Sys. 26 (1), 53–74.
Tonani, M., Sykes, P., King, R.R., McConnell, N., Péquignet, A.-C., O'Dea, E., Graham, J. A., Polton, J., Siddorn, J., 2019. The impact of a new high-resolution ocean model on the Met Office North-West European Shelf forecasting system. Ocean Sci. 15 (4), 1133–1158. https://doi.org/10.5194/os-15-1133-2019.
Ullgren, J.E., White, M., 2012. Observations of mesoscale variability in the Rockall Trough. Deep-Sea Res. I 64, 1–8.
Ulses, C., Estournel, C., Bonnin, J., Durrieu de Madron, X., Marsaleix, P., 2008a. Impact of storms and dense water cascading on shelf-slope exchanges in the Gulf of Lion (NW Mediterranean). J. Geophys. Res. 113, C02010. https://doi.org/10.1029/2006JC003795.
Ulses, C., Estournel, C., Puig, P., Durrieu de Madron, X., Marsaleix, P., 2008b. Dense shelf water cascading in the northwestern Mediterranean during the cold winter 2005: Quantification of the export through the Gulf of Lion and the Catalan margin. Geophys. Res. Lett. 35 (7), L07610.
van Aken, H.M., Maas, L.R.M., van Haren, H., 2005. Observations of inertial wave events near the continental slope off Goban Spur. J. Phys. Oceanogr. 35, 1329–1340.
van Haren, H., Hosegood, P.J., 2017. A downslope propagating thermal front over the continental slope. J. Geophys. Res. (Oceans) 122 (4), 3191–3199. https://doi.org/10.1002/2017JC012797.
Veitch, J., Penven, P., Shillington, F., 2009. The Benguela: A laboratory for comparative modeling studies. Prog. Oceanogr. 83 (1-4), 296–302.
Vilibić, I., Orlić, M., 2002. Adriatic water masses, their rates of formation and transport through the Otranto Strait. Deep-Sea Research I 49 (8), 1321–1340.
Vlasenko, V., Stashchuk, N., 2015. Internal tides near the Celtic Sea shelf break: A new look at a well known problem. Deep-Sea Research I 103, 24–36.
Vlasenko, V., Stashchuk, N., Inall, M.E., Hopkins, J.E., 2014. Tidal energy conversion in a global hot spot: on the 3-d dynamics of baroclinic tides at the Celtic Sea shelf break. *J. Geophys. Res. (Oceans)* 119, 3249–3265.
Vlasenko, V., Stashchuk, N., Inall, M.E., Porter, M., Aleynik, D., 2016. Focusing of baroclinic tidal energy in a canyon. *J. Geophys. Res. (Oceans)* 121, 2824–2840. https://doi.org/10.1002/2015JC011314.
Voss, M., Bange, H.W., Dippner, J.W., Middelburg, J.J., Montoya, J.P., Ward, B., 2013. The marine nitrogen cycle: recent discoveries, uncertainties and the potential relevance of climate change. Phil Trans R Soc B 368, 11. https://doi.org/10.1098/rstb.2013.0121.
Wakelin, S.L., Holt, J.T., Blackford, J.C., Allen, J.I., Butenschön, M., Artioli, Y., 2012. Modeling the carbon fluxes of the northwest European continental shelf: validation and budgets. J. Geophys. Res. 117, 1–17. https://doi.org/10.1029/2011JC007402.
Wakelin, S.L., Artioli, Y., Holt, J.T., Butenschön, M., Blackford, J., 2020. Controls on near-bed oxygen concentration on the Northwest European Continental Shelf under a potential future climate scenario. Prog. Oceanogr. 102400 https://doi.org/10.1016/j.pocean.2020.102400.
Walsh, J.J., Biscaye, P.E., Csanady, G.T., 1988. The 1983–84 Shelf Edge Exchange Processes (SEEP) – I experiment: hypotheses and highlights. Cont. Shelf Res. 8, 435–456.
White, M., Mohn, C., Orren, M.J., 1998. Nutrient distributions across the Porcupine Bank. ICES J. Marine Sci. 55, 1082–1094. https://doi.org/10.1006/jmsc.1998.0417.
Wilson, A.M., Raine, R., Mohn, C., White, M., 2015. Nepheloid layer distribution in the Whittard Canyon, NE Atlantic Margin. Mar. Geol. 367, 130–142.
Wollast, R., Chou, L., 2001. Ocean Margin EXchange in the northern Gulf of Biscay: OMEX I. An introduction. *Deep-Sea Res. II* 48, 2971–2978.

Xu, W., Miller, P.I., Quartly, G.D., Pingree, R.D., 2015. Seasonality and interannual variability of the European slope current from 20 years of altimeter data compared with in situ measurements. Remote Sensing of the Environment 162, 196–207.

Young, E.F., Brown, J., Aldridge, J.N., Horsburgh, K.J., Fernand, L., 2004. Development and application of a three-dimensional baroclinic model to the study of the seasonal circulation in the Celtic Sea. Cont. Shelf Res. 24 (1), 13–36. https://doi.org/10.1016/j.csr.2003.09.003.

Young, E.F., Thorpe, S.E., Banglawala, N., Murphy, E.J., 2014. Variability in transport pathways on and around the South Georgia shelf, Southern Ocean: Implications for recruitment and retention. *J. Geophys. Res. Oceans* 119, 241–252. https://doi.org/10.1002/2013JC009348.

Zhao, L., Guo, X., 2011. Influence of cross-shelf water transport on nutrients and phytoplankton in the East China Sea: a model study. Ocean Sci. 7, 27–43. https://doi.org/10.5194/os-7-27-2011.

Zhou, Q., Nost, O.A., 2013. The establishment of Atlantic Water transport as a topographically trapped slope current off Scotland. Tellus A65, #19978.